

Temperature-Controlled Assembly Kinetics for DNA-Functionalized Gold
Nanoparticles

by

Brittany Rae Dever

A thesis submitted in partial fulfillment of the requirements for the degree of

Doctor of Philosophy

Department of Chemistry
University of Alberta

© Brittany Rae Dever, 2014

Abstract

The assembly of nanoparticle building blocks into more complex nanostructures has important applications in analytical chemistry, materials science, medical science, optics, and electronics. Due to its exquisite specificity and programmable nature, DNA has emerged as a very promising biomolecule to facilitate the assembly of nanomaterials. DNA-conjugated gold nanoparticles (AuNP) have been used in a wide range of assays and have also been assembled into discrete nanostructures, two-dimensional arrays, and three-dimensional crystal structures.

This thesis focuses on how temperature impacts the assembly kinetics of DNA-functionalized AuNPs and applying the findings to the development of analytical assays. A temperature effect on the assembly kinetics of AuNPs was discovered. As the temperature increased, the assembly kinetics increased up to a critical temperature (T_{crit}). At temperatures higher than T_{crit} , the assembly kinetics were drastically reduced. This very sharp transition from maximal assembly kinetics at T_{crit} to minimal assembly kinetics at higher temperatures (2-3 °C) has not been reported in literature. The impact of various experimental parameters on the T_{crit} and the sharpness of the transition in the temperature-dependent assembly kinetics (TDAK) profile were studied. Parameters studied included the sodium chloride concentration, the amount of DNA on the AuNP surface, the linker concentration, and the presence of gaps and overhangs present in the linker sequence.

The temperature dependent assembly kinetic phenomenon was used to design a colorimetric assay that could detect single nucleotide polymorphisms (SNPs) within five minutes. This strategy was used to detect a SNP that conferred first line drug resistance in *Mycobacterium tuberculosis*. Temperature-dependent assembly kinetics was also applied to develop a strategy to sequentially control the assembly of three different DNA-AuNPs in a single solution.

These results demonstrate the broad applications that temperature-dependent assembly kinetics of DNA-AuNPs can have in assay development and the synthesis of more complex nanostructures from nanoparticle building blocks. With the promising applications that nanotechnology has to offer, temperature-dependent assembly kinetics offers a novel tool to selectively assemble nanomaterials in solution to aid in the advancement of nanoscience.

Preface

Parts of Chapter 1 of this thesis have been published as Zhang, H.; Li, F.; Dever, B.; Li, X.-F.; Le, X.C. DNA-mediated homogeneous binding assays for nucleic acids and proteins. (2013) *Chemical Reviews*, 113(4), 2812. I was responsible for manuscript composition and editing. Zhang, H. and Li, F. were involved with concept formation, manuscript composition, and manuscript edits. Li, X. -F and Le X. C were supervisory authors and were involved with concept formations, manuscript composition and manuscript edits.

The remainder of this thesis is original work by Brittany Dever. Chapters 2, 3, 4 and 5 have not been published.

Acknowledgements

I would first like to thank my supervisor, Dr. Chris Le, for his support and guidance not only in research, but also in my future career pathway. Working with Chris has been a huge pleasure, and I am very grateful for the opportunities that he has given me. From designing projects in the lab and presenting at group meetings, to showcasing my research findings at major conferences and writing manuscripts, the experience that I have gained is exceptional and will be extremely valuable for my future endeavors. Chris has also been very supportive in my professional development outside of the lab in terms of teaching and learning, and leadership initiatives. His constant faith in me has given me the freedom and opportunities to grow as a researcher and academic, and for that I will be forever grateful.

I would also like to thank my examining committee, Dr. Yingfu Li, Dr. Charles Lucy, Dr. Chris Cairo, and Dr. Robert Campbell for their helpful suggestions and comments. I would also like to thank Dr. Hongquan Zhang, for being an excellent mentor by teaching me in the lab and guiding me in my research pursuits. I would also like to thank Dr. Xing-Fang Li for her friendly conversations and guidance for my future endeavors. I would also like to thank Katerina Carastathis and Dianne Sergy, for their help throughout the years and my family and friends in Edmonton, the AET division and Chemistry Department at the University of Alberta for making these past few years a blast. Lastly, I would like to thank my funding sources, NSERC and AITF.

TABLE OF CONTENTS

CHAPTER 1 – INTRODUCTION¹	1
1.1 DNA-BASED ASSEMBLY OF NANOMATERIALS.....	1
1.2 DNA-BASED ASSEMBLY OF AuNPs FOR ASSAY DEVELOPMENT.....	4
1.2.1 DNA-AuNP aggregation-based assays.....	5
1.2.1.1 Crosslinking DNA-AuNP bioassay.....	6
1.2.2 Fluorescence-based DNA-AuNP bioassays.....	10
1.2.3 DNA-AuNP scanometric-based assays.....	13
1.2.4 SERS based DNA-AuNP assays.....	15
1.3 BOTTOM-UP ASSEMBLY OF NANOPARTICLE BUILDING BLOCKS TO FORM COMPLEX STRUCTURES.....	16
1.3.1 DNA-based assembly of discrete DNA-AuNP structures.....	17
1.3.2 Template assisted DNA-AuNP assembly.....	19
1.3.3 Three-dimensional DNA-assembled DNA-AuNP structures.....	21
1.4 CONTROLLING THE ASSEMBLY OF DNA-LINKED NANOSTRUCTURES.....	25
1.4.1 Sharp melting profile of DNA-AuNP aggregates.....	25
1.4.2 Controlling the assembly kinetics of DNA-AuNPs.....	27
1.5 OBJECTIVE AND RATIONALE.....	28
CHAPTER 2: A SHARP TRANSITION FROM MAXIMAL TO MINIMAL ASSEMBLY KINETICS FOR DNA-ASSEMBLED GOLD NANOPARTICLES	31
2.1 INTRODUCTION.....	31
2.2 EXPERIMENTAL.....	33
2.2.1 Materials and Reagents.....	33
2.2.2 Conjugation of DNA to gold nanoparticles.....	34

2.2.3 Assembly protocol.....	34
2.2.5 Melting experiments.....	36
2.3 RESULTS AND DISCUSSION.....	37
2.3.1 Temperature-dependent assembly kinetics.....	37
2.3.2 Comparison of the TDAK profile to the melting profile for DNA-assembled AuNPs.....	42
2.4 CONCLUSIONS.....	45

CHAPTER 3 – CHARACTERIZATION OF PARAMETERS THAT IMPACT

TEMPERATURE-DEPENDENT ASSEMBLY KINETICS OF DNA-GOLD

NANOPARTICLES.....	46
3.1 INTRODUCTION.....	46
3.2 EXPERIMENTAL.....	47
3.2.1 Materials and Reagents.....	47
3.2.2 Preparation of DNA-AuNPs.....	49
3.2.3 Quantification of ssDNA number on AuNP surface.....	50
3.2.4 Monitoring assembly kinetics.....	50
3.2.5 Monitoring melting profiles.....	51
3.3 RESULTS AND DISCUSSION.....	52
3.3.1 Impact of NaCl concentration on the TDAK of DNA-AuNPs.....	55
3.3.2 Impact of linker concentration on the TDAK of DNA-AuNPs.....	60
3.3.3. Impact of linker gaps and overhangs on the TDAK of DNA-AuNPs.....	66
3.3.4 Impact of the number of ssDNA per AuNP on the TDAK of DNA-AuNPs.....	70
3.4 CONCLUSIONS.....	73

CHAPTER 4 – DEVELOPMENT OF A RAPID COLORIMETRIC ASSAY FOR SINGLE NUCLEOTIDE POLYMORPHISM DETECTION	75
4.1 INTRODUCTION	75
4.2 EXPERIMENTAL	77
4.2.1 <i>Materials and Reagents</i>	77
4.2.2 <i>Preparation of DNA-AuNPs</i>	79
4.2.3 <i>Monitoring assembly of DNA-AuNPs</i>	80
4.2.4 <i>Monitoring melting profiles of DNA-AuNPs</i>	80
4.3 RESULTS AND DISCUSSION	81
4.3.1 <i>Temperature-dependent assembly kinetics for perfectly-matched vs mismatched linked DNA-AuNPs</i>	82
4.3.1 <i>Comparison of temperature-dependent assembly profiles to melting profiles for SNP discrimination</i>	85
4.3.3 <i>Optimization of the DNA-AuNP configuration for enhanced SNP discrimination</i>	88
4.3.4 <i>Optimization of NaCl concentration for enhanced selectivity in SNP detection</i>	93
4.3.5 <i>Concentration of Linker DNA that can be discriminated using temperature-dependent assembly kinetics</i>	95
4.3.6 <i>Application of assay to detect a clinically relevant SNP</i>	97
4.4. CONCLUSIONS	102
 CHAPTER 5: TEMPERATURE-CONTROLLED SEQUENTIAL ASSEMBLY OF DNA-FUNCTIONALIZED AUNPS	103
5.1 INTRODUCTION	103

5.2 Experimental	106
5.2.1 Materials and Reagents.....	106
5.2.2 Conjugation of DNA to gold nanoparticles.....	107
5.2.3 Assembly protocol.....	107
5.2.4 Temperature-dependent assembly rate (TDAK) profile.....	108
5.2.5 Temperature-controlled sequential assembly of nanoparticles.....	108
5.2.6 Transmission Electron Microscopy (TEM) experiments.....	110
5.3 RESULTS AND DISCUSSION.....	112
5.3.1 Temperature-dependent assembly kinetics of DNA-AuNPs with base mismatches	112
5.3.2 Temperature controlled assembly of 20 nm AuNPs differing by base mismatches	120
5.3.3 Temperature-controlled assembly of differently sized DNA-AuNPs.....	123
5.3.4 Controlling the assembly of different DNA-AuNPs by increasing the temperature.....	132
5.4 CONCLUSIONS	137
CHAPTER 6 – CONCLUSIONS AND FUTURE WORK.....	138
REFERENCES.....	142

LIST OF FIGURES

Figure 1-1. Cross-linking mechanism for the assembly of DNA-AuNPs for DNA detection.....	7
Figure 1-2. Non-crosslinking mechanism for the assembly of DNA-AuNPs for DNA detection.	9
Figure 1-3. Fluorescent biosensors that use DNA-AuNPs.	12
Figure 1-4. Schematic of the scanometric assay using DNA-AuNPs.....	14
Figure 1-5. DNA-based assembly of DNA-AuNPs to form discrete structures. ...	18
Figure 1-6. Templated assembly of DNA-AuNPs.....	20
Figure 1-7. DNA-AuNP crystal structures.....	23
Figure 2-1. Absorbance spectra of assembled and non-assembled AuNPs.	35
Figure 2-2. Schematic showing the temperature-dependent assembly of DNA-functionalized gold nanoparticles (AuNPs).	37
Figure 2-3. The effect of temperature on the absorbance ratio (700 nm/530 nm) for monitoring the assembly of 20 nm AuNP-DNA1 and 20 nm AuNP-DNA2 using Linker DNA.	40
Figure 2-4. The temperature-dependent assembly rate (TDAK) profile obtained from the assembly of 20 nm AuNP-DNA-Sequence-A and 20 nm AuNP-DNA-Sequence-B with a linker DNA.	41

Figure 2-5. Comparison of the temperature-dependent assembly rate profile and the melting curve under identical experimental conditions	43
Figure 3-1. Determination of the full width half maximum (FWHM) of the transition from maximum to minimum temperature-dependent assembly kinetics	54
Figure 3-2. The impact of NaCl concentration on the temperature-dependent assembly kinetics profile.....	57
Figure 3-3. Comparison of T_{crit} and T_m at different NaCl concentrations.....	59
Figure 3-4. The impact of Linker-A concentration on the temperature-dependent assembly kinetics profile.....	63
Figure 3-5. Comparison of T_{crit} and T_m at different Linker-A concentrations. ...	65
Figure 3-6. Schematic of variations of DNA linker sequences used in this study	68
Figure 3-7. The impact of linker variations on the temperature-dependent assembly kinetics profile.....	69
Figure 3-8. The impact of the number of DNA probes per AuNP on the temperature-dependent assembly kinetics profile.....	71
Figure 4-1. The extent of aggregation (monitored at 700 nm/530 nm) that occurs for Probe1-AuNP and Probe2-AuNP within five minutes using perfectly matched (PM) Linker DNA (black) or mismatched (MM) Linker DNA (red).	84

Figure 4-2. Melting profiles for Probe1-AuNP and Probe2-AuNP that are assembled with PM-Linker DNA (blue) and MM-Linker DNA (red).	87
Figure 4-3. Design of DNA-AuNP configurations to adjust the distance between DNA-AuNP probes when hybridized to target DNA.	89
Figure 4-4. Temperature-dependent assembly profiles for different configurations of DNA-assembled AuNPs.	92
Figure 4-5. Influence on the NaCl concentration on the temperature-dependent assembly profiles for PM-linked (blue) and MM-linked (red) DNA-AuNPs.	94
Figure 4-6. Extent of assembly that occurs for PM-linked (blue) and MM-linked (red) DNA-AuNPs at 64 °C within five minutes.	96
Figure 4-7. Temperature-dependent assembly profiles based on five minute of incubation for HisP1-AuNP and HisP2-AuNP assembled with His526-Linker DNA(blue) and Tyr526-Linker DNA (red).	98
Figure 4-8. The impact of time on the assembly of His1-AuNP and His2-AuNP probes assembled with His526 (black) and Tyr526 (red) linker DNA.	99
Figure 4-9. Colorimetric discrimination between His526-Linker and Tyr526-Linker induced aggregation of His1-AuNP and His2-AuNP probes after incubation at 56 °C for 20 minutes.	101

Figure 5-1. Schematic showing the temperature-dependent assembly of DNA-functionalized gold nanoparticles (AuNPs).....	105
Figure 5-2. Schematic showing assembly of AuNPs using DNA sequences containing no mismatch (a), a single-base mismatch (b) or two-base mismatches (c)..	113
Figure 5-3. Effect of temperature on the assembly of AuNP-DNA1 (20 nm) and AuNP-DNA0M (20 nm) using a Linker DNA.....	115
Figure 5-4. Effect of temperature on the assembly of AuNP-DNA1 (20 nm) and AuNP-DNA1M (20 nm) using a Linker DNA.....	116
Figure 5-5. Effect of temperature on the assembly of AuNP-DNA1 (20 nm) and AuNP-DNA2M (20 nm) using a Linker DNA.....	117
Figure 5-6. The TDAK profiles showing assembly rates as a function of temperature for assembling AuNPs functionalized with DNA that contains zero (black), one (red), or two (blue) base mismatches with respect to the linker DNA.....	118
Figure 5-7. Transmission electron microscope images showing DNA-assembled AuNPs at the T_{crit} (a, b, and c) and the absence of assembly at temperatures slightly higher than T_{crit} (d, e, and f).....	119

Figure 5-8. a) Temperature-controlled sequential assembly of AuNPs functionalized with DNA containing no mismatch (DNA0M) one-base mismatch (DNA1M), and two-base mismatches (DNA2M)..	122
Figure 5-9. Schematic showing assembly of AuNPs using DNA sequences containing no mismatch (a), a single-base mismatch (b), or two-base mismatches (c).	124
Figure 5-10. Effect of temperature on the assembly of AuNP-DNA0M (50 nm) and AuNP-DNA1 (20 nm) with a Linker DNA.	126
Figure 5-11. Effect of temperature on the assembly of AuNP-DNA2M (10 nm) and AuNP-DNA1 (20 nm) with a Linker DNA.	127
Figure 5-12. Temperature-controlled assembly of different sized DNA-AuNPs.	129
Figure 5-13. Transmission electron microscopy (TEM) images showing temperature-controlled sequential assembly of different sized AuNPs in a single solution.	131
Figure 5-14. Effect of temperature on the assembly of AuNP-DNA2M (50 nm) and AuNP-DNA1 (20 nm) and Linker DNA.	134
Figure 5-15. Controlling the assembly of DNA-AuNPs by increasing the temperature with time.	135

Figure 5-16. Transmission electron microscopy (TEM) images showing temperature-controlled sequential assembly of different-sized AuNPs by increasing temperature in a single solution..... 136

LIST OF TABLES

Table 2-1. DNA sequences and modifications used in the temperature-dependent assembly kinetic study.	33
Table 3-1. DNA sequences and modifications used to study how different parameters impact the TDAK of DNA-AuNPs.	48
Table 3-2. Effect of Linker-A concentration on the critical temperature for temperature-dependent assembly kinetics of DNA-assembled AuNPs.....	61
Table 3-3. Summary of parameters that impact the temperature-dependent assembly kinetic profile.	74
Table 4-1. Sequences used for the development of the rapid colorimetric SNP assay.....	78
Table 5-1. DNA sequences and modifications used to demonstrate temperature-controlled assembly of nanoparticles in a single solution.....	106

List of Abbreviations

Silver nanoparticles	AgNPs
Gold nanoparticle	AuNP
Base pair	bp
Deoxyribonucleic Acid	DNA
Double stranded DNA	dsDNA
Ethylenediaminetetraacetic acid	EDTA
Fluorescence resonance energy transfer	FRET
Full width half maximum	FWHM
High performance liquid chromatography	HPLC
Localized surface plasmon resonance	LSPR
Minutes	min
Millimolar	mM
Mismatched linker	MM-linker
Sodium chloride	NaCl
Nanometer	nm
Nanomolar	nM

Nucleotide	n.t.
Oligonucleotide	Oligo
Perfectly matched linker	PM-linker
Quantum dots	QD
Surface-enhanced raman spectroscopy	SERS
Selectivity factor	SF
Thiol	-SH
Single nucleotide polymorphism	SNP
Single stranded DNA	ssDNA
Thymine	T
Critical temperature	T_{crit}
Temperature-dependent assembly kinetics	TDAK
Transmission electron microscopy	TEM
Melting temperature	T_{m}
Tris hydrogen chloride	Tris-HCl
Microliter	μL
Two-dimensional	2D

Three-dimensional

3D

Chapter 1 – Introduction¹

1.1 DNA-based assembly of nanomaterials¹

Compared to bulk materials, those on the nanoscale (1-100 nm) have unique chemical and physical properties. For example CdSe nanoparticles, also known as quantum dots (QDs), have desirable photophysical properties including composition and size-dependent emission properties, high fluorescence quantum yields, resistance to photobleaching and a broad absorption spectra.¹⁻³ Gold nanoparticles (AuNPs) have localized surface plasmon resonance (LSPR) properties that result from the interaction of light with electrons confined on the AuNP surface.⁴ Magnetic nanoparticles are superparamagnetic but experience no magnetization in the absence of an applied magnetic field.⁵ Many of these properties are predicted by the morphology of the nanoparticle, which is the basis behind developing synthetic strategies devised on producing nanoparticles with novel properties.⁶ As a result of these unique properties, nanomaterials can be applied to medical imaging and therapeutics,⁷⁻⁹ diagnostics,^{10,11} development of metamaterials, assembly of optical and electronic devices,¹²⁻¹⁴ and photonic circuits.¹⁵

Functionalizing the surface of nanoparticles is important because this provides stability for nanoparticles in solution also and provides the functionality required for various applications.¹⁶ The surface molecules also define the intermolecular interactions and therefore play an important role in the assembly of the

¹ Zhang, H., Li, F., Dever, B., Li, X.-F., Le, X.C. DNA-mediated homogeneous binding assays for nucleic acids and proteins. *Chemical Reviews*, **113**, 2812.

nanoparticles.¹⁷ DNA is an advantageous material to assemble nanoparticles because it can be readily synthesized and modified, has very specific complementary base pairing, and is programmable. By modifying one end of DNA with a thiol-group, AuNPs can be functionalized through a covalent gold-thiolate bond. With this approach, many thiol-modified oligonucleotides can be conjugated to a single AuNP. Since 1996, Mirkin and co-workers have extensively studied DNA-AuNPs.¹⁸ These particles maintain the unique properties of AuNPs along with the recognition and stability properties of DNA and have been used to develop therapeutics and diagnostic tools.¹⁹⁻²¹ DNA also provides a powerful way to control the assembly of AuNPs. For example, by varying the length of the connecting DNA, it is possible to control the interparticle spacing between AuNPs. Also, by manipulating how many DNA molecules are attached on the AuNP surface, the structures that assemble can be controlled. For example, by limiting the number of DNA strands per AuNP, it is possible to form dimers and trimers.^{22,23} DNA superstructures, such as DNA origami, can also be used as a template to control the assembly of DNA-functionalized AuNPs.²⁴⁻²⁸

Other nanoparticles, such as silver nanoparticles (AgNPs),²⁹ magnetic nanoparticles,³⁰ and QDs³¹ can also be modified and assembled with DNA. However, most studies have been performed using DNA-AuNPs. This is due to advantageous properties of AuNPs including easy control of size during synthesis,³² stability in aqueous environments, strong plasmonic bands,³³ catalytic properties,³⁴ and potential in biological applications.³⁵ Additionally, the amount of DNA that can be loaded on to a AuNP surface can be controlled through ionic

strength conditions,²⁰ the size of the AuNP,³⁶ DNA sequence and structure,³⁷ and sonication during the conjugation reaction.³⁷

In this Introduction Chapter I will review the progress of DNA-based assembly of AuNPs for the development of assays, and formation of more complex nanostructures. I will also discuss the methods to control DNA-based assembly of AuNPs and ways to increase the assembly kinetics of DNA-AuNPs. This will lead into the body of my thesis where I explore the study of temperature to kinetically control the assembly of DNA-AuNPs. I present a unique temperature-dependent assembly kinetic trend, study parameters that impact this trend, and apply this phenomenon to develop a colorimetric assay to detecting single nucleotide polymorphisms (SNPs) and a strategy to sequentially control the assembly of different DNA-AuNPs in a single solution.

1.2 DNA-based assembly of AuNPs for assay development

Recent technological advances in nanoscience have remarkably improved the ability to design and fabricate nanomaterials with novel properties. The unique properties of nanomaterials give several advantages over traditional assays such as enhanced selectivity, sensitivity and practicality. As a result, nanomaterials have advanced assay development. Specifically, nanomaterials can serve as a scaffold for recognition molecules or as a reporter to generate a detectable signal. AuNPs have several desirable properties that have been harnessed to make novel biosensors for nucleic acids, proteins and small molecules.^{10,38-40} The most common method for AuNP synthesis is the citrate reduction of HAuCl₄ in water.^{4,41} This well-established technique enables the synthesis of highly uniform particles that range in size from 5 to 250 nm. Although relatively unreactive towards most functional groups, AuNPs can be readily functionalized through the formation of stable gold-thiolate bonds with molecules containing thiol (-SH) or disulfide (S-S) groups. Gold-thiolate chemistry has been applied extensively for the conjugation of different types of recognition molecules such as antibodies, aptamers, and nucleic acids.^{38,42}

By combining the unique properties of AuNPs with DNA nanotechnology, the assembly of AuNPs can be controlled and manipulated through the specific Watson-Crick base pairing. DNA-AuNPs can act as biosensors by recognizing and assembling in the presence of target DNA. This is achieved by functionalizing AuNPs with DNA probes that are complementary to the target DNA. Other biomolecules, such as proteins and small molecules, can also be recognized by

DNA-AuNPs when AuNPs are functionalized with functional nucleic acids.⁴³ Aptamers are examples of functional nucleic acids, which are short synthetic oligonucleotides that are generated using the systematic evolution of ligands by exponential enrichment (SELEX) technique.⁴⁴⁻⁵¹ Highly specific aptamers have the ability to bind to targets such as proteins, small molecules and cells with high affinity, making them ideal ligands for the construction of DNA-AuNP based biosensors.^{45,52,53} In this section, I will discuss the properties of AuNPs that how they have led to advancements in analytical chemistry.

1.2.1 DNA-AuNP aggregation-based assays

Localized surface plasmon resonance occurs when incident light at an appropriate wavelength induces collective oscillations of electrons at the surface of AuNPs.⁴⁰ The LSPR response is dependent on factors such as the size and shape of the AuNP, dielectric constant of the environment, and interactions with neighbouring particles. By rationally controlling these factors to manipulate the LSPR, AuNP-based bioassays have been developed. For example, 20 nm AuNPs have a plasmon band at 530 nm. When neighbouring AuNPs are brought into close proximity, the surface plasmons couple, resulting in a redshift in the absorbance spectra.⁵⁴ This effect is so pronounced that when AuNPs are suspended they appear red in solution, and when aggregation-induced coupling of the surface plasmons occurs, the solution turns blue. This phenomenon provides a practical colorimetric signal readout that can be used to detect analyte-induced aggregation or disaggregation of AuNPs. The colorimetric change upon aggregation makes AuNPs a practical nanomaterial for point-of-care detection since no expensive

instrumentation is required. Several strategies have been demonstrated to induce aggregation or disaggregation of AuNPs based on crosslinking or non-crosslinking mechanisms. These mechanisms rely on the target molecule to either induce or dissociate aggregates through a linkage between the particles and non-crosslinking mechanisms require the target to disrupt the stability of AuNPs in solution. Here I will discuss both of these assay formats.

1.2.1.1 Crosslinking DNA-AuNP bioassay

The first DNA-AuNP crosslinking assay was demonstrated by Mirkin and co-workers in 1996.²⁷ In their assay format, two DNA-AuNP probes were used to recognize a complementary target oligonucleotide. The DNA-AuNP probes were designed to be complementary to the target oligonucleotide, but not complementary to one another. Therefore, hybridization of the target oligonucleotide would induce aggregation of the DNA-AuNP probes and a colour change from red to blue (Figure 1-1). Also, compared to molecular DNA, the melting transition for DNA-assembled AuNPs was extraordinarily sharp.⁵⁵ They made use of this phenomenon to develop an assay to detect single base mismatches in oligonucleotide sequences.^{20,56}

This DNA-AuNP aggregation-induced colorimetric detection strategy has also been applied for the detection of proteins and small molecules. For example, functionalizing AuNPs with aptamers that recognize platelet derived growth factor (PDGF) results in the aggregation of DNA-AuNPs in the presence of PDGF.⁵⁷

Another approach that has been used for the crosslinking DNA-AuNP assays is to disrupt an aggregate network that already been formed as a result of the target analyte being present. This was first demonstrated by Lu and coworkers where they assembled DNA-AuNPs with a linking substrate strand.⁵⁸ In the presence of Pb^{2+} , a DNAzyme would cleave the linking substrate strand, resulting in the disruption of the DNA-AuNP network and a colour change from blue to red would occur. This approach has been used to detect other biomolecules including adenosine and cocaine.^{59,60}

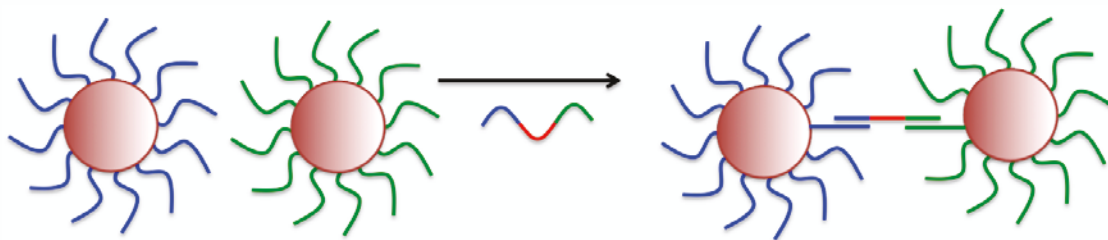


Figure 1-1. Cross-linking mechanism for the assembly of DNA-AuNPs for DNA detection.

1.2.1.2 Non-crosslinking based DNA-AuNP assays

The non-crosslinking mechanism to induce AuNP aggregation is dependent on the stability of AuNPs in solution rather than an interparticle crosslinker. The ability of AuNPs to remain suspended in solution depends on electrostatic repulsions. When AuNPs are synthesized through the citrate reduction of HAuCl₄, the AuNPs are capped with a negatively charged citrate layer. If this layer was not present, van der Waals attractive forces would dominate, resulting in aggregation of the particles.⁶¹ When NaCl is added to a solution of AuNPs, the negative charge on the AuNP surface is screened, resulting in aggregation. Li and Rothberg found that negatively charged single stranded DNA (ssDNA) will interact with the AuNP surface and provide electrostatic repulsion to keep the AuNPs stable in solution in the presence of 200 nM NaCl.⁶² In the presence of DNA that is complementary to the ssDNA adsorbed to the AuNP surface, hybridization results in the removal of the ssDNA from the surface of the AuNP (Figure 1-2). The AuNPs therefore aggregate in the presence of NaCl. This approach is selective enough to detect single nucleotide polymorphisms (SNPs).^{62,63} Aptamers can also be used so that this assay can be extended to the detection of proteins and small molecules.⁶⁴⁻⁶⁶

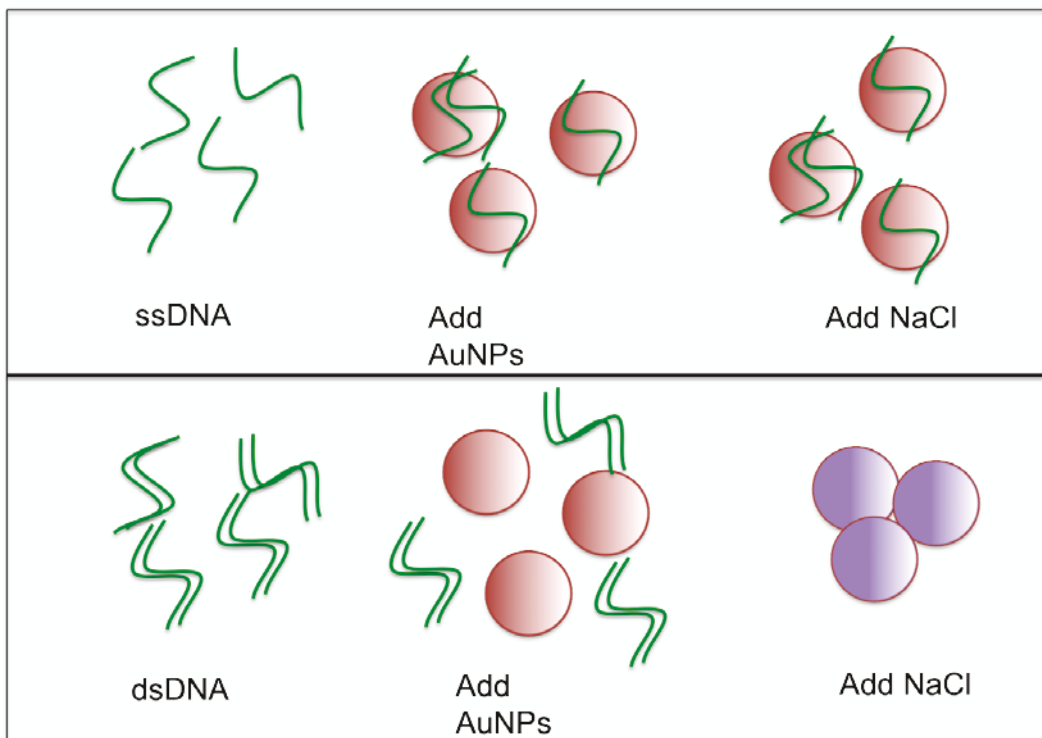


Figure 1-2. Non-crosslinking mechanism for the assembly of DNA-AuNPs for DNA detection.

1.2.2 Fluorescence-based DNA-AuNP bioassays

AuNPs can also be used as powerful fluorescence quenchers through either a fluorescence resonance energy transfer (FRET) or a surface energy transfer (SET) mechanism.⁶⁷⁻⁶⁹ Compared to conventional quenchers, AuNPs have a higher quenching efficiency and can quench over longer intermolecular distances. Also, because of their polyvalent nature, a single AuNP can quench many fluorescent molecules. AuNPs can also quench a broad range of fluorescent molecules including fluorescent dyes, fluorescent proteins, and quantum dots. These properties make AuNPs a superior component for constructing fluorescent-based biosensors.

Molecular beacons were developed by Tyagi and Kramer in 1996 and has shown to be an effective method to homogeneously detect nucleic acids in solution. One way that AuNPs can enhance fluorescent assays is to replace the traditional quencher in a molecular beacon format (Figure 1-3a). In doing so, AuNPs have been demonstrated to be more efficient quenchers and enhanced the sensitivity up to 100-fold.⁷⁰ AuNP-based molecular beacons are also more selective than traditional molecular beacons for single-base mismatch detection. Additionally, because you can modify AuNP with many DNA probes and AuNPs are able to quench many fluorophores, it is possible to achieve multiplex detection using this assay format. Song and co-workers conjugated three different DNA hairpin probes with different fluorescent dyes to the AuNP surface.⁷¹ Three different target oligonucleotides could then hybridize to the probes to generate three distinct signals. By replacing DNA hairpins with aptamer sequences, this assay

format has been used to detect small molecules.⁷² A variation of this assay depends on the adsorption of the fluorescent dye attached to the end of the oligonucleotide probe onto the surface of the AuNP.⁷³ In the absence of complementary DNA, the fluorescent dye adsorbs to the AuNP surface so that fluorescence is quenched. Hybridization with complementary target DNA results in the release of the dye from the surface so that the fluorescence signal is restored.

In another DNA-AuNP-based fluorescent assay, DNA-AuNPs are assembled with DNA-functionalized fluorescent probes, such as quantum dots.⁷⁴ Binding of the target analyte to the DNA probe on the AuNP surface results in the release of the fluorescently labeled probe to restore fluorescence (Figure 1-3b). DNA-AuNPs have been used as fluorescent probes to monitor the intracellular concentration of mRNA in living cells. Mirkin and co-workers developed biosensors called “nano-flares”, where fluorescently labeled DNA hybridize to DNA on the surface of AuNPs (Figure 1-3c).¹⁹ When target mRNA is present, it binds to the DNA on the AuNP surface and displaces the fluorescently labeled DNA to generate a signal. This detection scheme can achieve multiplexed detection by functionalizing the AuNP with different DNA sequences that are hybridized to differently labeled DNA fluorescent probes.⁷⁵ Also, by modifying the AuNP with aptamers, it is possible to detect intracellular concentrations of small molecules, such as adenosine.⁷⁶ Compared to traditional transfection agents, DNA-AuNPs have enhanced cellular uptake and can evade degradation, making them very powerful tools for monitoring and manipulating cellular functions.⁷⁷⁻⁷⁹

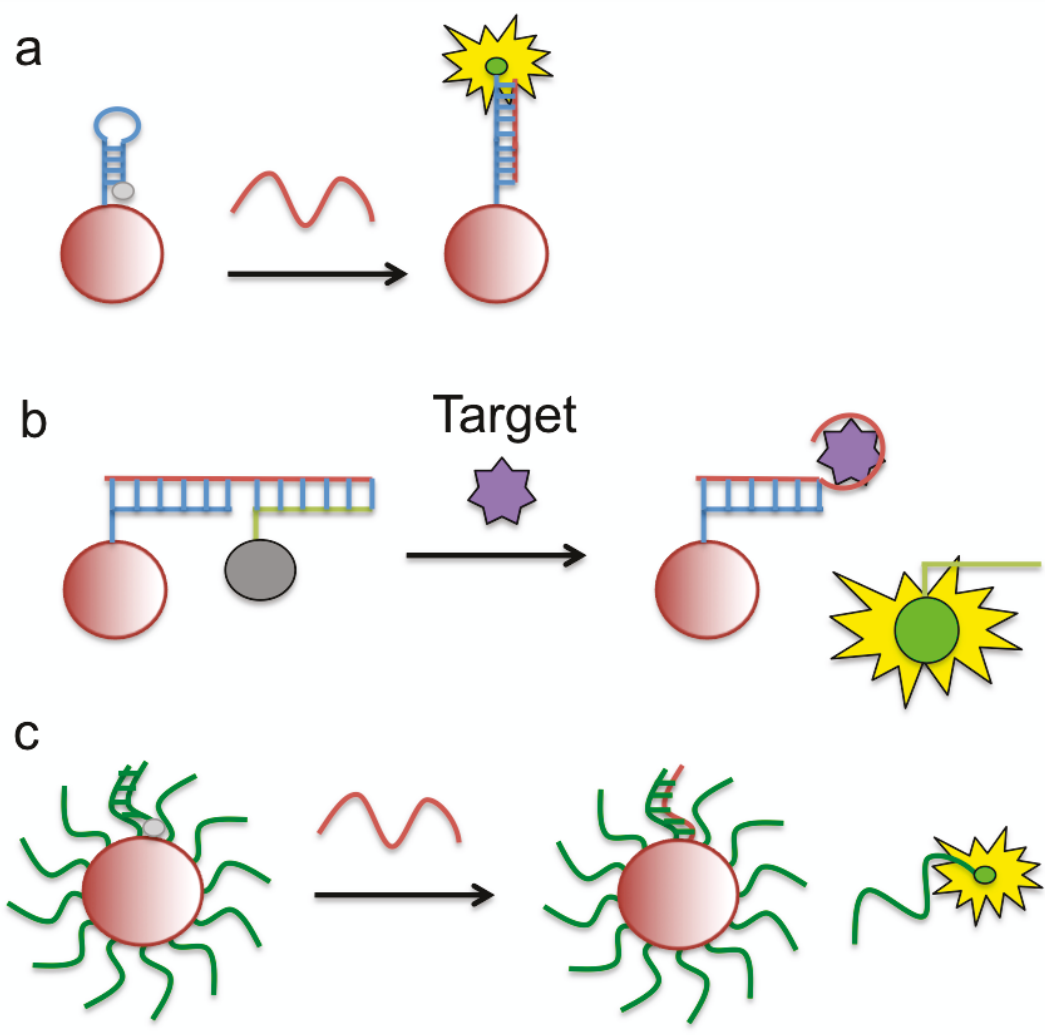


Figure 1-3. Fluorescent biosensors that make use of DNA-AuNPs.

1.2.3 DNA-AuNP scanometric-based assays

The fluorescent and colorimetric-based detection schemes that have been discussed thus far are all homogenous in nature, i.e. the detection takes place in a single tube. DNA-AuNPs can also be assembled on solid supports to provide a colorimetric signal read-out. A scanometric DNA-AuNP array assay has been developed where capture DNA immobilized on a glass chip is recognized by target DNA (Figure 1-4).⁸⁰ A DNA-AuNP probe then recognizes the extended portion of the target DNA. In the presence of target DNA, the DNA-AuNP probes will be captured onto the glass chip. The chip is then washed to remove non-specific binding and silver is catalytically reduced on the AuNP surface to amplify the binding signal. After silver reduction, the array can be visualized with a flatbed scanner to yield a detection limit of 50 fM. This approach can also be used to detect other targets, such as thrombin, by utilizing a thrombin aptamer on the surface of the AuNPs.⁸¹ Lateral flow assays have also been designed using this approach.⁸²

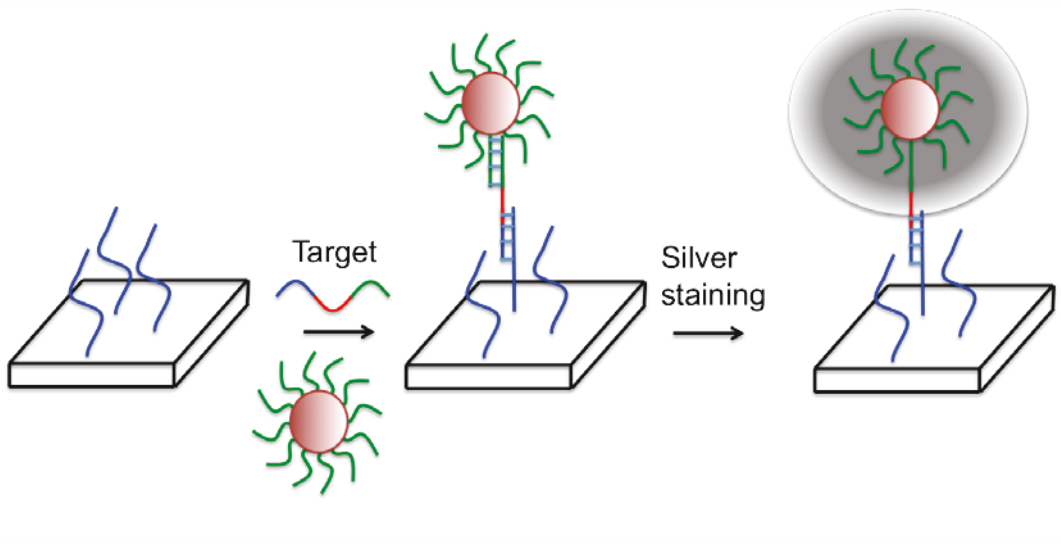


Figure 1-4. Schematic of the scanometric assay using DNA-AuNPs.

1.2.4 SERS based DNA-AuNP assays

LSPR is also responsible for the process known as surface-enhanced Raman spectroscopy (SERS), where the LSPR generates a strong electromagnetic field which can be used to enhance the signal for Raman active molecules.⁸³ This phenomenon is attributed to a combination of chemical and electromagnetic enhancement effects.^{84,85} In the chemical enhancement process, a charge is transferred between the Raman active molecule and the AuNP surface. Chemical enhancement contributes about two orders of magnitude to the overall enhancement. Generally, the electromagnetic effect accounts for the larger contribution to the overall enhancement. When incident light strikes the AuNP surface, LSPR and a localized magnetic field are induced, which subsequently enhances the Raman signal of molecules close to the AuNP surface. SERS circumvents some limitations of normal Raman scattering enabling single molecule detection with fingerprinting molecular specificity.⁸⁶⁻⁸⁸ The SERS effect is even stronger in the gap between two metallic nanoparticles where the surface plasmons are coupled.^{89,90} These regions are also referred to as “hotspots”.⁹¹ When target molecules interact with a “hotspot”, a SERS signal is generated. SERS has demonstrated to be a more sensitive method to detect labeled DNA compared to fluorescence-based methods.⁹²⁻⁹⁴ Recently, DNA-based assembly of DNA-AuNPs has been used to synthesize gold nanobridged nanogap particles, which have a gap size of 1 nm.⁹⁵ This SERS probe was found to generate a very sensitive and reproducible signal.

1.3 Bottom-up assembly of nanoparticle building blocks to form complex structures

The formation of more complex nanostructures from nanoparticle building blocks has important applications in medical science,^{9,96} materials science,⁹⁷ electronics,^{12,13} optics¹⁴ and catalysis.⁹⁸ Novel properties that arise from nanoparticle assemblies are attributed to the size, shape, composition and orientation of nanoparticles with respect to one another. Through synthetic control, it is possible to tune the optical responses of nanoparticles.³²⁶ These optical properties can then be predicted based on Mie Theory.⁵⁴ Another way to manipulate the properties of nanoparticles is to assemble them into more complex structures.⁹⁹ When the surface plasmons between nanoparticles couple, the region between the particles experience an enhanced electric field, known as a hot-spot. This effect has been harnessed to enhance Raman signals in SERS.⁹⁰ To optimize the electric field enhancement, it is important that nanoparticles have correct positioning with respect to one another.^{100,101} Developing strategies that produce nanostructures with well-defined geometries at high yields remains a challenge. One way to overcome this challenge is to utilize the programmable nature of DNA to devise strategies to assemble well-defined nanostructures.^{22,27} Since the introduction of DNA-functionalized AuNPs, a lot of progress has been made in controlling the spatial arrangement of nanoparticles using linking DNA.^{26,102-104} Research has focused on orienting nanoparticles to form discrete,¹⁰⁵ two dimensional (2D), and three dimensional (3D) structures. In this section, I will highlight advances in using DNA to assemble more complex nanostructures.

1.3.1 DNA-based assembly of discrete DNA-AuNP structures

The ability to anisotropically functionalize AuNPs with DNA offers the opportunity to construct novel structures. By controlling the number and the position of the DNA on the AuNP surface, DNA-AuNPs can be assembled into specific nanostructures with unique properties.^{99,106} Alivisatos and coworkers were the first to demonstrate this, when they synthesized mono-functionalized AuNPs to form dimers and trimers (Figure 1-5a).²² This approach however, was limited to very small AuNPs (2 nm). Larger AuNPs functionalized with a single oligonucleotide could be obtained through electrophoretic separation¹⁰⁷ and anion exchange high performance liquid chromatography.¹⁰⁸ Mono-functionalized AuNPs have been used to construct more complex nanostructures such as chiral pyramidal plasmonic assemblies.^{109,110}

Another strategy to form a mono-functionalized DNA-AuNP is to functionalize the AuNP surface with two different oligonucleotides. One that will recognize a linking strand and one that will not recognize a linking sequence in a 1: 99 ratio, respectively.²³ In that way, approximately only one DNA that recognizes the assembling DNA will be present on the AuNP surface. This strategy is advantageous, as coverage of DNA on the AuNP surface will stabilize the AuNPs in solution to prevent aggregation that occurs in the absence of the DNA-assembly. This approach was used to assemble dimer DNA-AuNP structures where a silver shell was then grown on the surface of the AuNPs to increase the electromagnetic field enhancement between the particles.²³ This structure was then used as a SERS platform.

Anisotropic DNA-AuNPs can also be achieved by only functionalizing one side of the AuNP with DNA. These type of particles are called ‘Janus’ nanoparticles. ‘Janus’ nanoparticles have can be formed by using geometric restrictions, such as a magnetic nanoparticle¹¹¹ or a solid support¹¹² to prevent the binding of DNA to the DNA-AuNP on one side. Janus nanoparticles can then be used to assemble dimers and asymmetric core-satellite structures (Figure 1-5b).^{111,112}

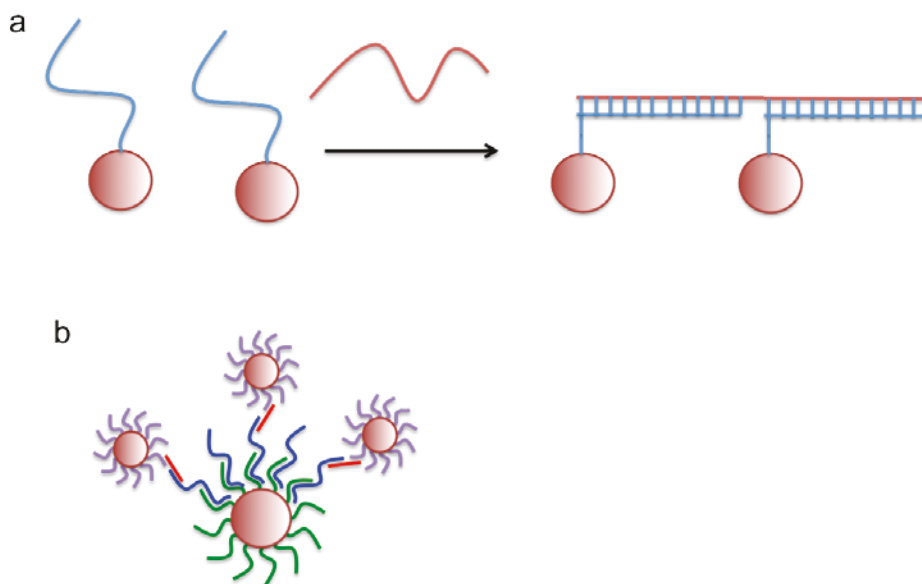


Figure 1-5. DNA-based assembly of DNA-AuNPs to form discrete structures.

1.3.2 Template assisted DNA-AuNP assembly

Precise organization of metallic nanoparticles is important for applications such as their integration into nanoelectronic devices. DNA can be used also be used as template to assemble and spatially arrange DNA-AuNPs through complementary base pairing. For example, products from rolling circle DNA amplification contain repeating DNA sequences and can be used to direct the assembly DNA-AuNPs into linear chains.^{113,114} DNA-origami,^{115,116} DNA-tiles,^{117,118} DNA crossover triangles,¹¹⁹ can also be used as a scaffold for directing the assembly of DNA-AuNPs through complementary base-pairing (Figure 1-6). This strategy is advantageous because unlike flexible DNA strands, DNA-origami structures are relatively fixed and can therefore generate assemblies that are more defined in terms of interparticle distance. DNA-AuNPs have also shown to direct the assembly of DNA structures. For example, DNA-modified AuNPs were used to control the assembly of DNA through size-dependent steric repulsion effects to form various nanotubes.¹²⁰

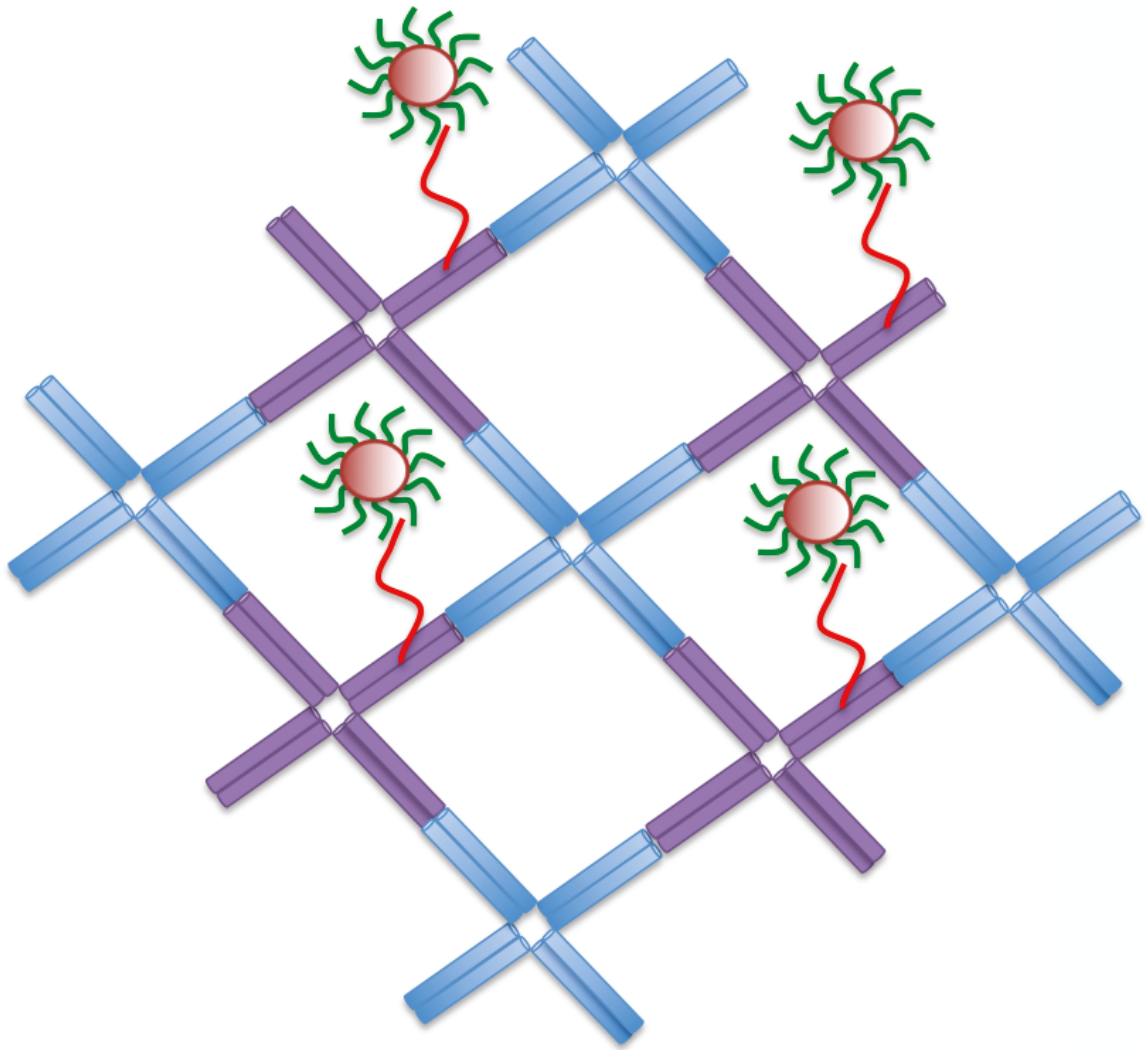


Figure 1-6. Templated assembly of DNA-AuNPs.

1.3.3 Three-dimensional DNA-assembled DNA-AuNP structures

3D DNA-AuNP networks form when polyvalent DNA-AuNPs assemble through a linker DNA or direct hybridization. The first DNA-assembled DNA-AuNP aggregate was demonstrated by Mirkin and coworkers, where they functionalized 13 nm AuNPs with two different thiol-alkane terminated DNA that were not complementary to one another.²⁷ In the presence of complementary linker DNA, the DNA-AuNPs hybridize to either end of the linker, resulting in the formation of networks of DNA-AuNPs. Because of the colorimetric change that occurs when AuNPs assemble, this discovery initiated the development of several analytical assays.^{20,21,56,121} The assembly of DNA-AuNPs was reversible with temperature.⁵⁵ The formation of DNA-AuNP aggregates has been described as an ‘Ostwald-ripening’ process, where DNA-AuNPs are first assembled into small clusters.¹²² These small clusters then coalesce to form a larger aggregate and then the DNA-linkers dehybridize and rehybridize to form a more compact structure.^{122,123} Because DNA-AuNPs are polyvalent in nature, there are often multiple linkages that form between particles. Therefore, hybridization events that would be considered unstable at the molecular level can assemble DNA-AuNP aggregates. For example, a few complementary base pairs¹²⁴ and g-quartet interactions¹²⁵ were strong enough to induce DNA-AuNP aggregation.

In 2008 both the Mirkin and the Gang research groups demonstrated that DNA-AuNPs could form 3D crystal structures.^{126,127} Under annealing conditions, DNA-AuNPs form the most thermodynamically stable structure by maximizing the number of neighboring DNA hybridization interactions.^{126–131} This is achieved

through the hybridization and dehybridization processes of the linking DNA with the DNA-AuNPs. Design rules have been developed for assembling DNA-AuNPs into different crystal lattice structures.^{129,132} By controlling certain parameters (ex. particle size and interparticle distance, which are dictated by designable DNA hybridization interactions), different crystal lattices can be achieved. Theoretical simulations for the crystallization of DNA-AuNPs agree with experimental results.¹³³

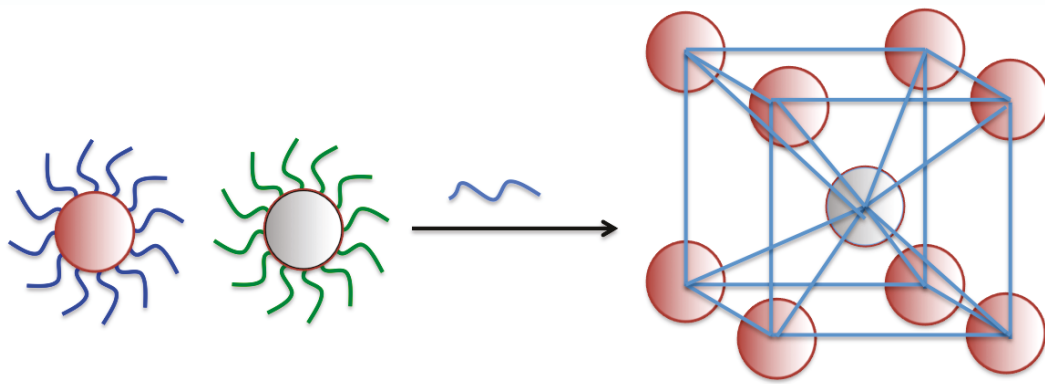


Figure 1-7. DNA-AuNP crystal structures.

One very promising application for the construction of 3D networks using DNA-assembled nanoparticles is to generate designer plasmonic metamaterials. This could provide a means to manipulate electromagnetic fields, resulting in materials with novel properties.¹³⁴ Computational methods can now identify nanoparticle assemblies that may display desirable properties,¹³⁵ but it remains a challenge to synthesize these structures on the nanoscale. Current approaches rely on lithograph approaches, and it has been very challenging to design a bottom-up assembly approach that could generate well-defined architectures.⁹⁷ Recently, DNA has been used to assemble silver nanoparticle (AgNP) superlattices that display metamaterial behaviors such as epsilon-near-zero (ENZ) behavior and a region with an optically metallic response (DC insulator that reflects in the visible spectrum).¹³⁶ Electrodynamic simulations were used to identify superlattices that would exhibit these behaviors. DNA-functionalized silver nanoparticles were then assembled into 3D structures using a linker sequence. The optical response of the superlattices was dependent on the spacing between the particles. Therefore, by controlling the linker length, the desired spacing could be achieved. This demonstrates that DNA-based assembly of DNA-functionalized AuNPs can serve as an attractive method to assemble designer materials.

1.4 Controlling the assembly of DNA-linked nanostructures

1.4.1 Sharp melting profile of DNA-AuNP aggregates

Compared to that of molecular DNA, the melting profiles for polyvalent DNA-AuNPs that are assembled with a linker DNA are extraordinarily sharp (Figure 1-8a).²⁰ In a DNA-assembled aggregate, there are multiple hybridization events that occur between the AuNPs. As the temperature increases, the weaker hybridization events may dissociate, but the aggregate will still remain intact. Because of the insensitivity to the weaker dissociations, the melting transition for DNA-assembled AuNP aggregates is much more cooperative and stable compared to that of molecular DNA.^{55,137,138} The neighboring duplex interactions induce cooperativity in the melting behavior of DNA-AuNP aggregates.¹³⁹ Molecular simulations have shown that when neighboring duplexes are within 5 nm of one another, the cation cloud that is associated with the duplex combine to form a shared cloud.¹⁴⁰ When the first duplex dissociates, the cations from that duplex are removed. This disrupts the shared cation cloud, which destabilizes neighbouring duplex. As a result, a melting cascade occurs which gives rise to the very sharp melting profile of DNA-assembled AuNP aggregates.

This novel phenomenon for DNA-assembled AuNPs has been harnessed to develop assays to detect single base mismatches in DNA sequences.^{20,56} An aggregate that is assembled with complementary DNA will have a higher melting temperature (T_m) compared to an aggregate that contains a single base mismatch with respect to the DNA attached to the AuNP surface. Therefore, an aggregate assembled with a single base mismatch will dissociate at a lower temperature,

which can be visualized by a colour change from blue to red. By spotting the solution on a C₁₈ thin-layer chromatography plate, this colour differentiation can be enhanced.²⁰ Due to the applications that this phenomenon can be applied to, the impact of several experimental parameters on the melting transitions have been studied.⁵⁵ For example, when solution sodium chloride concentration or interparticle distance increase, the melting temperature (T_m) of the aggregate increases. DNA-AuNPs with a moderate loading of DNA-probes on the AuNP surface also have enhanced thermal stability.¹⁴¹⁵⁵

1.4.2 Controlling the assembly kinetics of DNA-AuNPs

Compared to molecular DNA that is free to diffuse rapidly in solution, DNA-AuNP hybridization is relatively slower (several hours) due to the DNA being confined to the nanoparticle environment.¹⁴²⁻¹⁴⁴ Because of the important applications of DNA-based assembly of AuNPs, it is crucial to understand and develop strategies to increase the kinetics. When considering DNA-AuNPs, there are different forces that affect assembly. The complementary base pairing between DNA-AuNPs provides an attractive force that promotes assembly and the electrostatic repulsion of the negatively charged DNA on the AuNP surface discourages assembly.^{20,145,146} Factors that influence the hybridization of DNA between the AuNPs and electrostatic repulsion can then influence the rate. One strategy is to design DNA so that it will not adsorb to the AuNP surface so that the DNA is more available for binding. This can be achieved by hybridizing the portion of the DNA closest to the AuNP with a short complementary DNA sequence.¹⁴³ This results in the formation of a rigid duplex structure which projects the DNA from the surface of the AuNP making the DNA more available to hybridize with complementary DNA.¹⁴⁷ Strategies that reduce the electrostatic repulsion when the AuNPs hybridize also increase the rate of assembly. The strategies include increasing the NaCl concentration,^{60,148} minimizing non-complementary DNA,¹⁴⁹ decreasing the loading of DNA on the AuNP surface,¹⁴⁸ increasing the interparticle distance,⁶⁰ and increasing the assembly temperature.⁶⁰ Other factors such as the linker length,^{123,150} and the presence or absence of a gap or overhanging in linking DNA can also impact the assembly kinetics.^{150,151}

1.5 Objective and Rationale

As discussed in this chapter, DNA-based assembly has many important applications in the development of diagnostics and novel materials. The assembly of DNA-functionalized nanomaterials is facilitated through DNA hybridization between nanoparticles directly or through a linking DNA strand. When considering DNA-assembled AuNPs it is very important to consider the kinetics. Compared to molecular DNA, DNA that is attached to a AuNP surface experiences slower hybridization kinetics due to the presence of the relatively large AuNP. This thesis was started with the exploration of strategies to increase the rate of assembly for DNA-AuNPs. When exploring the impact of temperature on the assembly kinetics, a unreported phenomenon was found. For a three-component system (two DNA-AuNPs joined by a complementary linker DNA), the assembly kinetics increased with an increase in temperature up to a critical temperature (T_{crit}). With a further increase in temperature past T_{crit} (~ 3 °C), a drastic decrease in assembly kinetics was observed. This unique profile is central to the studies described in this thesis. I explore the phenomenon itself, parameters that impact the phenomenon and its potential applications in colorimetric assay development and controlled assembly strategies. The rationale of this thesis is to demonstrate that temperature-dependent assembly kinetics of DNA-AuNP can be used as a novel tool to control the assembly of nanomaterials. The thesis projects are:

Chapter 2: A sharp transition from maximal to minimal assembly kinetics for DNA-assembled gold nanoparticles. I systematically studied the assembly

kinetics of DNA—assembled gold nanoparticles at various temperatures. Within a very narrow temperature window, maximal to minimal assemble kinetics are observed. This is the first time that this temperature-dependent transition in assembly kinetics has been reported. Comparison of this temperature-dependent assembly kinetic phenomenon to the melting profile of a pre-assembled aggregate shows that this temperature-dependent assembly phenomenon is unique.

Chapter 3: Characterization of parameters that impact temperature-dependent assembly kinetic of DNA-gold nanoparticles. I studied various experimental parameters that influence the temperature-dependent assembly kinetics of DNA-AuNP such as salt concentration, linker concentration, linker length, and DNA density on the AuNP surface. It is important to understand how these parameters influence the critical temperature and the sharpness of the transition, and it is pertinent to have a firm understanding of the impact of these experimental variables on the temperature-dependents assembly kinetics in order to apply this phenomenon to bioassay developments and strategies to control the assembly of nanomaterials.

Chapter 4: Development of a rapid colorimetric assay for single nucleotide polymorphism detection. I designed and optimized a colorimetric assay to detect single nucleotide polymorphisms (SNPs) using the temperature-dependent assembly kinetics phenomenon. Using this strategy, I can differentiate between single base mismatches in target DNA sequences within five minutes with very

high selectivity. I applied this strategy to detect a clinically relevant SNP that confers drug resistance in *Mycobacterium tuberculosis*.

Chapter 5. Temperature-controlled sequential assembly of DNA-functionalized AuNPs. I designed a strategy that uses the temperature-dependent assembly kinetics to sequentially control the assembly of different DNA-AuNPs in a single solution. I found that by inducing mismatches into the probe DNA on the AuNP surface with respect to the linking DNA, the temperature-dependent assembly profiles are shifted. By identifying temperatures where there is rapid assembly for some DNA-AuNPs, and negligible assembly for others, I developed a temperature program that can selectively assemble nanomaterials as a function of time.

Chapter 6. Conclusions. This chapter summarizes the research in this thesis, as well as future directions.

Chapter 2: A sharp transition from maximal to minimal assembly kinetics for DNA-assembled gold nanoparticles

2.1 Introduction

Nanoparticles can serve as basic building blocks for the assembly of more complex plasmonic nanostructures. One of the most promising techniques uses DNA to assemble nanoparticles through the exquisite specificity of complementary base pairing.⁹⁹ This was first demonstrated over a decade ago, when DNA-functionalized gold nanoparticles (AuNPs) were assembled into periodic structures, dimers and trimers via DNA linkers.^{22,27} Since then, DNA-mediated assembly of DNA-functionalized gold nanoparticles have found important applications in analytical chemistry,^{10,20,56,152} formation of crystal structures,^{126,127,129,153,154} and spatially arranging nanoparticles in one and two-dimensional patterns.^{113,118,155–157} When considering DNA-driven assembly of DNA-AuNPs, it is crucial to understand assembly kinetics because this parameter can be used to control assembly in solution¹⁵⁸ and is important to optimize in assay development. Compared to molecular DNA hybridization, DNA-mediated AuNP assembly is slower and is influenced by complex factors such as multiple linkers forming between particles,¹³⁹ electrostatic repulsion,¹⁴⁵ DNA surface density¹⁴¹ and DNA-AuNP interactions.¹⁵⁹ To this extent, several parameters have been studied on the impact of DNA-mediated AuNP assembly kinetics including the presence of non-base pairing DNA¹⁴⁹ gaps and overhangs in the linker sequence,^{150,151} linker concentration,⁶⁰ DNA-spacer length,¹⁴⁸ NaCl concentration,^{60,148} DNA-AuNP configuration,⁶⁰ the structure of the DNA,^{143,144}

and temperature.^{20,60,160-162} Temperature is a particularly interesting parameter to study as an increase in temperature has been reported to both increase^{20,60} and decrease^{161,162} the assembly kinetics. Here we systematically study how assembly temperature impacts the assembly kinetics for DNA-assembled AuNPs and find that as temperature increases, an increase in assembly rate is observed. Further increases in temperature past a critical temperature (T_{crit}) results in a dramatic decrease in the assembly rate. The unique feature about this finding is that temperature range from maximal to minimal assembly kinetics is extremely narrow (2 – 3 °C) compared to the range that has previously been reported (~10 °C).^{60,161,162} We compare the temperature-dependent assembly kinetic profile to another unique melting profile for DNA-assembled AuNPs. We also study how temperature impacts other DNA-based assembly, such as on the surface of a single DNA-AuNP and between molecular DNA.

2.2 Experimental

2.2.1 Materials and Reagents

HPLC purified DNA sequences (Table 2-1) were purchased from Integrated DNA Technologies (Coralville, IA). Gold nanoparticles were purchased from Ted Pella (Redding, CA). 18 M Ω water was used for all experiments. Tween 20 and sodium chloride (NaCl) were purchased from Fisher Scientific (Nepean, ON, Canada).

Table 2-1 DNA sequences and modifications used to study temperature-dependent assembly kinetics of DNA-AuNPs.

Name	Sequence and modification (5' to 3')
Linker	CTA CCA CAC CAC CAC CAG AGT CCC AGC CCA CCG TCC ACA CAC CCA CTT G
DNA1	Thiol Modifier C6 S-S /TTT TTT TTT TTT TTT GTG GTG GTG TGG TAG
DNA2	Thiol Modifier C6 S-S /TTT TTT TTT TTT TTT CAA GTG GGT GTG TGG
Sequence-A	Thiol Modifier C6 S-S /TTT TTT TTT TTT TTT CTT GTG GGT CAA C
Sequence-B	Thiol Modifier C6 S-S /TTT TTT TTT TTT TTT GAC AGT CGG CG
Linker-A	GTT GAC CCA CAA GCG CCG ACT GTC

2.2.2 Conjugation of DNA to gold nanoparticles

Alkyl thiol modified DNA was added to gold nanoparticle (AuNPs) solutions at a 1000:1 ratio. Solutions were vortexed and incubated at room temperature overnight. The NaCl was then added to the mixture so that its concentration was 100 mM. The solution was vortexed for 30 s and sonicated with a FS60 Fisher Scientific Ultrasonic Cleaner for 30 s. After a 20 min incubation period at room temperature, the NaCl addition procedure was repeated twice to bring the total NaCl concentration to 300 mM. The DNA-AuNP conjugates were further aged overnight at room temperature. 0.05% Tween 20 was added and the conjugates were centrifuged at 16,000 g for 20 min. The supernatant was removed and the pellet was washed through resuspension in 10 mM Tris-HCl pH 7.4 containing 0.05% Tween 20. The conjugates were centrifuged and washed twice more before being resuspended in 10 mM Tris-HCl pH 7.4.

2.2.3 Assembly protocol

Reaction mixtures containing AuNP-DNA1, AuNP-DNA2 and Linker DNA were incubated at various temperatures in a MJ mini PCR thermal cycler (Bio-Rad, Hercules, CA). In control experiments, the reaction mixtures did not contain Linker DNA. At different time intervals, the reaction mixtures were transferred to a 384 microwell plate and the absorbance ratio of 700 nm/530 nm was determined on a Benchmark Plus microplate spectrophotometer (Bio-Rad, Hercules, CA). This absorbance ratio was chosen because non-assembled AuNPs have a plasmon peak at 530 nm. When assembled, there is a decrease in absorbance at 530 nm and an increase in absorbance at 700 nm (Figure 2-2). The time allotted for transfer of

the solutions prior to the absorbance measurement was kept constant at 10 min. Absorbance ratios of 700 nm/530 nm from the control mixtures containing no linking DNA were subtracted from the same measurements of the samples.

In all studies on the impact of temperature on the assembly of 20 nm AuNP-DNA1 and 20 nm AuNP-DNA2, each reaction mixture contained 0.75 nM 20 nm AuNP-DNA1, 0.75 nM 20 nm AuNP-DNA2, 75 nM Linker DNA, and 300 mM NaCl in 10 mM Tris-HCl buffer pH 7.4.

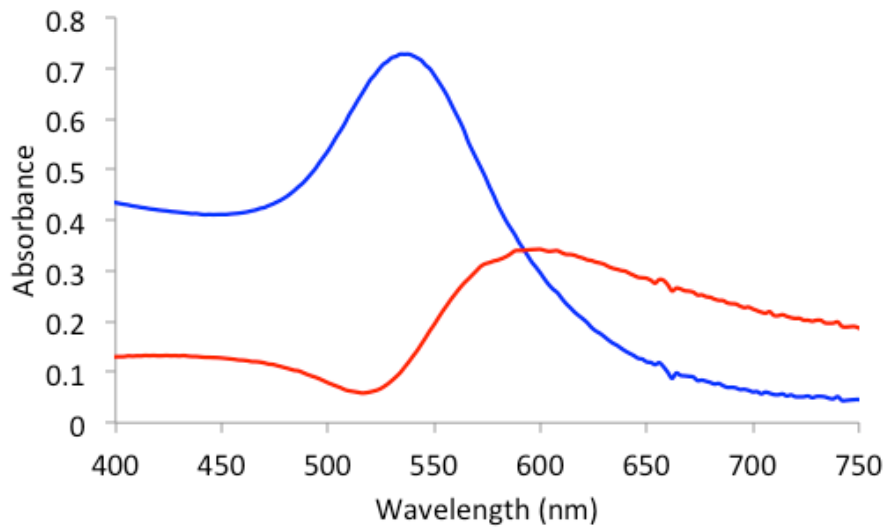


Figure 2-1 Absorbance spectra of solutions containing freely suspended 20 nm AuNPs (blue) and assembled AuNPs (red). The AuNPs were functionalized with either DNA1 or DNA2 as shown in Figure 2-1. For the assembly, the solution contained 0.75 nM AuNP-DNA1, 0.75 nM AuNP-DNA2, 75 nM Linker DNA, 300 mM NaCl and 10 mM Tris-HCl buffer (pH 7.4).

2.2.4 Temperature-dependent assembly kinetics (TDAK) profile

Absorbance ratios of 700 nm/530nm were measured at various time intervals during the assembly process. The initial assembly rate was determined from the slope in the initial linear region of the kinetic curve. The initial assembly rate was plotted as a function of temperature to give rise to the temperature-dependent assembly kinetics (TDAK) profile.

2.2.5 Melting experiments

Reaction mixtures were prepared as described in section 2.2.3 and were heated to 70 °C for 5 min and allowed to cool slowly overnight to induce aggregate formation. Melting experiments were performed using a Hewlett Packard 8452 Diode Array Spectrophotometer with a temperature controller. The temperature was increased from 40 °C to 80 °C at 1°C/min with stirring while monitoring the absorbance of 260 nm.

2.3 Results and discussion

2.3.1 Temperature-dependent assembly kinetics

To study the assembly rates as a function of temperature, we used a three-component system that involved a linker DNA and two different AuNPs that are each functionalized with thiol-modified single-stranded DNA (Figure 2-2). We designed the sequences of these probes in such a way that DNA1 was complementary to one end of the linker DNA, and DNA2 was complementary to the other end of the linker DNA. DNA1 and DNA2 were not complementary to each other. The hybridization of the Linker with DNA1 and DNA2 assembled AuNP-DNA1 and AuNP-DNA2 into close proximity.

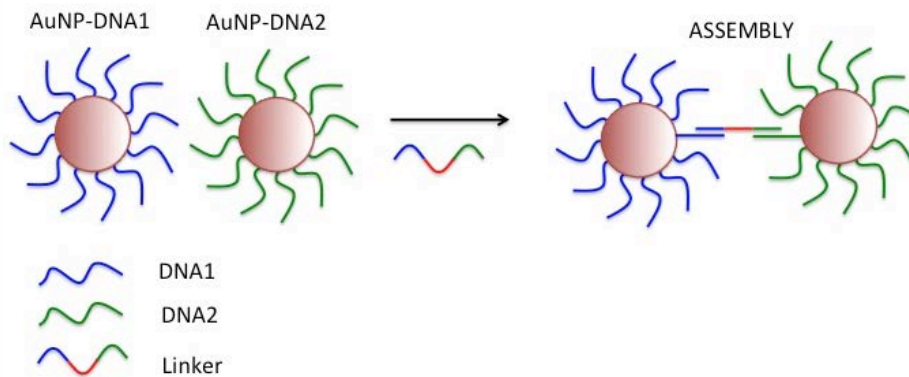


Figure 2-2 Schematic showing the temperature-dependent assembly of DNA-functionalized gold nanoparticles (AuNPs). AuNPs were functionalized with either DNA1 or DNA2. The Linker contains DNA sequences at either ends that are complementary to DNA1 and DNA2, so that AuNP-DNA1 and AuNP-DNA2 can hybridize to the Linker to result in assembly.

We first examined the effect of temperature on the assembly by monitoring the absorbance ratio of 700 nm/530 nm because a red shift occurs as dispersed nanoparticles assemble (Figure 2-1). As the temperature increased from 40 °C to 64 °C (Figure 2-3a), the assembly kinetics increased. With further increase of temperature higher than 64 °C, however, the assembly kinetics decreased drastically (Figure 2-3b). We plotted the initial assembly rate as a function of temperature to yield what we termed a temperature-dependent assembly kinetics (TDAK) profile (Figure 2-3c). This TDAK profile highlights the very narrow temperature range in which the maximal assembly rate is achieved at 64 °C and the minimal assembly rate is observed at 67 °C. We termed the temperature with maximal assembly kinetics the critical temperature (T_{crit}) because a further increase in incubation temperature results in a dramatic decrease in the assembly rate. At a temperature only 3 °C higher than T_{crit} , the assembly rate was minimal. To demonstrate the generality of the TDAK profile for DNA-assembled AuNPs, we also performed similar experiments with different probe sequences. A similar TDAK profile was obtained (Figure 2-4). At a critical temperature (T_{crit}) of 56 °C, the maximum assembly rate was achieved.

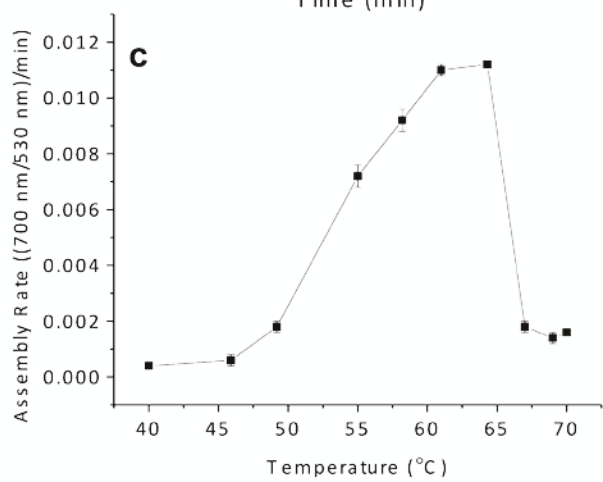
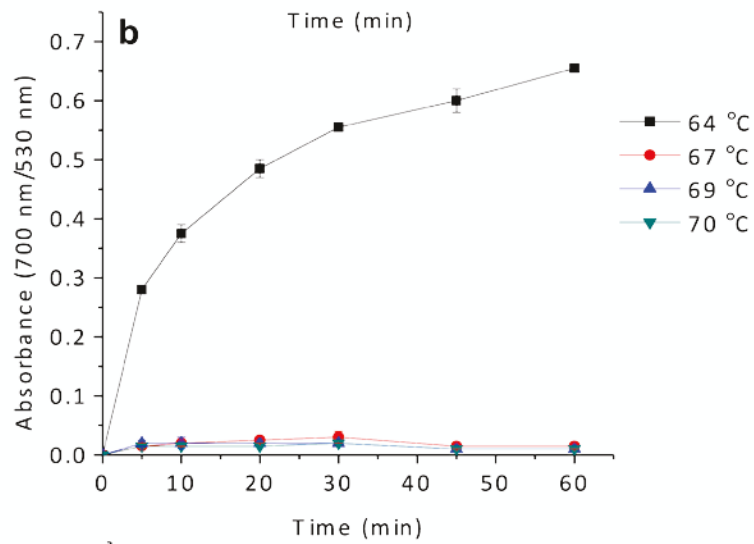
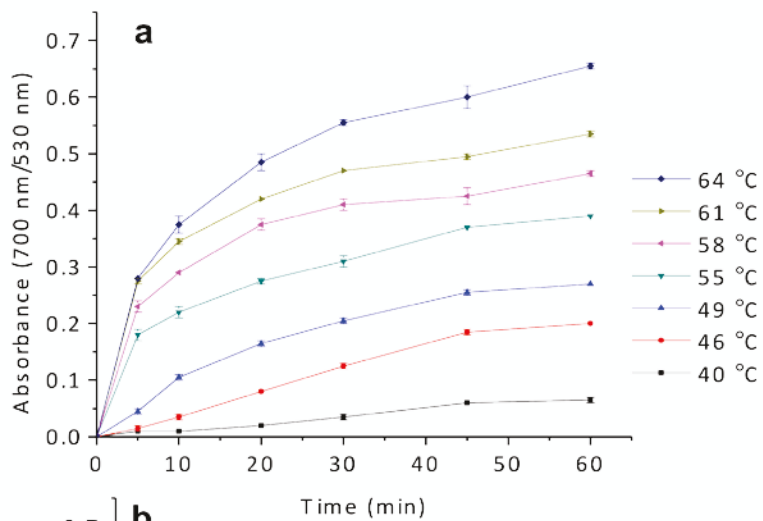


Figure 2-3. The effect of temperature on the absorbance ratio (700 nm/530 nm) for monitoring the assembly of 20 nm AuNP-DNA1 and 20 nm AuNP-DNA2 using Linker DNA. (a) The assembly rate increases with the increase of temperature from 40 °C to 64 °C. (b) Assembly rate drastically decreases with the further increase of temperatures higher than 64 °C. (c) The temperature-dependent assembly kinetics (TDAK) profile for the assembly of 20 nm AuNP-DNA1 and 20 nm AuNP-DNA2 with the Linker DNA. The assembly rate was determined from the slope of the absorbance ratio (700 nm/530 nm) as a function of time in the initial linear region of the kinetic curves (from (a) and (b)).

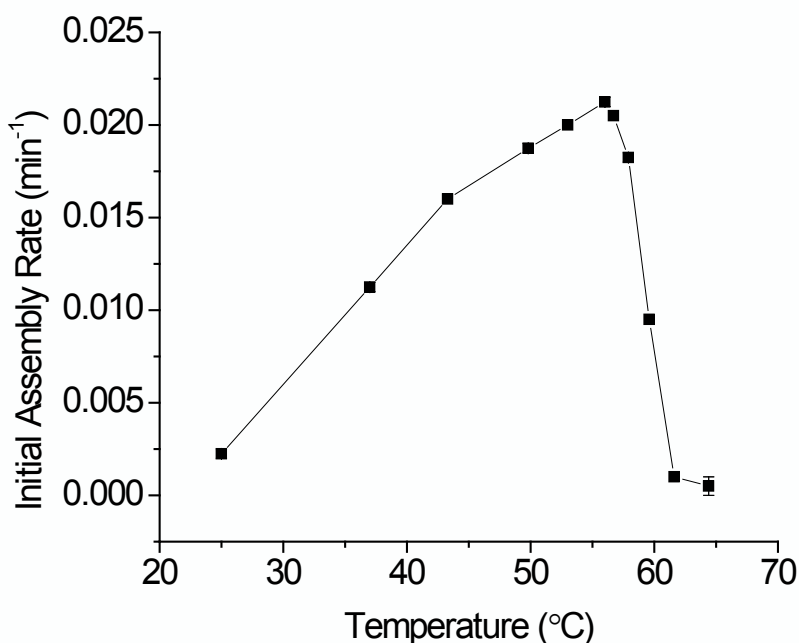


Figure 2-4. The temperature-dependent assembly kinetics (TDAK) profile obtained from the assembly of 20 nm AuNP-DNA-Sequence-A and 20 nm AuNP-DNA-Sequence-B with a linker DNA. DNA Sequence-A was conjugated to the first AuNP (20 nm in size) and DNA Sequence-B was conjugated to the second AuNP (20 nm in size). DNA Linker has one end complementary to Sequence-A and the other end complementary to Sequence-B. 0.75 nM AuNP-Sequence-A and 0.75 nM AuNP-Sequence-B were mixed with 75 nM Linker DNA and incubated at temperatures ranging from 25 °C to 64 °C. At each temperature, the absorbance ratio (700 nm/530 nm) was monitored as a function of time. The assembly rate was determined from the slope in the initial linear region of the curve.

The sharp transition from maximal to minimal with increasing temperature is unique compared to the broader transitions that have been reported previously and therefore the potential for applications of this phenomenon have not been explored.^{60,162,163} In previous studies, the decrease in assembly kinetics with an increase in temperature was seen over a 10 °C temperature range whereas in this study we found the transition to take place over a 3 °C temperature range. A possible explanation for the difference in the TDAK's observed could be due to difference is the DNA-AuNP systems used to study the impact of temperature. For example, these studies involved two component systems,^{161,162} where DNA hybridization occurred directly between DNA-AuNP without a DNA linker, or involved the presence of a duplex structure within the linker DNA.⁶⁰ These differences could cause the hybridization kinetics to not behave the same with respect to temperature as these structural differences could impede the cooperativity of hybridization.^{55,139}

2.3.2 Comparison of the TDAK profile to the melting profile for DNA-assembled AuNPs

The most probable explanation for the sharp decrease in assembly kinetics at temperatures past T_{crit} is the dehybridization of DNA. This could be due to T_{crit} coinciding at the melting temperature (T_m). T_m is as the temperature in which 50% of DNA dehybridization has occurred. To test this hypothesis, the TDAK profile was compared to the melting profile under identical conditions. In the melting experiment, the AuNPs were already assembled and the temperature was increased while monitoring the absorption at 260 nm. An increase in absorption at

260 nm signifies that the assembled AuNPs had been disrupted due to the crosslinking target DNA strands dehybridizing from the complementary probe strands on the surface of the AuNPs. For the assembly experiment, the assembly rates of non-assembled AuNPs-DNA at different temperatures were monitored.

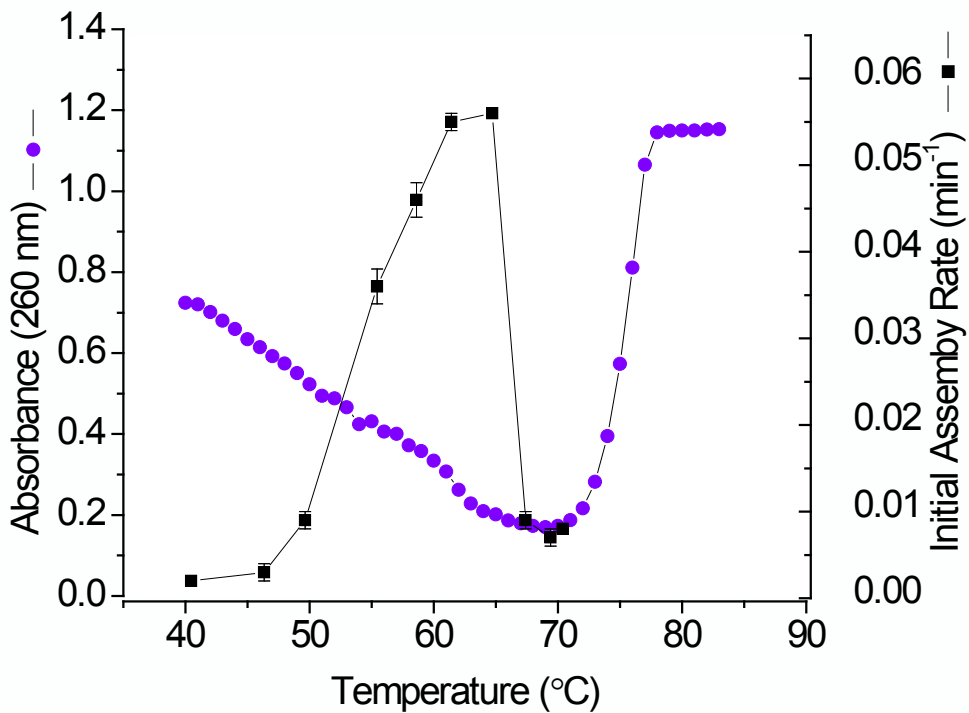


Figure 2-5. Comparison of the temperature-dependent assembly rate profile (black) and the melting curve (purple) under identical experimental conditions.

As shown in Figure 2-5, T_{crit} and T_{m} are not the same. Under the same experimental conditions, T_{m} was determined to be 75.5 °C while T_{crit} was 64.0 °C. The difference between the T_{m} and T_{crit} could be explained when the temperature dependent assembly kinetics and the disassembly (melting) processes are considered. For the melting process, DNA-linked AuNP-DNA aggregates contain multiple linkages between AuNPs in the aggregate structure.⁵⁵ The aggregate also has a shared cation cloud.^{139,140} Both of these factors can stabilize the aggregates, resulting in a higher temperature for DNA dehybridization to occur (T_{m}). In contrast, for the assembly process, the rate of hybridization at different temperatures was monitored. There is no aggregate that contains multiple linkages and a higher localized NaCl concentration to stabilize DNA hybridization.¹⁶⁴ Thus, the higher T_{m} compared to T_{crit} could be explained by a higher localized salt concentration and multiple linkages existing within a preformed aggregate that stabilizes the duplexes formed. Nonetheless, it is important to realize that T_{crit} and T_{m} are distinct from one another.

2.4 Conclusions

We have investigated the impact of temperature on the assembly kinetics of DNA-functionalized AuNPs and have found a novel trend. As the temperature is increased, the assembly rate increased up to a T_{crit} . At temperatures 2-3 °C higher than T_{crit} , the kinetics for assembly are drastically reduced. This very sharp transition from maximal assembly kinetics at T_{crit} to minimal assembly kinetics at temperatures slightly higher, has not been reported in literature. This phenomenon could serve as the basis for the development of diagnostics and strategies to control assembly. These opportunities will be explored in the remainder of this thesis.

Chapter 3 – Characterization of parameters that impact temperature-dependent assembly kinetics of DNA-gold nanoparticles

3.1 Introduction

Due to the sequence-specific hybridization properties of DNA, DNA-functionalized nanoparticles have found applications in the development of assays and the bottom-up synthesis of novel materials.^{4,22,24,27,28,165–170} This is based on the recognition capability of DNA to assemble nanomaterials into aggregate, discrete, and ordered three dimensional structures.^{22,27,123,126–128} Detection schemes that have been developed from DNA-functionalized nanomaterials exhibit enhanced sensitivity and selectivity compared to those of molecular probes. For example, single-base mismatches can be distinguished from fully complementary sequences based on the sharp melting transition that is observed when DNA-assembled gold nanoparticles (AuNP) are heated.^{20,55,56} In addition to the sharp melting profile that is observed to DNA-assembled AuNPs in Chapter 2, we found that an increase in assembly rate results as the temperature is increased up to a critical temperature (T_{crit}). By increasing the temperature past T_{crit} the assembly kinetics are drastically decreased. What is interesting about this phenomenon is that the transition from maximal assembly kinetics to minimal assembly kinetics, occurs within a 2-3 °C temperature range. This sharp transition from maximum to minimum assembly kinetics could possibly be used to develop bioassays^{20,58–60,171–173} and strategies to control the assembly of different DNA-AuNPs. These applications will be explored in Chapters 4 and 5 of this thesis.

Because of the important potential applications, it is crucial to understand what variables impact temperature-dependent assembly kinetics as fluctuations in the narrow temperature range could adversely affect these applications. In Chapter 3, we study how different experimental parameters such as NaCl concentration, linker concentration, linker hybridization positioning, and DNA surface density impact the temperature-dependent assembly kinetics.

3.2 Experimental

3.2.1 Materials and Reagents

HPLC purified DNA sequences (Table 3-1) were purchased from Integrated DNA Technologies (Coralville, IA). Gold nanoparticles (20 nm) were purchased from Ted Pella (Redding, CA). 18 M Ω water was used for all experiments. Tween 20 and sodium chloride (NaCl) were purchased from Fisher Scientific (Nepean, ON, Canada). Quant-iT™ Oligreen ssDNA reagent was purchased from Life Technologies (Burlington, ON).

Table 3-1. DNA sequences and modifications used to study the impact of experimental parameters on the temperature dependent assembly kinetics of DNA-AuNPs.

Name	Sequence and modification (5' to 3')
Linker-B	CTA CCA CAC CAC CAC CCA CAC AC C CAC TTG
Linker-A	CTA CCA CAC CAC CAC CAG AGT CCC AGC CCA CCG TCC ACA CAC CCA CTT G
Linker-C	CAG AGT CCC CTA CCA CAC CAC CAC CCA CAC ACC CAC TTG AGC CCA CCG T
Oligo-1	Thiol Modifier C6 S-S /TTT TTT TTT TTT TTT GTG GTG GTG TGG TAG
Oligo-2	Thiol Modifier C6 S-S /TTT TTT TTT TTT TTT CAA GTG GGT GTG TGG

3.2.2 Preparation of DNA-AuNPs

Alkyl thiol modified DNA (Oligo-1) was added to gold nanoparticle (AuNPs) solutions at a 1000:1 ratio. Solutions were vortexed and incubated at room temperature overnight. NaCl was then added to the mixture so that its concentration was 100 mM. The solution was vortexed for 30 s and sonicated with a FS60 Fisher Scientific Ultrasonic Cleaner for 30 s. After a 20 min incubation period at room temperature, the NaCl addition procedure was repeated twice to bring the total NaCl concentration to 300 mM. The DNA-AuNP conjugates were further aged overnight at room temperature. 0.05% Tween 20 was added and the conjugates were centrifuged at 16,000 g for 20 min. The supernatant was removed and the pellet was washed through resuspension in 10 mM Tris-HCl pH 7.4 containing 0.05% Tween 20. The conjugates were centrifuged and washed twice more before being resuspended in 10 mM Tris-HCl pH 7.4.

Note, to obtain DNA-AuNP conjugates with higher and lower surface densities, the ratio of DNA:AuNPs in the initial reaction mixture was varied. To achieve a high surface density we reacted a DNA:AuNP of 2000:1 with a final NaCl concentration of 500 mM; for medium-high surface density we reacted a DNA:AuNP ratio of 1000:1 with a final NaCl concentration of 300 mM; for a medium-low surface density we reacted DNA:AuNP ratio of 500:1 with a final NaCl concentration of 200 mM; and for a low surface density we reacted DNA:AuNP ratio of 250:1 with a final NaCl concentration of 100 mM.

3.2.3 Quantification of ssDNA number on AuNP surface

Similar to a method reported in literature,¹⁷⁴ DNA was first displaced from AuNP surfaces by incubating 15 μL of 2.3 nM DNA-AuNP conjugates with 8.4 μL of 0.1425 M 2-mercaptoethanol, 10 μL of 1 M NaCl and 66.6 μL of 10 mM Tris-HCl buffer with 1 mM EDTA at pH 7.4 overnight at room temperature. The digest was then vortexed at 16,000 g for 20 min and 90 μL of the supernatant was removed. Using standard calibration, the concentration of oligonucleotides was determined using Quant-iT OliGreen ssDNA reagent as outline by the manufacturer's guidelines. The number of oligonucleotides per nanoparticle was then calculated by dividing the total number of oligonucleotides by the total number of nanoparticles present in solution.

3.2.4 Monitoring assembly kinetics

Reaction mixtures containing 0.75 nM Oligo-1-AuNP, 0.75 nM Oligo-2-AuNP and 75 nM Linker-A DNA were incubated at various temperatures in a MJ mini PCR thermal cycler (Bio-Rad, Hercules, CA). In control experiments, the reaction mixtures did not contain Linker-A DNA. At different time intervals, the reaction mixtures were transferred to a 384 microwell plate and the absorbance ratio of 700 nm/530 nm was determined on a Benchmark Plus microplate spectrophotometer (Bio-Rad, Hercules, CA). This absorbance ratio was chosen because non-assembled AuNPs have a plasmon peak at 530 nm. When assembled, there is a decrease in absorbance at 530 nm and an increase in absorbance at 700 nm. The time allotted for transfer of the solutions prior to the absorbance measurement was kept constant at 10 min. Absorbance ratios of 700 nm/530 nm

from the control mixtures containing no linking DNA were subtracted from the same measurements of the samples.

3.2.5 Monitoring melting profiles

Reaction mixtures were prepared as described in section 3.2.4 and were then heated to 70 °C for 5 min and were allowed to cool slowly overnight to induce aggregate formation. Melting experiments were performed on a Hewlett Packard 8452 Diode Array Spectrophotometer with a temperature controller. The temperature was increased from 40 °C to 80 °C at 1°C/min with stirring while monitoring the absorbance of 260 nm, which is responsive to the disruption of the gold nanoparticle aggregate.

3.3 Results and Discussion

By understanding the temperature-dependent assembly rate profiles for DNA-assembled nanomaterials, temperature programs can be designed to control the assembly of different nanomaterials in solution and to develop DNA detection assays. This will be explored in Chapters 4 and 5 of this thesis. Because of the important potential applications that the temperature-dependent assembly rate of DNA-AuNPs strategy provides, it is important to understand how different experimental variables will impact the temperature-dependent assembly kinetics. Experimental variables that could fluctuate include the concentration of linker DNA, the concentration of NaCl and the number of probe DNA attached to the AuNP surface. Therefore, it is of great importance to determine the impact of these parameters on the temperature dependent assembly kinetics.

A key feature of the temperature-dependent assembly rate profile is the sharp transition that occurs from maximal assembly kinetics at T_{crit} to minimal assembly kinetics when the temperature is increased slightly. The sharpness of this transition essentially defines the maximum number of transitions that can be fit within any given temperature window. With this regard, it is also important to understand how different experimental variables impact the sharpness of the transition. Specifically, it is crucial to study how these parameters affect the temperature-dependent assembly kinetics to determine optimal conditions for achieving the sharpest possible transitions.

To study how different experimental parameters impact the temperature-dependent assembly kinetics we used two DNA-AuNPs, oligo-1-AuNP and oligo-

2-AuNP. Oligo-1 and oligo-2 are not complementary to each other, but are complementary to Linker-A DNA. The assembly of oligo-1-AuNP, oligo-2-AuNP, and Linker-A can be monitored using UV/Vis spectroscopy (700 nm/530 nm) based on the coupling of surface plasmons of the AuNPs. We used two metrics to study how different experimental parameters impact the temperature-dependent assembly kinetics. The first metric was the critical temperature (T_{crit}), which is defined as the temperature in which maximal assembly kinetics is observed. Upon increasing the temperature past T_{crit} , a drastic decrease in assembly kinetics was observed. We also monitored the sharpness of the transition of the temperature range from T_{crit} to minimal assembly kinetics. To measure this we took the full-width half maximum (FWHM) of the first derivative of the temperature-dependent assembly rate profile (Figure 3-1)

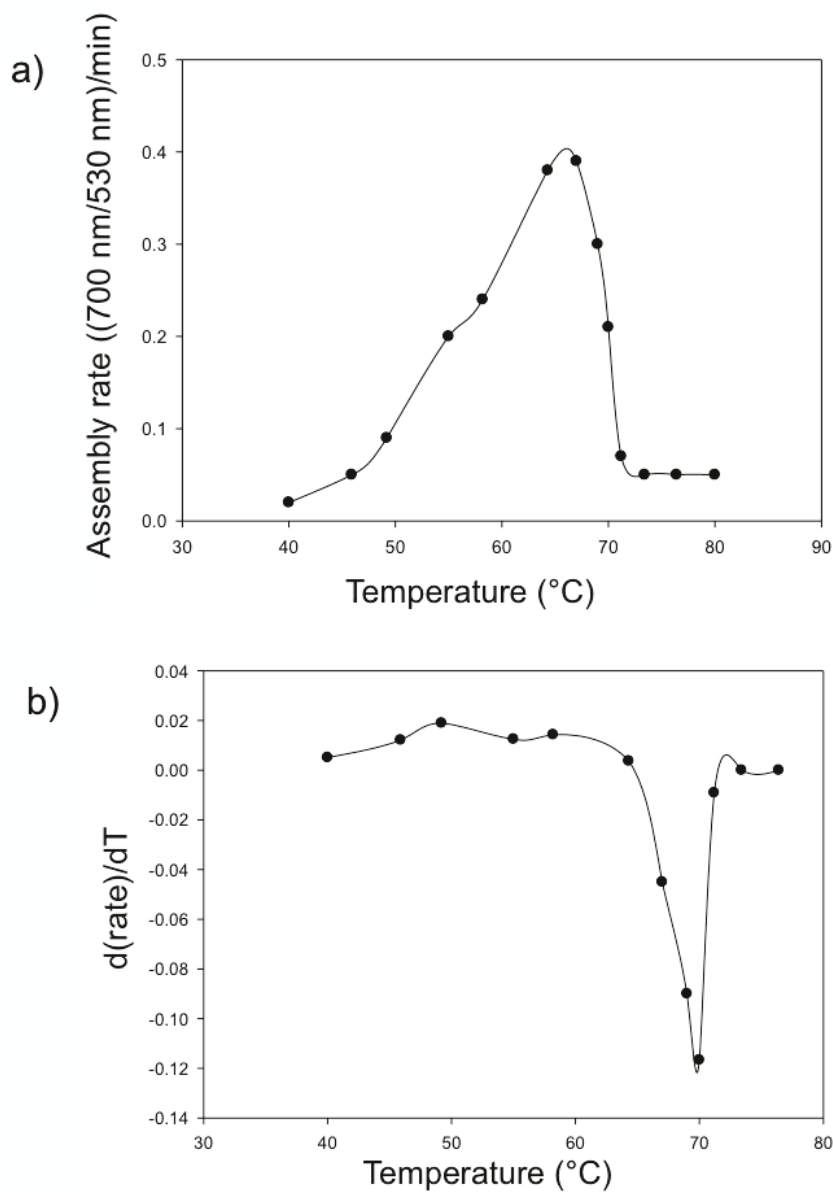


Figure 3-1 Determination of the full width half maximum (FWHM) of the transition from maximum to minimum temperature-dependent assembly kinetics, we first (a) monitored the assembly rate of as a function of incubation temperature and then (b) determined the FWHM of the first derivative of the assembly kinetic profile as a metric to monitor how sharp the transition was.

3.3.1 Impact of NaCl concentration on the TDAK of DNA-AuNPs

Salt has a strong impact on the assembly of DNA-functionalized gold nanoparticles.^{60,148} This is because DNA has a high negative charge due to phosphate groups present within the backbone. Although, DNA increases the stability of gold nanoparticles because the negative charge repels other DNA conjugated nanoparticles and prevents aggregation, the electrostatic repulsion can also hinder the target-induced aggregation. Salt can be used to screen these negative repulsions, and to increase the hybridization kinetics on the surface of gold nanoparticles.¹⁴⁸ Additionally, salt has a dramatic impact on the melting temperature of DNA-assembled gold nanoparticles.^{55,175} Reduced salt concentration can induce aggregation of AuNPs.¹⁷⁶ Because NaCl is used in the buffer solution and is present in biological matrices, the impact of NaCl on the temperature-dependent assembly rate profile was investigated. In these experiments, the concentrations of oligo-1-AuNP, oligo-2-AuNP and Linker-A were kept constant and the NaCl concentration in the reaction solutions was varied between 100 mM to 500 mM. As shown in Figure 3-2 as the NaCl concentration was increased from 100 mM to 500 mM, T_{crit} increased from 49 °C to 67 °C. This is likely due to the screening effect of NaCl minimizing the electrostatic repulsions of the DNA so that hybridization is more stable at higher temperatures. When the concentration of NaCl increases from 100 mM to 300 mM, an increase in the sharpness of the transition was enhanced from a FWHM of 5.9 °C to 2.0 °C, respectively. Further increase of the NaCl concentration to 500 mM did not make the transition any sharper. This trend of seeing a narrower

temperature window where maximal to minimal assembly kinetics and a higher T_{crit} that is observed could be due to higher cooperation in the binding of DNA between the AuNPs.^{139,140} Because NaCl screens negatively charged DNA, at higher NaCl concentrations DNA-hybridization becomes more stable. The increased hybridization stability at higher NaCl concentrations can therefore account for the increase in T_{crit} . The screening of the charges could also promote many DNA-hybridization events to occur between the particles to enhance the cooperativity, leading to a sharper transition.

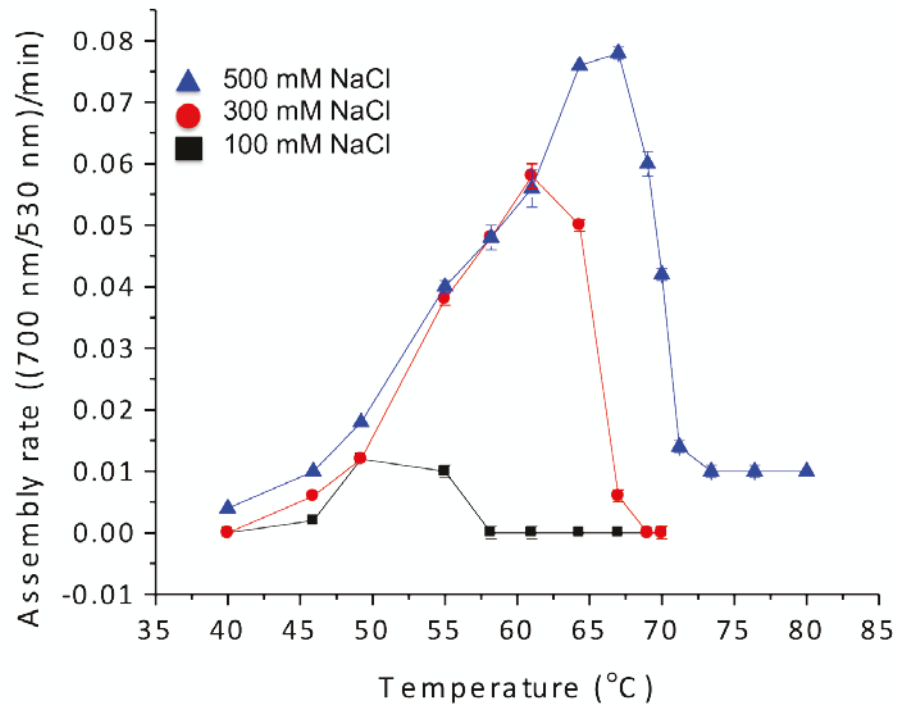


Figure 3-2 The impact of NaCl concentration on the temperature-dependent assembly kinetics profile. As the NaCl concentration was increased from 100 to 500 mM, an increase in the T_{crit} was observed. Additionally, an increase in NaCl concentration resulted in a sharper transition in the temperature-dependent assembly kinetic profile.

The impact of salt concentration on the melting temperature (T_m) has been studied.⁵⁵ The T_m is described as the temperature at which 50 % of DNA hybridized becomes dissociated. Similar to the transition that is observed for the temperature-dependent assembly rate profile, the melting transition is also extraordinarily sharp. The steep melting profile has been attributed to the decrease in the cations associated with the aggregate as the melting process proceeds and the presence of multiple linkers between the particles.^{55,139,140} To support that these processes also impact the temperature-dependent assembly rate transition, we compared how the change in salt concentration impacts both the melting and the temperature-dependent assembly rate profile. In Figure 3-3, at each NaCl concentration, the T_m is consistently higher than the T_{crit} . These results reflect what was discussed in Chapter 2. However, the increase in T_m and T_{crit} showed similar trends in response to NaCl concentration suggesting similar mechanisms for the transitions.¹⁷⁵

To summarize, the increase in NaCl concentration does increase the T_{crit} as well as the sharpness of the transition in the temperature-dependent assembly rate profile. Higher T_{crit} values for a given DNA-assembled AuNP system can be achieved through increased concentrations of NaCl that lead to the formation of more stable duplexes. To achieve the sharpest possible transition, a higher concentration of NaCl should be present in the reaction. The concentration of NaCl that can be used however, is limited to the fact that at higher concentrations of NaCl can induce aggregation of AuNPs could occur. This NaCl induced

aggregation at higher NaCl concentrations can occur in the absence of linker DNA.

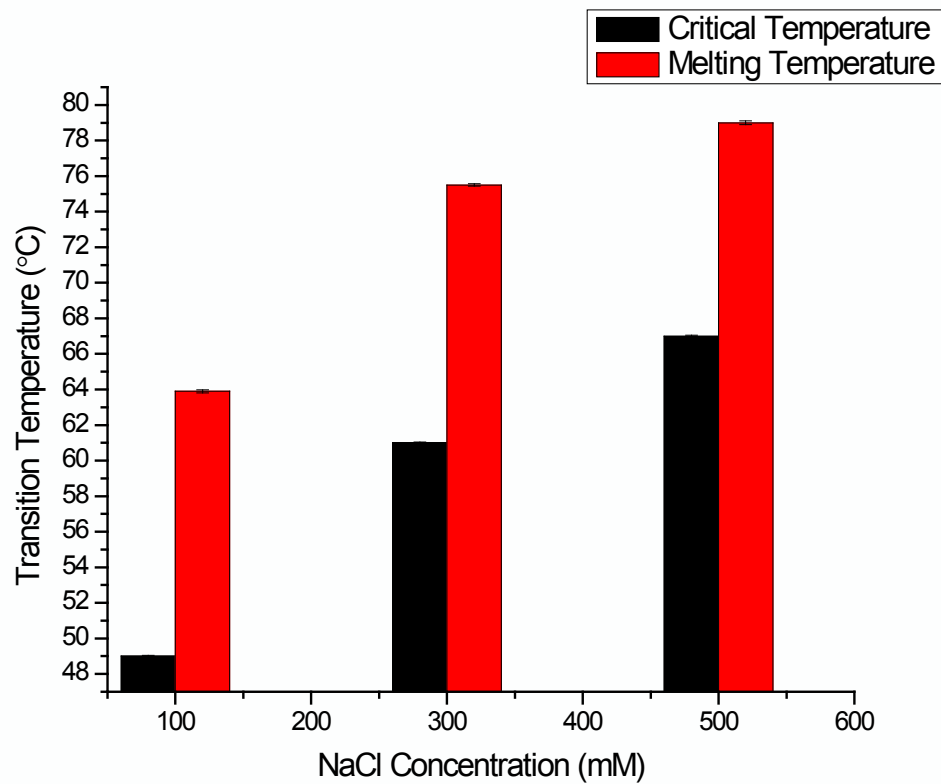


Figure 3-3. Comparison of T_{crit} and T_m at different NaCl concentration. As the NaCl concentration increases, the T_{crit} and T_m both increase. However, at any NaCl concentration, T_{crit} is consistently lower than T_m .

3.3.2 Impact of linker concentration on the TDAK of DNA-AuNPs

Applications for temperature-dependent assembly kinetics include DNA-detection and controlled assembly. Particularly for DNA detection, it is not always certain what the concentration of DNA present in solution is. Therefore, it is very important to understand how the concentration of the linking DNA impacts the temperature-dependent assembly kinetics. For example, if T_{crit} is linker concentration dependent it is important to determine the temperature-dependent assembly kinetics at various linker concentrations.

To study the impact of linker concentration, parameters such as NaCl concentration, oligo-1-AuNP concentration, and oligo-2-AuNP concentration were kept constant. We examined how the linker concentration affects the temperature-dependent assembly kinetics for DNA-linked AuNPs with concentrations of Linker-A ranging from 20 nM to 460 nM. As the linker concentration increases, T_{crit} increases as well (Table 3-2).

Table 3-2. Effect of Linker-A concentration on the critical temperature for temperature-dependent assembly kinetics of DNA-assembled AuNPs

Linker-A Concentration (nM)	T _{crit} (°C)
20	55
40	58
60	61
80	61
150	64
460	64

The increase in T_{crit} observed as the Linker-A concentration is increased suggests that at higher link concentrations, the DNA-hybridization that occurs is more stable and can withstand higher temperatures. This increase in DNA hybridization stability with increase in linker concentration could be explained by the number of linkages that are forming between oligo-1-AuNP and oligo-2-AuNP. With higher concentrations of linker DNA, more hybridization events can occur between the particles, resulting in increased stability.⁵⁵

We also studied how the linker concentration affects the transition in the temperature-dependent assembly kinetic profile. With regard to controlling the assembly using temperature-dependent kinetics, it is important for the transition to be as sharp as possible so that the maximum number of temperature-controlled assembly events can occur in a given temperature window. Generally, that as the concentration of Linker-A is increased, the sharpness of the transition increases. As shown in Figure 3-4, as the Linker concentration is increased from 40 nM to 80 nM to 150 nM, the FWHM of the transition decreases from 4.0 °C to 2.7 °C to 2.0 °C. Further increase of the concentration past 150 nM does not increase the sharpness of the transition. The increased cooperativity of this transition with increased concentration could be explained in terms of the presence of more linkers between the particles.

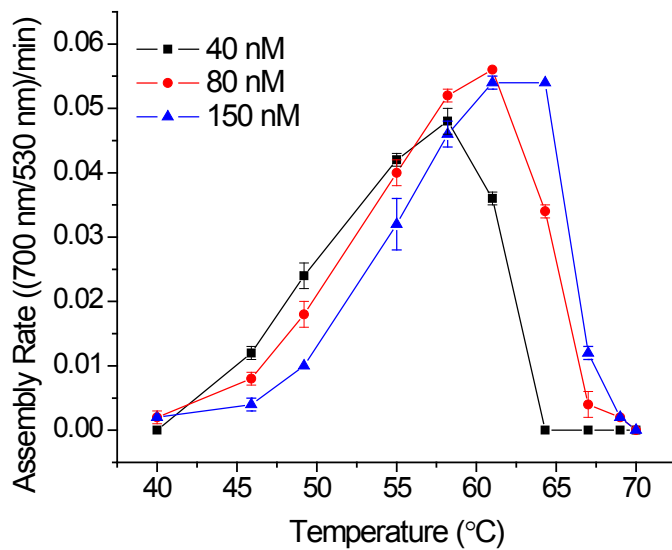


Figure 3-4. The impact of Linker-A concentration on the temperature-dependent assembly kinetics profile. As the Linker-A concentration was increased from 40 to 150 nM, an increase in the T_{crit} was observed. Additionally, an increase in Linker-A concentration resulted in a sharper transition in the temperature-dependent assembly kinetic profile.

We also compared how the linker concentration impacts the temperature-dependent assembly kinetics and the melting profile (Figure 3-5). When comparing the temperature-dependent assembly kinetic profiles to the melting temperature, T_{crit} is consistently lower than T_m . This is similar to what was observed for the impact of salt (Figure 3-5). However, the impact of linker concentration on the melting profile and the TDAK profile are similar as both profiles are shifted to higher temperatures in response to increased linker concentration. This could be because at higher linker concentrations, more linkages between DNA-AuNPs can form to stabilize the aggregate (in the melting profile) or to stabilize the hybridization occurring between DNA-AuNPs at higher temperature (in the temperature-dependent assembly kinetic profile).^{55,124}

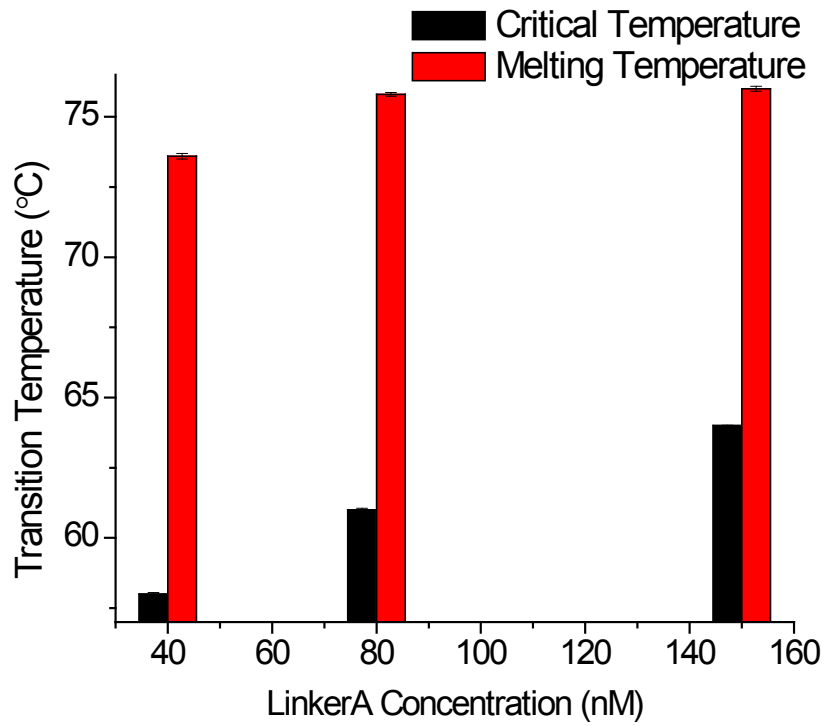


Figure 3-5. Comparison of T_{crit} and T_m at different Linker-A concentrations. As the Linker-A concentration increases, the T_{crit} and T_m both increase. However, at any Linker-A concentration, T_{crit} is consistently lower than T_m .

3.3.3. Impact of linker gaps and overhangs on the TDAK of DNA-AuNPs

When considering applications for the detection of DNA using DNA-AuNP probes, sometimes there can be cases where the sequences to be detected are adjacent, contain a DNA gap between them, or have DNA overhangs on either side (Figure 3-6). For example, to detect DNA in a biological sample, it is likely that the DNA-AuNP probes will only hybridize to a portion of the target DNA. This could result in the presence of DNA gaps or overhangs between the DNA-AuNP sequences. Additionally, when considering controlled assembly of DNA-AuNP, by inserting nucleotides (n.t.) into the linker sequence to produce a gap, the interparticle distance can be regulated.¹⁷⁷ Therefore, the length of the linker that hybridizes to the complementary probes on the surface of gold nanoparticles is important as it regulates the interparticle distance of the aggregates that are formed.

In these experiments, linking DNA was varied while keeping the complementary regions constant (Figure 3-6). All other parameters, such as salt concentration, linker concentration, oligo-1-AuNP and oligo-2-AuNP, were kept constant. As the number of linking n.t. is increased from 0 (Linker-B), where there no additional n.t. between the complementary probe region, to 19 (Linker-A), where there are 19 n.t. between the complementary regions, the T_{crit} decreases from 67 °C to 64 °C (Figure 3-7). Since Linker-B does not have any additional n.t. between the complementary regions on the probe DNA, a nicked duplex structure is formed that can maintain base stacking interactions. These base stacking interactions stabilize the duplexes formed so that they are stable at higher temperatures.^{178,179}

Linker-A has 19 n.t. inserted between the complementary regions with the probe DNA-AuNPs. Therefore the base stacking interactions are interrupted and the duplexes are less stable and will dissociate at lower temperatures. In agreement with these results, Liu and coworkers reported that a decrease in melting temperature of pre-formed aggregates as the gap sequence in the linker DNA increases.¹⁵¹

For the Linker-C sequence, the base stacking was maintained as there were no n.t. inserted between the complementary regions but the T_{crit} was suppressed ($T_{\text{crit}} = 61\text{ }^{\circ}\text{C}$) compared to Linker-B that contains no overhang DNA region ($T_{\text{crit}} = 67\text{ }^{\circ}\text{C}$) (Figure 3-7). Two factors that could attribute to the destabilization of duplexes and thus a lower T_{crit} could be steric hindrance induced by the overhanging sequences adjacent to the complementary regions or electrostatic repulsion between the overhanging sequence and the connecting AuNPs.¹⁵¹ Overhangs in DNA linker sequences destabilize and reduce the melting temperature of pre-formed DNA-assembled aggregates.¹⁵¹

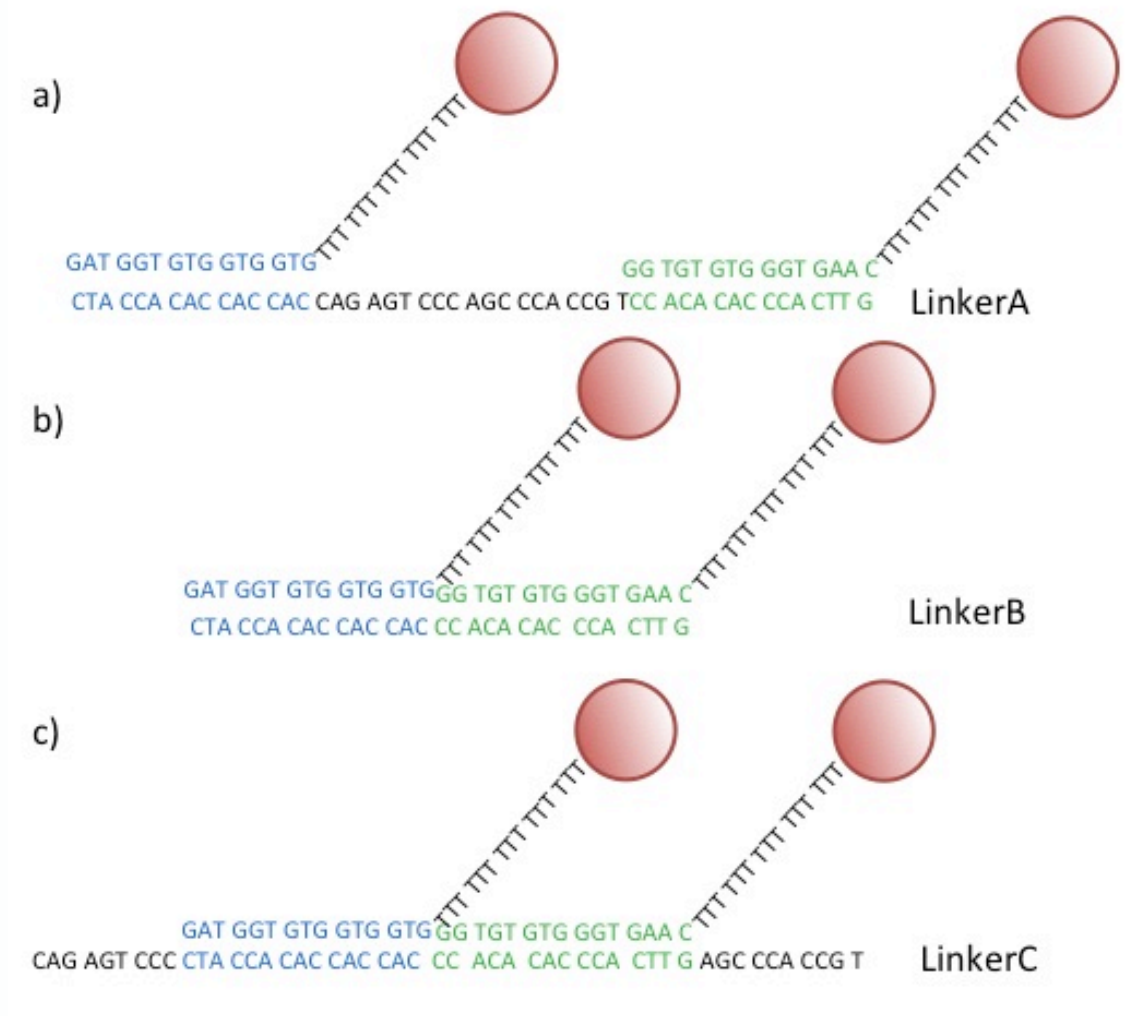


Figure 3-6. Schematic of variations of DNA linker sequences used in this study. a) Linker-A contains a 19 bp gap between the complementary DNA-AuNP probe sequences. b) Linker-B contains no gap between the complementary DNA-AuNP probe sequences. c) Linker-C contains 9 and 10 bp overhangs on either side of the complementary DNA-AuNP probe sequences.

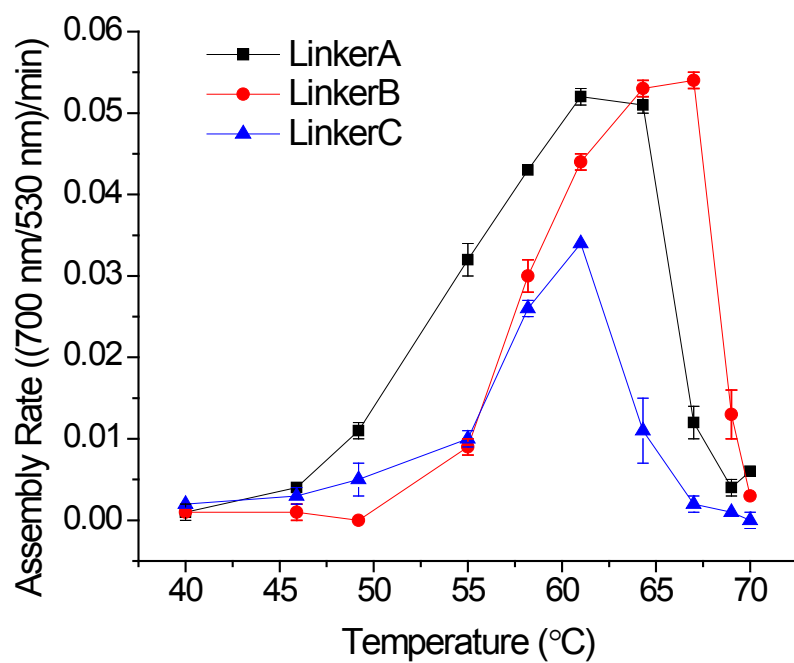


Figure 3-7. The impact of linker variations on the temperature-dependent assembly kinetics profile. When a gap is introduced into the linker sequence (Linker-A), the T_{crit} is lower compared to when gap is present (Linker-B). When overhanging sequences are present (Linker-C) with respect to the DNA-AuNP probes, T_{crit} is decreased compared to when no overhang is present (Linker-B).

3.3.4 Impact of the number of ssDNA per AuNP on the TDAK of DNA-AuNPs

Significant research effort has been dedicated to understanding the effect of probe density on the hybridization of DNA at surfaces,^{180–182} including at the surface of gold nanoparticles.^{55,141} Generally, a modest probe density yields faster aggregation kinetics¹⁴⁸ and stronger duplex stability associated with a higher melting temperature¹⁴¹ compared to AuNPs modified with a high probe density. The impact of probe density on the temperature-dependent assembly kinetics was therefore investigated. To achieve AuNPs with different density of DNA probes, the probe DNA:AuNP ratio in the conjugation reaction was adjusted to 250, 500, 1000 and 2000 by the addition of 100, 200, 300 and 500 mM of NaCl added during the salt aging process, respectively. Using this procedure, 20 nm DNA-AuNPs were prepared with 74 ± 2 , 105 ± 3 , 117 ± 1 and 125 ± 1 probe DNA molecules attached to the surface.

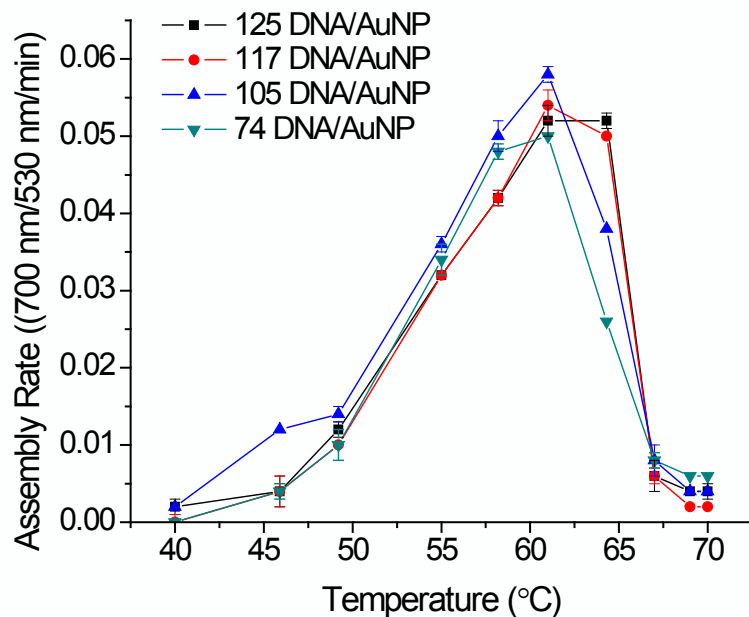


Figure 3-8. The impact of the number of DNA probes per AuNP on the temperature-dependent assembly kinetics profile. As the number of DNA probes on the surface of AuNPs was increased from 74 to 125, an increase in the T_{crit} was observed. Additionally, an increase in the number of DNA probes per AuNP resulted in a sharper transition in the temperature-dependent assembly kinetic profile.

As the probe surface density decreases, the T_{crit} also decreases (Figure 3-8). This could be attributed to the fewer linkers present between the AuNPs which stabilize the duplex.⁵⁵ This would also explain why the temperature-dependent assembly transition broadens as the probe density decreases, as the aggregate would act less cooperatively.⁵⁵

Overall, this impact of the DNA surface density on the temperature-dependent assembly rate of DNA-AuNPs impacts both the T_{crit} value and the transition. Thus it will be important to monitor the surface probe density when applying temperature-dependent assembly kinetics for controlled assembly and analytical detection applications. It is important to mention that the variation in the number of DNA probes attached to the AuNP surface was due to the adjustment of reagents in the conjugation reaction. Under identical conjugation reaction conditions, the number of DNA/AuNP was repeatable.

3.4 Conclusions

The results from this study can be used to understand how and to what extent different parameters impact the temperature-dependent assembly kinetic profile (Table 3-3). When designing kinetic-based strategies to control the sequence of assembly of nanomaterials, it is ideal to have conditions where maximum to minimum assembly kinetics is observed in a small temperature window. To achieve this, the transition should be as sharp as possible. Sharper transitions are associated with conditions that promote multiple linkages forming between AuNPs such as higher NaCl concentration, higher linker concentration, and a higher number of DNA attached on the surface of the AuNP. Overhanging DNA in the linker sequence interferes with the cooperativity of the transition found in the temperature-dependent assembly kinetic profile. T_{crit} increases when conditions favor the formation of stable hybridization between AuNPs, such as high NaCl concentration and high linker concentration. Base-stacking interactions are important for hybridization stability, and when base-stacking interactions are interrupted (through the introduction of a gap in the linker sequence), T_{crit} decreases. For biological applications it is important to realize that both NaCl and linker concentration will impact the temperature-dependent assembly kinetics as both of these parameters will be present and may vary in biological systems.

Table 3-3. Summary of parameters that impact the temperature-dependent assembly kinetic profile of DNA-AuNPs.

Parameter	Critical Temperature (°C)	FWHM (°C)
<i>NaCl concentration</i>		
100 mM	49.	5.9
300 mM	61	2.2
500 mM	67	2.0
<i>Linker-A Concentration (nM)</i>		
40.0	58	4.0
80.0	61	2.7
150.0	64	2.0
<i>Linker design</i>		
19 n.t. gap	64	2.0
no gap	67	2.0
19 n.t. overhang	61	2.7
<i>Surface density</i>		
74 ±2	61	6.0
105 ±3	61	4.0
117 ±1	64	2.0
125 ±1	64	2.0

Chapter 4 – Development of a rapid colorimetric assay for single nucleotide polymorphism detection

4.1 Introduction

Single nucleotide polymorphisms (SNPs) are common genetic variations linked to the predisposition of diseases and bacterial drug-resistance.¹⁸³ Because of the important potential in personalized medicine, reliable methods to detect SNPs are necessary. Current techniques rely on sequence-specific hybridization of molecular probes^{70,184} or on enzymatic approaches to determine the sequence of target strands.^{185–189} When considering diagnostics that can be utilized at the point-of-care, it is ideal to develop assays that are sensitive, stable, simple and rapid. It is also advantageous if the signal read-out for the assay does not require expensive instrumentation, especially in high-burden areas that are resource-limited.

Gold nanoparticles (AuNPs) have unique properties that are advantageous in the design of colorimetric read-out assays.⁴ For example, AuNPs have extremely high extinction coefficients (up to $10^{11} \text{ M}^{-1} \text{ cm}^{-1}$), which are several orders of magnitude higher than that of organic dyes and are ideal labels for sandwich-based assays. The localized surface plasmon resonance (LSPR) of AuNPs can also be manipulated based on the interaction with neighbouring particles to elicit a colorimetric response.⁴⁰ For example, freely suspended AuNPs that are functionalized with DNA are red in solution. However DNA hybridization-guided aggregation of AuNPs results in the coupling of the surface plasmons results and a

redshift in the absorbance spectra and a consequent colour change to blue.²⁷ Controlling the DNA-based aggregation of AuNPs has been used in the development of assays for enzyme activity,¹⁹⁰ metal ions,^{58,60,172,191,192} small molecules,^{59,149,193} proteins,¹⁹⁴ and SNPs.^{20,56,148,175} For example, perfectly matched (PM) and mismatched (MM) DNA sequences can be differentiated based on the melting temperature (T_m) of the target assembled DNA-AuNP aggregates.^{20,56,175}

In Chapter 2 we described a novel phenomenon where the assembly kinetics of DNA-linked AuNPs is heavily dependent on the assembly temperature. Generally, assembly kinetics increases with an increase in temperature up to a critical temperature (T_{crit}). At temperatures higher than the T_{crit} , assembly kinetics is drastically reduced. In Chapter 3, we found that experimental parameters can shift the entire temperature-dependent assembly kinetic profile to higher or lower temperature. In this chapter, we study the impact of base-mismatches present in the linking DNA on the temperature-dependent assembly profile. We design and optimize a rapid colorimetric assay to detect SNPs based on the temperature-dependent kinetic phenomenon. By understanding the assembly kinetics, we can identify temperatures where PM sequences assemble DNA-AuNP probes, and MM sequences do not. Based on the differential assembly kinetics, we can discriminate a PM and MM sequence colorimetrically within five minutes. We applied this technique to detect a clinically relevant SNP that confers drug resistance in *Mycobacterium tuberculosis*.

4.2 Experimental

4.2.1 Materials and Reagents

HPLC purified DNA sequences (Table 4.1) were purchased from Integrated DNA Technologies (Coralville, IA). Gold nanoparticles (20 nm) were purchased from Ted Pella (Redding, CA). 18 M Ω water, was used for all experiments. Tween 20 and sodium chloride (NaCl) were purchased from Fisher Scientific (Nepean, ON, Canada).

Table 4-1. Sequences used for the development of rapid colorimetric SNP assay

Name	Sequence and modification (5' to 3')
PM Linker	CTA CCA CAC CAC CAC CAG AGT CCC AGC CCA CCG TCC ACA CAC CCA CTT G
MM Linker	CTA CCA CAC CAC CAC CAG AGT CCC AGC CCA CCG TCC ACA CA <u>I</u> CCA CTT G
Probe1	Thiol Modifier C6 S-S /TTT TTT TTT TTT TTT GTG GTG GTG TGG TAG
Probe2	Thiol Modifier C6 S-S /TTT TTT TTT TTT TTT CAA GTG GGT GTG TGG
Probe3	GTG GTG GTG TGG TAG TTT TTT TTT TTT TTT/ Thiol Modifier C3 S-S
Probe4	Thiol Modifier C6 S-S/TTT GTG GTG GTG TGG TAG
Probe5	Thiol Modifier C6 S-S /TTT GTG GTG GTG TGG TAG
HisP1	Thiol Modifier C6 S-S /TTT TTT TTT TTT TTT CTT GTG GGT CAA C
HisP2	Thiol Modifier C6 S-S /TTT TTT TTT TTT TTT GAC AGT CGG CG
His526	GTT GAC CCA CAA GCG CCG ACT GTC
Tyr526	GTT GAC C <u>I</u> A CAA GCG CCG ACT GTC

4.2.2 Preparation of DNA-AuNPs

Alkyl thiol modified DNA (Probe1 or Probe2) was added to gold nanoparticle (AuNPs) solutions at a 1000:1 ratio. Solutions were vortexed and incubated at room temperature overnight. NaCl was then added to the mixture so that its concentration was 100 mM. The solution was vortexed for 30 s and sonicated with a FS60 Fisher Scientific Ultrasonic Cleaner for 30 s. After a 20 min incubation period at room temperature, the NaCl addition procedure was repeated twice to bring the total NaCl concentration to 300 mM. The DNA-AuNP conjugates were further aged overnight at room temperature. 0.05% Tween 20 was added and the conjugates were centrifuged at 16,000 g for 20 min. The supernatant was removed and the pellet was washed through resuspension in 10 mM Tris-HCl pH 7.4 containing 0.05% Tween 20. The conjugates were centrifuged and washed twice more before being resuspended in 10 mM Tris-HCl pH 7.4.

To prepare AuNP conjugates to study the impact of AuNP configuration, we conjugated AuNPs with different probe DNA. For the head-to-tail 15T spacer configuration, we conjugated AuNPs with Probe1 and Probe2 DNA; for the tail-to-tail 15T spacer configuration, we conjugated AuNPs with Probe2 and Probe3 DNA; and for the head-to-tail 3T spacer configuration, we conjugated AuNPs with Probe4 and Probe5 DNA.

4.2.3 Monitoring assembly of DNA-AuNPs

Reaction mixtures containing Probe1-AuNP, Probe2-AuNP and linker DNA were incubated at various temperatures in an MJ mini PCR thermal cycler (Bio-Rad, Hercules, CA). In control experiments, the reaction mixtures did not contain Linker-A DNA. At different time intervals, the reaction mixtures were transferred to a 384 microwell plate and the absorbance ratio of 700 nm/530 nm was determined on a Benchmark Plus microplate spectrophotometer (Bio-Rad, Hercules, CA). This absorbance ratio was chosen because non-assembled AuNPs have a plasmon peak at 530 nm, and when assembled, there is a decrease in absorbance at 530 nm and an increase in absorbance at 700 nm. The time allotted for transfer of the solutions prior to the absorbance measurement was kept constant at 10 min. Absorbance ratios of 700 nm/530 nm from the control mixtures containing no linking DNA were subtracted from the same measurements of the samples.

4.2.4 Monitoring melting profiles of DNA-AuNPs

Reaction mixtures were prepared as described in section 4.2.4 and were then heated to 70 °C for 5 min and were allowed to cool slowly overnight to induce aggregate formation. Melting experiments were performed on a Hewlett Packard 8452 Diode Array Spectrophotometer with a temperature controller. The temperature was increased from 40°C to 80°C at 1°C/min with stirring while monitoring the absorbance of 260 nm, which is responsive to the disruption of the gold nanoparticle aggregate.

4.3 Results and Discussion

In Chapter 2 we described a kinetic phenomenon for DNA-assembled DNA-AuNPs. In a three-component system, where complementary linker DNA assembles two different DNA functionalized AuNPs, the assembly temperature can influence the assembly kinetics. Generally, as the temperature is increased, assembly kinetics increased up to a critical temperature (T_{crit}). At temperatures higher than the T_{crit} (within 2-3 °C) the assembly kinetics is drastically reduced. Here, we investigate the application of the temperature-dependent assembly kinetic phenomenon for the development of a rapid colorimetric SNP assay. We find that there is a shift in the temperature-dependent assembly profile for DNA-AuNP probes assembled with perfectly matched (PM) Linker verses mismatched (MM) Linker DNA. Based on this, we can identify temperatures where only the PM Linker will assemble the DNA-AuNP probes. Conditions, such as the AuNP configuration and NaCl concentration were optimized to enhance the selectivity of the assay. We then use this approach to detect a SNP that confers drug resistance in *Mycobacterium tuberculosis*.

4.3.1 Temperature-dependent assembly kinetics for perfectly-matched vs mismatched linked DNA-AuNPs

To study the impact of PM Linker versus MM Linker DNA on the temperature-dependent assembly of DNA-AuNPs, we functionalized 20 nm AuNPs with Probe1 and Probe2 DNA (Table 4-1). Probe1 and Probe2 are complementary with respect to the perfectly matched (PM Linker) and contain a single base mismatch with respect to the mismatched (MM) Linker. We then monitored the assembly that occurs within five minutes, using either PM Linker or mismatched MM Linker DNA.

To monitor aggregation, an absorbance ratio of 700 nm/530 nm was used. AuNPs that are not aggregated have a plasmon peak at 530 nm. Upon DNA hybridization, AuNPs are brought within close proximity and the surface plasmons couple, resulting in a red shift in the absorbance spectra with a decrease in absorbance at 530 nm and an increase in absorbance at 700 nm. Therefore, as aggregation increases, an increase in the absorbance ratio of 700 nm/530 nm can be observed. This can also be observed in a change of solution colour, from red to blue.

We incubated Probe1-AuNP and Probe2-AuNP with PM Linker or MM Linker at temperatures ranging from 40 °C to 70 °C for five minutes and then determined the extent of aggregation. For both PM Linker and MM Linker, aggregation increased with temperature up to the T_{crit} (Figure 4-1). At temperatures higher than T_{crit} , the aggregation was drastically reduced. However, compared to the PM Linker, the temperature dependent assembly profile for the MM Linker was

shifted to a lower temperature range. At 64 °C the PM Linker induced maximal aggregation. However, the MM Linker had minimal aggregation. This is because 64 °C is the T_{crit} for the PM Linker, so maximal assembly kinetics occurs. However, 64 °C is higher than the T_{crit} (58 °C) for the MM Linker system, and minimal assembly kinetics occur. Therefore, to discriminate between the PM and MM Linker DNA, we can incubate the Linker DNA with the Probe1-AuNP and Probe2-AuNP at 64 °C. At this temperature, PM DNA Linker will hybridize with the AuNP probes with maximal assembly kinetics to produce an increase in the absorbance ratio and a color change. MM DNA Linker will not hybridize with the AuNP probes and no absorbance ratio or colour change will result.

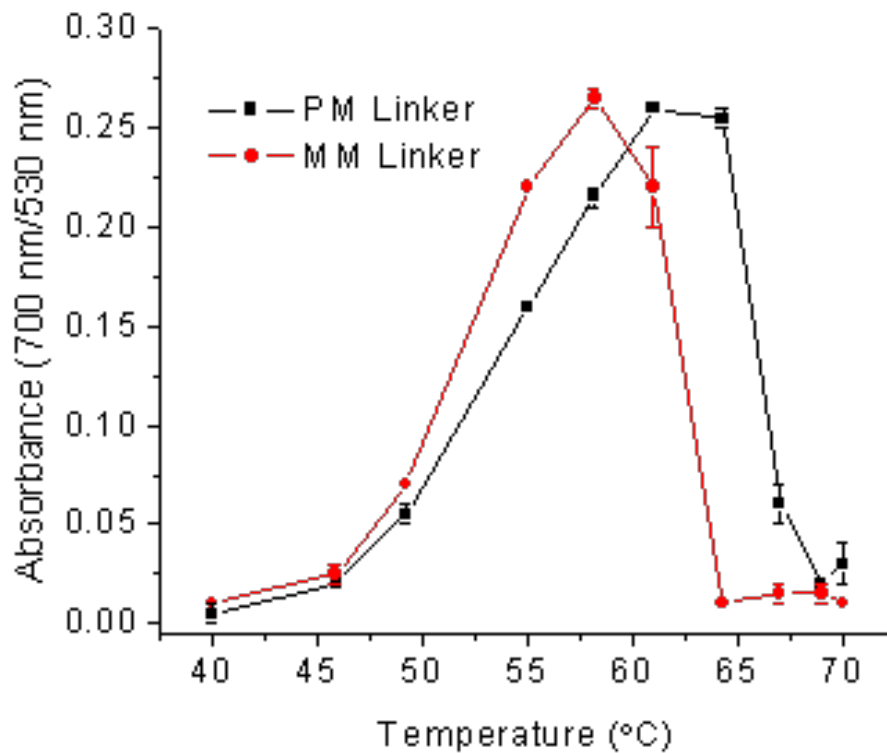


Figure 4-1. The extent of aggregation (monitored at 700 nm/530 nm) that occurs for Probe1-AuNP and Probe2-AuNP within five minutes using perfectly matched (PM) Linker DNA (black) or mismatched (MM) Linker DNA (red).

4.3.1 Comparison of temperature-dependent assembly profiles to melting profiles for SNP discrimination

The shift in the temperature-dependent assembly profiles between the PM-linked and the MM-linked DNA-AuNPs gives rise to the ability to discriminate between PM and MM sequences. Another way that DNA-functionalized AuNPs can be used for the discrimination of SNPs is to observe the melting transition of the aggregate that is assembled with either the PM Linker or MM Linker DNA.^{20,27,55,56} DNA-AuNP aggregates assembled with the PM Linker DNA are more stable than aggregates that are assembled with the MM Linker DNA. Therefore the melting temperature (T_m) for the aggregate assembled with PM Linker DNA is higher than that for assembled with MM Linker DNA. The main advantage of using DNA-AuNP probes for SNP detection via melting analyses is that the melting transition is extremely sharp compared to that of molecular DNA. This enables the full dissociation of an aggregate assembled with MM Linker at lower temperatures, while aggregates with PM Linker remain assembled. Therefore, it is ideal to have a large temperature difference between the two T_m 's. We determined the melting transition for DNA-AuNP aggregates assembled with PM Linker and MM Linker DNA (Figure 4-2) so that we could compare the effectiveness of using the melting profile compared to the temperature-dependent assembly profile for SNP discrimination. PM-linked DNA-AuNP aggregates dissociated at 75 °C, whereas MM-linked DNA-AuNP aggregates dissociated at 68 °C, resulting in a 13 °C difference. When comparing the temperature-dependent assembly profile for the PM-linked DNA-AuNPs, maximal assembly

occurred at 64 °C. MM-linked DNA-AuNP aggregates experience maximal assembly at 58 °C, resulting in a 6 °C difference. Although the temperature difference is not as great, the advantage of using the temperature-dependent assembly kinetics to discriminate between base mismatches is that pre-assembly of the aggregate is not required. By incubating the probes at 64 °C for five minutes, discrimination can be achieved.

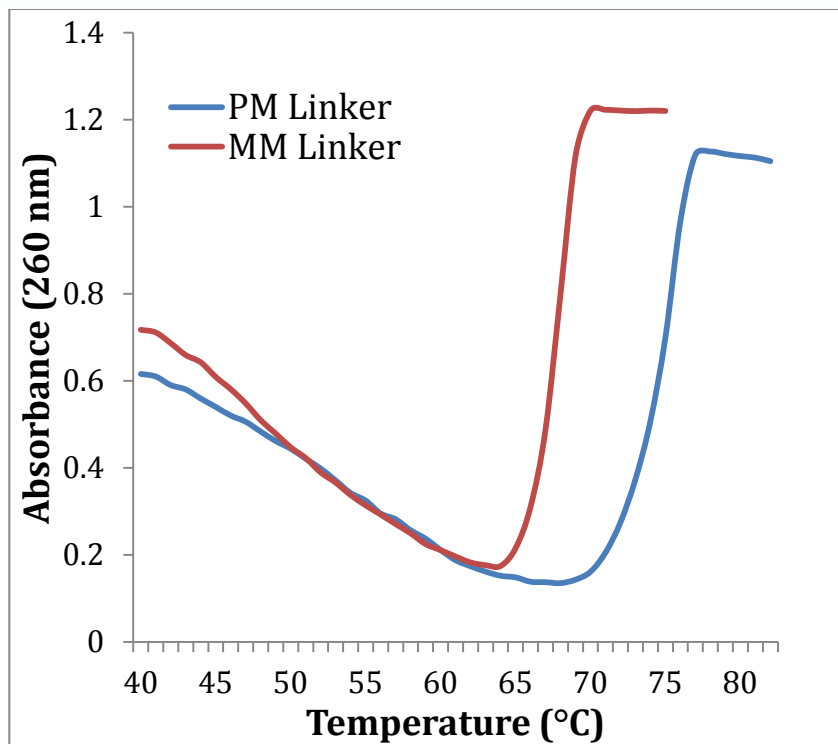


Figure 4-2. Melting profiles for Probe1-AuNP and Probe2-AuNP that are assembled with PM-Linker DNA (blue) and MM-Linker DNA (red).

4.3.3 Optimization of the DNA-AuNP configuration for enhanced SNP discrimination

For the discrimination of SNPs, it is crucial to design the assay to be as selective as possible. For this assay design, it is important to have maximal assembly occur for the PM Linker and no assembly occur for the MM linker. To optimize the selectivity of the assay, we studied the impact of the DNA-AuNP configuration. The DNA-AuNP configuration ultimately gives rise to the distance between the DNA-AuNP probes when hybridized with Linker DNA. It is important to consider the distance between DNA-AuNP probes because of the electrostatic repulsions and steric hindrance that heavily DNA-functionalized AuNPs experience. When there is a larger distance between the DNA-AuNP probes, less electrostatic repulsion occurs and DNA hybridization is promoted. In Figure 4-3, we studied three different DNA-AuNP configurations, including a tail-to-tail configuration with a 15 T spacer (longest distance between AuNP probes), a head-to-tail configuration with a 15 T spacer (moderate distance between AuNP probes), and a head-to-tail configuration with a 3T spacer (shortest distance between AuNP probes).

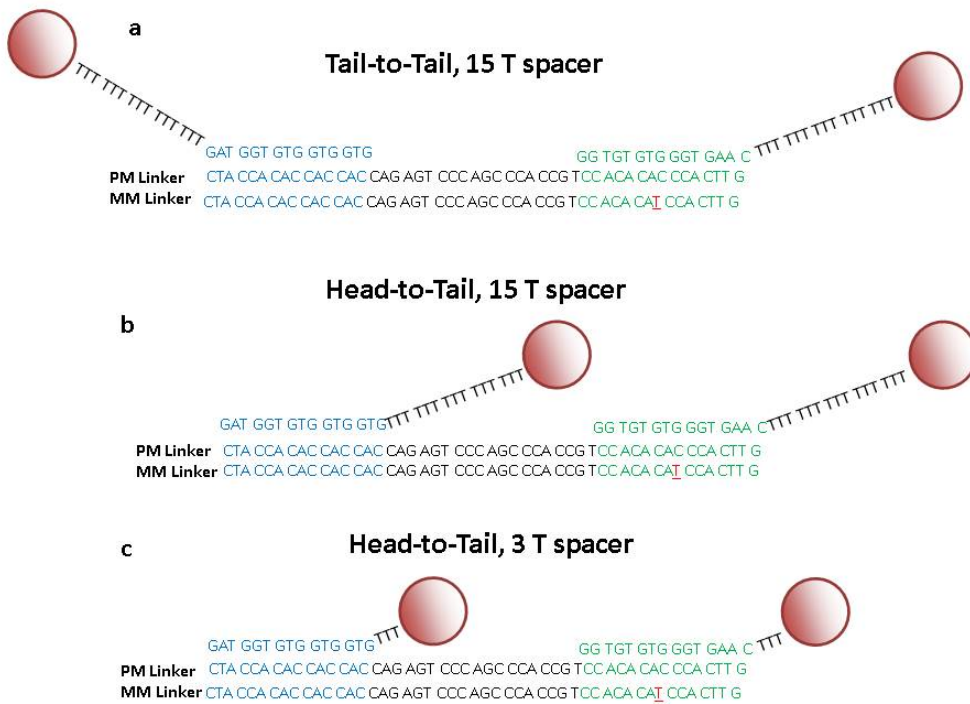


Figure 4-3. Design of DNA-AuNP configurations to adjust the distance between DNA-AuNP probes when hybridized to target DNA. a) The tail-to-tail 15 T spacer configuration has the greatest distance between DNA-AuNP probes; b) The head-to-tail 15T spacer has moderate distance between the DNA-AuNP probes; c) The head-to-tail 3T spacer has the shortest distance between the DNA-AuNP probes.

Using the three different DNA-AuNP configurations, we then studied which system will give the highest selectivity for discriminating between single base mismatches in the linker DNA. We determined the temperature-dependent assembly profile for both PM-linked and MM-linked DNA-AuNPs for each system (Figure 4-4), and then determined the selectivity factor (SF) at the temperature that provided highest selectivity. The SF was determined by dividing the signal of the PM Linker by the signal of the MM Linker at the temperature where the difference between the signals was the greatest. The SF for the tail-to-tail 15 T spacer configuration was 9.3 at 64 °C, the SF for the head-to-tail 15 T spacer configuration was 25.5 at 64 °C. The SF for the head-to-tail 3T spacer configuration was 2.8 at 58 °C. The tail-to-tail 15 T configuration (DNA-AuNP probes are the farthest distance apart) experienced more assembly for both the PM Linker and MM Linker at 64 °C, which compromised the SF compared to the head-to-tail 15T spacer (moderate interparticle distance). For the head-to-tail 15T spacer configuration, at 64 °C the PM Linker assembled the AuNP probes and relatively minimal assembly occurred for the MM Linker assembled AuNP probes to generate the highest SF. For the head-to-tail 3T spacer configuration, where the separation between the DNA-AuNP probes is the shortest, the temperature-dependent assembly profiles generated with PM Linker and MM Linker overlapped to a greater extent, resulting in the lowest SF at a lower temperature. It is likely that steric hindrance and electrostatic repulsion influenced the hybridization of the linker DNA to the DNA-AuNP probes, resulting in a lower T_{crit} values and less cooperative temperature-dependent assembly profiles.

Because the moderate distance between DNA-AuNP probes (head-to-tail 15 T spacer) generated the greatest SF, this configuration was used for the remainder of the study.

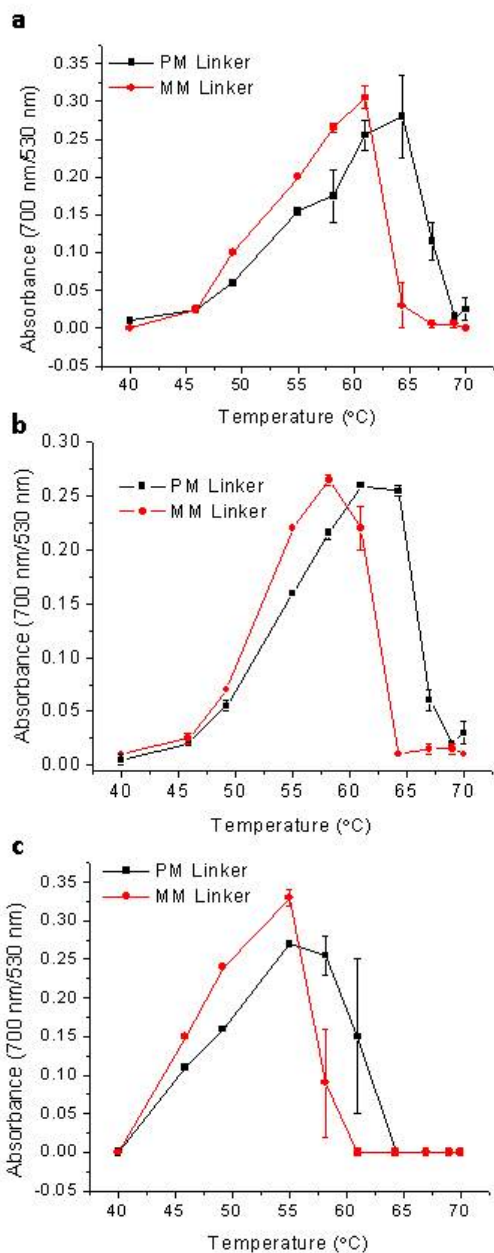


Figure 4-4. Temperature-dependent assembly profiles for different configurations for DNA-assembled AuNPs. a) Tail-to-tail 15T spacer (longest interparticle distance), b) head-to-tail 15T spacer (moderate interparticle distance), c) head-to-tail 3T spacer (shortest interparticle distance).

4.3.4 Optimization of NaCl concentration for enhanced selectivity in SNP detection

Another parameter that can influence the temperature-dependent assembly profile is the concentration of NaCl in solution. In Chapter 3, higher NaCl concentrations resulted in the shift of the temperature-dependent assembly profiles to higher temperatures and can also influence the sharpness of the transition from maximal to minimal assembly kinetics with temperature. Here we investigated the impact of NaCl concentration on the SF for SNP detection. The concentration of NaCl ranged from 200 to 400 mM (Figure 4-5). Similar to Chapter 3, as the NaCl concentration increased, the temperature-dependent assemble profile shifted to higher temperatures for both the MM Linker and PM Linker. As a result, as the NaCl concentration increased, the ideal temperature to determine the SF increased. For 200 mM NaCl the SF was 21 at 61 °C, for 300 mM NaCl, the SF was 25.5 at 64 °C, and for 400 mM NaCl the SF was 21 at 67 °C. At the lowest NaCl concentration (200 mM), screening of the electrostatic repulsion from the DNA-AuNPs is the lowest, and the extent of aggregation that the PM Linker induces is lower compared to that at higher concentrations (300 mM), while the MM Linker induces minimal aggregation for both NaCl concentrations. As a result, 300 mM NaCl yielded a higher SF. When the NaCl concentration was further increased (400 mM), hybridization from the MM Linker occurred at temperatures where maximal assembly for the PM Linker was observed. This sacrificed the SF. Therefore, the optimal NaCl concentration for discriminating SNPs was determined to be 300 mM.

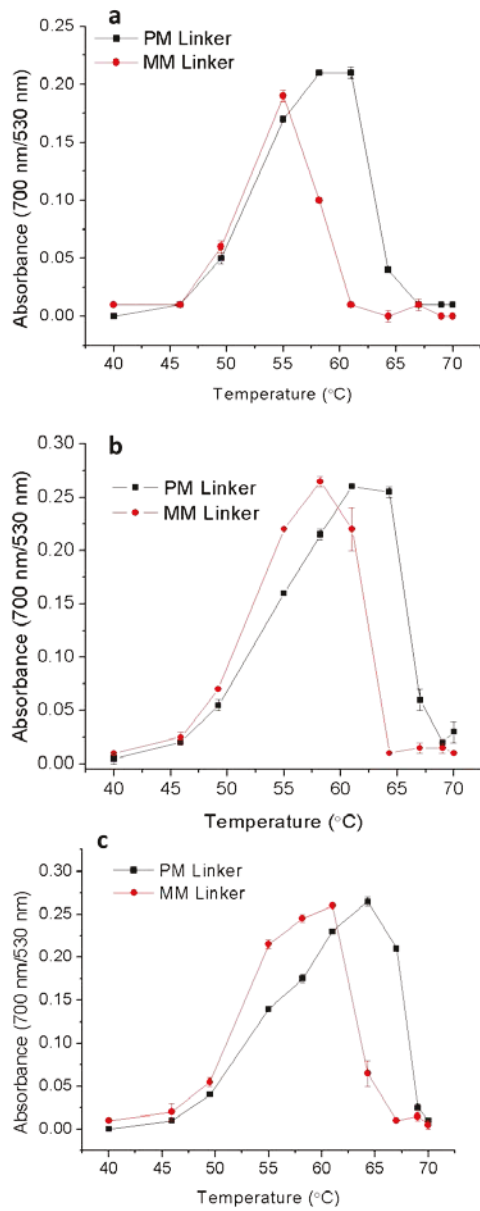


Figure 4-5 Influence on the NaCl concentration on the temperature-dependent assembly profiles within five minutes for PM-linked (blue) and MM-linked (red) DNA-AuNPs. a) 200 mM NaCl; b) 300 mM NaCl; c) 400 mM NaCl.

4.3.5 Concentration of Linker DNA that can be discriminated using temperature-dependent assembly kinetics

The concentration of linker DNA influences the temperature-dependent assembly profile. In Chapter 3, we found that as the concentration of DNA linker is increased, the temperature-dependent assembly profile is shifted to higher temperatures and higher T_{crit} values are observed. When considering the design of an assay for SNP detection, it is critical to understand the concentration range that can achieve the discrimination of SNPs based on the temperature chosen for differentiation. For example, at lower linker concentrations, the ideal temperature for the highest SF may be lower compared to that with higher linker concentrations. Based on our optimized experimental conditions for NaCl concentration and AuNP configuration, for 75 nM Linker DNA, the temperature that yields the highest SF is 64 °C. We investigated the linker DNA concentration range that would facilitate the discrimination between SNPs at 64 °C (Figure 4-6). Between 30 – 100 nM, PM Linker would assemble DNA-AuNP probes within five minutes, whereas the MM Linker would not. However, the SF decreased with linker concentration. For example, the SF for 100 nM, 75 nM, 45 nM and 30 nM linker DNA were 27, 25.5, 18, and 15, respectively. The linear range of detection was therefore determined to be between 30 – 100 nM with an R^2 value of 0.995. At concentrations lower than 30 nM, the temperature assembly profiles were shifted to lower temperatures, such that at 64 °C the PM Linker would not assemble the DNA-AuNP probes. It is interesting that, at lower concentrations (10

nM) SNPs could still be differentiated within five minutes (SF = 12), however a lower temperature would be required (58 °C).

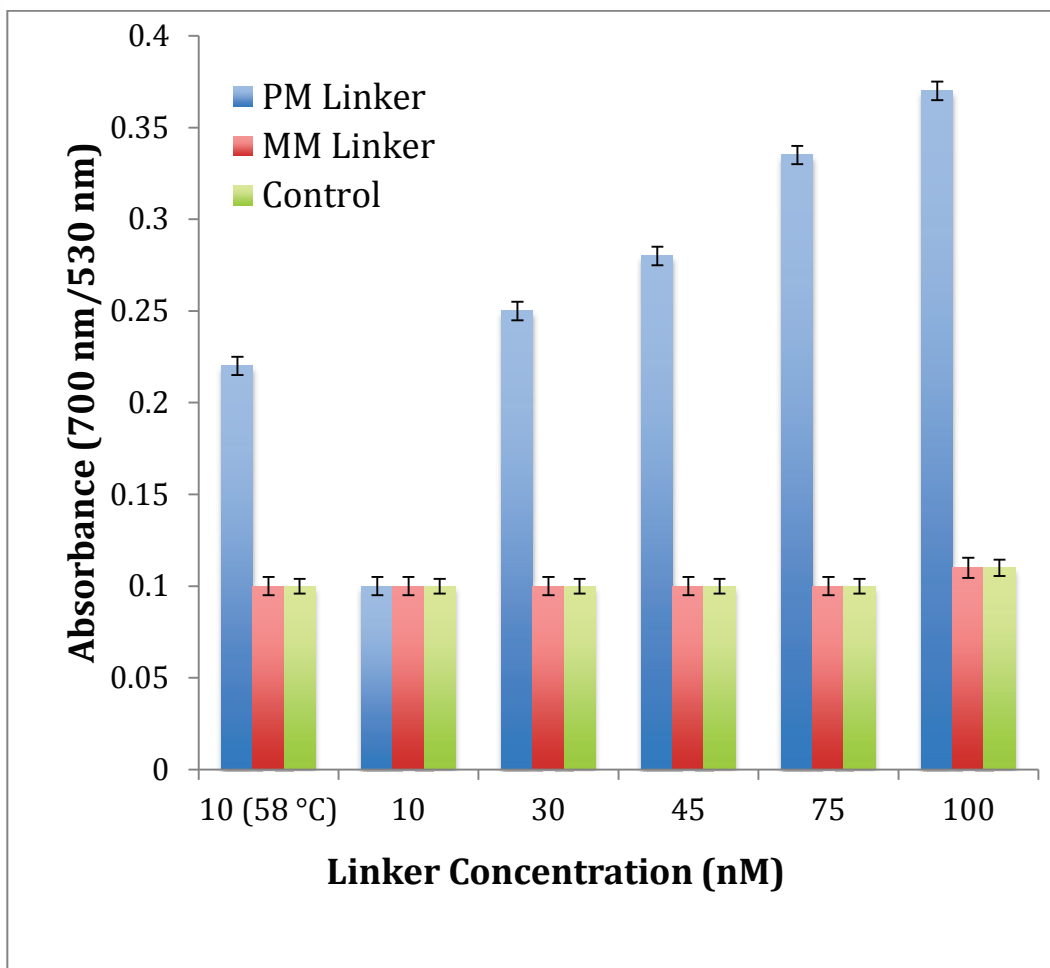


Figure 4-6. Extent of assembly that occurs for PM-linked (blue) and MM-linked (red) DNA-AuNPs at 64 °C within five minutes for different concentrations of linking DNA. The control contains no linking DNA.

4.3.6 Application of assay to detect a clinically relevant SNP

To demonstrate the utility of this technology for detecting SNPs in DNA sequences, we applied temperature-dependent assembly for the detection of a clinically relevant SNP. SNPs present in the *rpoB* gene from *Mycobacterium tuberculosis* confers resistance to first line drugs used to treat infection, such as rifamycin. The *rpoB* genes encodes for the RNA polymerase β -subunit,¹⁹⁵ and one SNP that confers a high-level of drug resistance is found in codon 526. Here, a cytosine residue is mutated to a thymine residue resulting in the change of the amino acid translated from a histidine (His526) to a tyrosine (Tyr526). To design a temperature-dependent assembly assay for the detection of this SNP, we designed two DNA-AuNP probes, HisP1-AuNP and HisP2-AuNP. Both of these probes are perfectly complementary to the segment of the *rpoB* gene that has no SNP present. However, when the His526Tyr mutation is present, there is a mismatch between the target sequence and HisP1-AuNP. It is important to note that there are also other SNPs that can occur within the *rpoB* gene will result in drug resistance. Therefore, in reality it is important to consider these SNPs as well.

Using the optimized experimental conditions, we determined the temperature-dependent assembly profiles for HisP1-AuNP and HisP2-AuNP within five minutes in the presence of 75 nM His526-Linker DNA (no SNP present) and 75 nM Tyr526-Linker DNA (SNP present) (Figure 4-7). For both His526-Linker DNA and Tyr526-Linker DNA increase in assembly within five minutes occurs with an increase in temperature up to a critical temperature, after which a decrease

in assembly results from a further increase of temperature. However, the perfectly matched His526-Linker DNA has a T_{crit} of 56 °C and the mismatched Tyr526-Linker DNA has a T_{crit} of 49 °C. Therefore, at 56 °C, maximal assembly of the AuNP probes occurs with the His526-Linker DNA, and no assembly occurs for the Tyr526-Linker DNA.

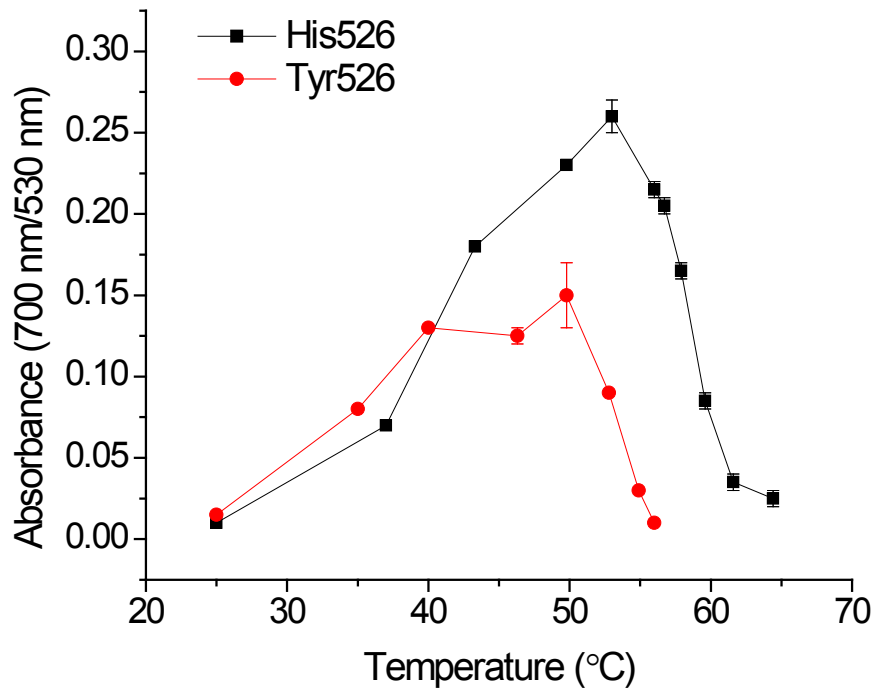


Figure 4-7. Temperature-dependent assembly profiles based on five minutes of incubation for HisP1-AuNP and HisP2-AuNP assembled with His526-Linker DNA (blue) and Tyr526-Linker DNA (red).

For an assay time of five minutes, the SF factor was 21.5. One possible way to increase the SF would be to increase the incubation time. Because His526-Linker would assemble AuNP probes with maximal assembly kinetics, was observable after five minutes. However, because 56 °C is past the T_{crit} for Try526-Linker assembled AuNP probes, no assembly occurs for the Tyr526-Linker at this temperature. We therefore studied how the increase in assembly time impacts the SF for the assay (Figure 4-8). As the assay time increased, an increase in the SF was observed up to 20 minutes (SF = 42.5). Further incubation time past 20 minutes only resulted in minimal increases in the SF.

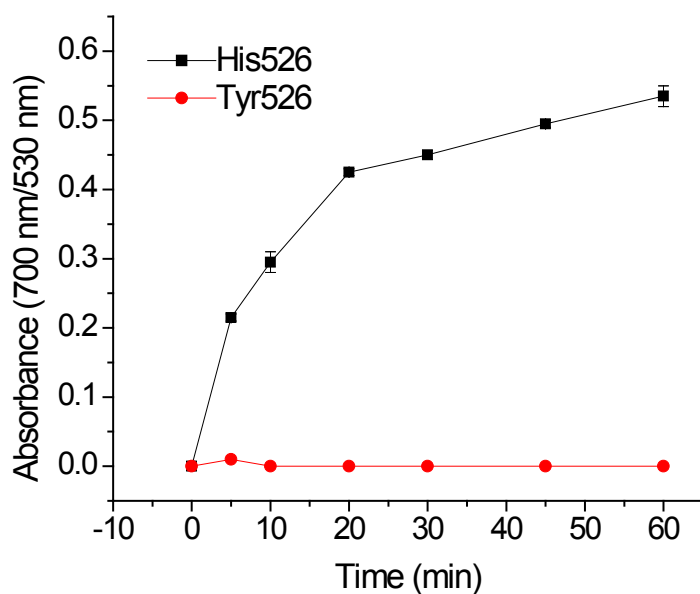


Figure 4-8. The impact of time on the assembly of His1-AuNP and His2-AuNP probes assembled with His526 (black) and Tyr526 (red) linker DNA.

As mentioned, a main advantage of target induced aggregation of AuNPs is that a solution of AuNPs will change colour from red to blue upon aggregation. This enables direct readout for assays, without the requirement of expensive instrumentation. High-burden areas, where tuberculosis infections are more predominant, are often resource-limited setting making the use of colorimetric signal readouts highly desirable. To demonstrate that we could use this assay for colorimetric detection of the His526Tyr SNP, we incubated His1-AuNP and His2-AuNP probes with His526-Linker and Tyr526-Linker for 20 minutes at 56 °C and monitored the colour change. In Figure 4-9, after incubation, the Tyr526-Linker DNA, which represents a target DNA that contains the SNP that confers drug resistance, does not assemble and the solution colour remains red. The His526-Linker DNA, which is perfectly complementary to the AuNP probes and represents a target DNA that does not confer drug resistance, does assemble. Therefore, the colour of the solution changes to a purple colour. When no Linker-DNA is present, no assembly occurs and the solution remains red (control).

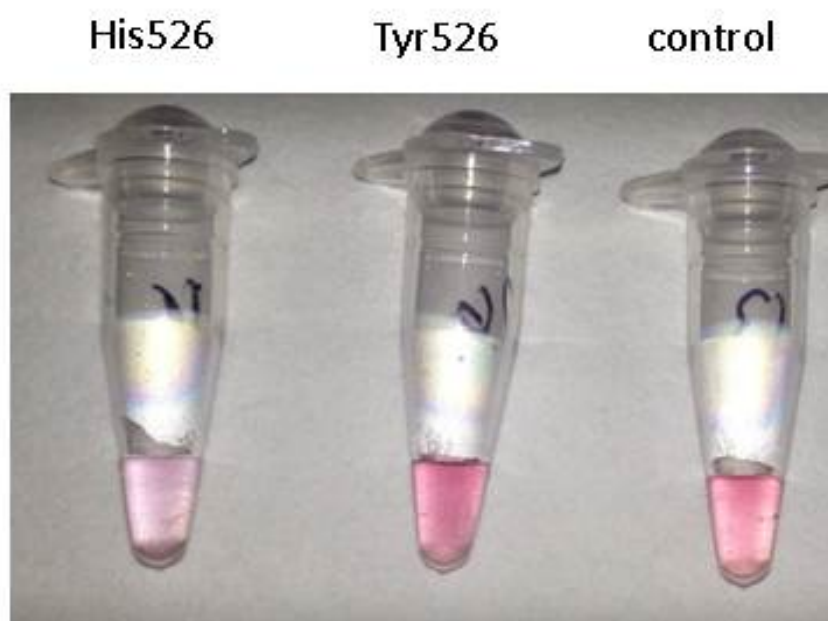


Figure 4-9. Figure 4-9. Colorimetric discrimination between His526-Linker and Tyr526-Linker induced aggregation of His1-AuNP and His2-AuNP probes after incubation at 56 °C for 20 minutes.

4.4. Conclusions

We have demonstrated that temperature-dependent assembly of DNA-functionalized AuNPs can be used for the development of assays to detect SNPs. By conjugating AuNPs with DNA probes that are complementary to the SNP region of interest and studying the temperature-dependent assembly, we can identify temperatures where only the fully complementary linking DNA sequence will induce aggregation. This technique is very simple, as incubation at a single temperature is required. Additionally, SNPs can be discriminated rapidly (within five minutes) and colorimetrically, making this approach amenable to point-of-care detection.

Chapter 5: Temperature-controlled sequential assembly of DNA-functionalized AuNPs

5.1 Introduction

The use of DNA to assemble nanoparticle building blocks into more complex structures has shown to be a very effective strategy.⁹⁹ Since the Mirkin research group first introduced this concept in 1996,^{22,27} many efforts have been made to use DNA-assembly of nanoparticles to develop diagnostic applications,^{10,20,56} ordered three dimensional crystal structures,^{126,127,129,153,154} and two dimensional nanoparticle arrays.^{113,118,155–157} Most research on DNA-mediated assembly of nanoparticles has focused on the positioning of nanoparticles using DNA. Designing strategies to sequentially control the assembly of different nanoparticles in a single solution has not been explored as extensively. This aspect of assembly is also important for achieving the bottom-up assembly of more complex nanostructures, particularly when it is desirable to assemble one nanostructure prior to another, homogenously. One unique characteristic of gold nanoparticles that are heavily functionalized with single stranded DNA (ssDNA), is that when these materials are assembled through complementary linking DNA, a very sharp melting transition occurs compared to that of free DNA. The sharp melting transition of DNA-AuNPs has been harnessed to control the sequence of assembly, however this strategy took several hours.¹⁹⁶ Temperature has a profound impact on accelerating the assembly of DNA nanostructures.^{20,60,160–162,197} Other factors such as non-base pairing DNA¹⁴⁹ gaps and overhangs in the linker sequence,^{150,151} linker concentration,⁶⁰ DNA-spacer length,¹⁴⁸ NaCl

concentration,^{60,148} DNA-AuNP configuration,⁶⁰ the structure of DNA,^{143,144} also impact the assembly kinetics of DNA-AuNPs. In Chapter 2, temperature-dependent assembly kinetics of DNA-AuNPs was introduced (Figure 5-1). Here, we demonstrate the use of assembly rates at different temperatures as a means to precisely control the sequential assembly of different nanoparticles in a single solution. The maximum assembly rates were achieved within a narrow temperature range and the assembly rate drastically decreased above a critical temperature (T_{crit}). Additionally, by incorporating base mismatches into the DNA sequences immobilized on the AuNP surface, the T_{crit} values were reduced. By identifying temperatures where assembly rates differ significantly for DNA-AuNPs containing complementary and mismatched sequences, we can design a temperature program to selectively and sequentially control the assembly of different nanoparticles in a single solution with maximal kinetics.

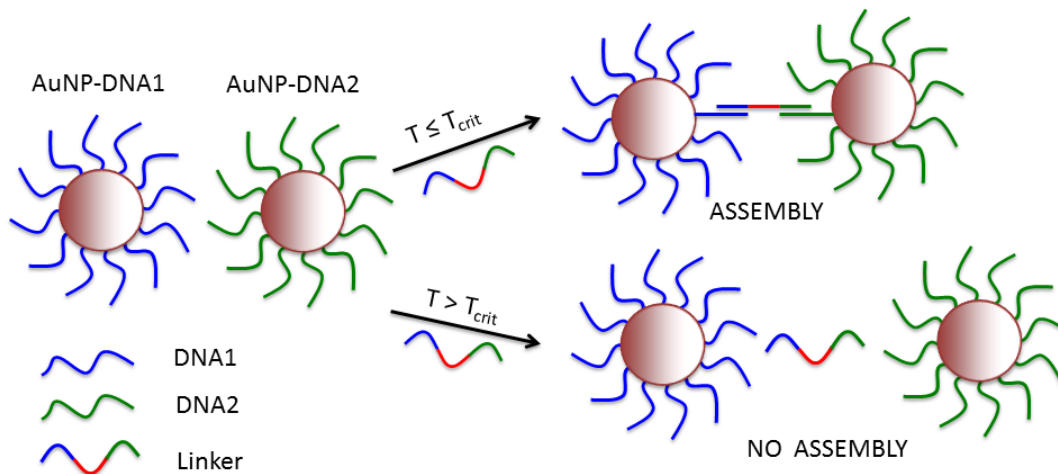


Figure 5-1. Schematic showing the temperature-dependent assembly of DNA-functionalized gold nanoparticles (AuNPs). AuNPs were functionalized with either DNA1 or DNA2. The Linker contains DNA sequences at either ends that are complementary to DNA1 and DNA2, so that AuNP-DNA1 and AuNP-DNA2 can hybridize to the Linker to result in assembly. At temperatures equal to or lower than the critical temperature (T_{crit}), assembly of AuNP-DNA1-Linker-DNA2-AuNP occurs. At temperatures greater than T_{crit} , the assembly does not occur. Three different versions of DNA2 were used in this study including DNA0M, DNA1M and DNA2M, which contained zero, one and two base mismatches with respect to the Linker DNA, respectively.

5.2 Experimental

5.2.1 Materials and Reagents

HPLC purified DNA sequences (Table 5-1) were purchased from Integrated DNA Technologies (Coralville, IA). Gold nanoparticles were purchased from Ted Pella (Redding, CA). 18 M Ω water was used for all experiments. Tween 20 and sodium chloride (NaCl) were purchased from Fisher Scientific (Nepean, ON, Canada).

Table 5-1. DNA sequences and modifications used to demonstrate temperature-controlled assembly of nanoparticles in a single solution.

Name	Sequence and modification (5' to 3')
Linker	CTA CCA CAC CAC CAC CAG AGT CCC AGC CCA CCG TCC ACA CAC CCA CTT G
DNA1	Thiol Modifier C6 S-S/TTT TTT TTT TTT TTT GTG GTG GTG TGG TAG
DNA0M	Thiol Modifier C6 S-S/TTT TTT TTT TTT TTT CAA GTG GGT GTG TGG
DNA1M	Thiol Modifier C6 S-S/TTT TTT TTT TTT TTT CAA GTG GTT GTG TGG
DNA2M	Thiol Modifier C6 S-S/TTT TTT TTT TTT TTT CAA GTT GGT TTG TGG

5.2.2 Conjugation of DNA to gold nanoparticles

Alkyl thiol modified DNA was added to gold nanoparticle (AuNPs) solutions at a 1000:1 ratio. Solutions were vortexed and incubated at room temperature overnight. The NaCl was then added to the mixture, so that its concentration was 100 mM. The solution was vortexed for 30 s and sonicated with a FS60 Fisher Scientific Ultrasonic Cleaner for 30 s. After a 20 min incubation period at room temperature, the NaCl addition procedure was repeated twice to bring the total NaCl concentration to 300 mM. The DNA-AuNP conjugates were further aged overnight at room temperature. 0.05% Tween 20 was added and the conjugates were centrifuged at 16,000 g for 20 min. The supernatant was removed and the pellet was washed through resuspension in 10 mM Tris-HCl pH 7.4 containing 0.05% Tween 20. The conjugates were centrifuged and washed twice more, before being resuspended in 10 mM Tris-HCl pH 7.4.

5.2.3 Assembly protocol

Reaction mixtures containing AuNP-DNA1, AuNP-DNA0M and Linker DNA were incubated at various temperatures in a MJ mini PCR thermal cycler (Bio-Rad, Hercules, CA). In control experiments, the reaction mixtures did not contain Linker DNA. At different time intervals, the reaction mixtures were transferred to a 384 microwell plate and the absorbance ratio of 700 nm/530 nm was determined on a Benchmark Plus microplate spectrophotometer (Bio-Rad, Hercules, CA). The time allotted for transfer of the solutions prior to the absorbance measurement was kept constant at 10 min. Absorbance ratios of 700 nm/530 nm from the

control mixtures containing no linking DNA were subtracted from the same measurements of the samples.

In all studies on the impact of temperature on the assembly of 20 nm AuNP-DNA1 and 20 nm AuNP-DNA0M, each reaction mixture contained 0.75 nM of 20 nm AuNP-DNA1, 0.75 nM of 20 nm AuNP-DNA0M, 75 nM Linker DNA, and 300 mM NaCl in 10 mM Tris-HCl buffer pH 7.4. For assembly of other AuNP systems used in this study, the concentrations of the AuNP-DNA probes vary, but the assembly protocol remains constant.

5.2.4 Temperature-dependent assembly rate (TDAK) profile

Absorbance ratios of 700 nm/530nm were measured at various time intervals during the assemble process. The initial assembly rate was determined from the slope in the initial linear region of the kinetic curve. The initial assembly rate was plotted as a function of temperature to give rise to the temperature-dependent assembly rate (TDAK) profile.

5.2.5 Temperature-controlled sequential assembly of nanoparticles

Sequential assembly of 20 nm gold nanoparticles

In a single tube, the reaction mixture contained 75 nM of Linker DNA in 300 mM NaCl and 10 mM Tris-HCl pH 7.4, 0.75 nM 20 nm AuNP-DNA1, 0.25 nM 20 nm AuNP-DNA0M, 0.25 nM 20 nm AuNP-DNA1M and 0.25 nM 20 nm AuNP-DNA2M. These concentrations were chosen so that AuNP-DNA differ by 0, 1 and 2 base mismatch would hybridize to AuNP-DNA1 in a 1:1:1:3 ratio, respectively. This mixture was aliquoted in 200 μ L PCR tubes and incubated first

at 61 °C for 30 min, then at 55 °C for another 30 min, and finally at 45 °C for 30 min. The absorbance ratio of 700 nm/530 nm was determined as a function of time to monitor the assembly progression.

Figure 5-2 shows temperature-controlled sequential assembly of DNA-AuNPs first with complete complementary sequences (no mismatch), then with DNA sequences containing a single-base mismatch, and finally with DNA sequences containing two-base mismatches. The reaction mixture was first incubated at 61 °C for 30 min. At 61 °C, AuNPs functionalized with complementary 15 n.t. sequences were assembled, and the assembly was complete after 30 min. The incubation temperature was then decreased to 55 °C. Reducing the incubation temperature to 55 °C resulted in the assembly of AuNPs functionalized with the 15 n.t. DNA sequences that contained a single base mismatch. After 30 min at 55 °C, the incubation temperature was further lowered to 45 °C. This further decrease of the incubation temperature to 45 °C gave rise to the assembly of AuNPs functionalized with the DNA sequences that contained two base mismatches.

Sequential assembly of 50 nm, 20 nm and 10 nm gold nanoparticles

In a single tube, a solution contained the Linker DNA, 20 nm AuNP-DNA1 and all three AuNP-DNA (50 nm, 20 nm, and 10 nm) probes as shown in Figure 5-9, representing no mismatch, a single mismatch, and two mismatches. Concentrations of these DNA probes were 0.03 nM 50 nm AuNP-DNA0M, 0.25 nM 20 nm AuNP-DNA1M, 2.3 nM 10 nm AuNP-DNA2M, 0.75 nM 20 nm

AuNP-DNA1 and 75 nm Linker DNA in 300 mM NaCl and 10 mM Tris-HCl pH 7.4. A lower concentration of 50 nm AuNPs and a higher concentration of 10 nm AuNPs were chosen because larger particles give a stronger spectroscopic signal compared to smaller ones. The difference in concentrations permitted the assembly of the different sized AuNPs to be monitored using UV-Vis spectroscopy. This mixture was aliquoted in 200 μ L PCR tubes and incubated at 61 °C for the first 60 min, 55 °C for the second 60 min and 45 °C for the final 60 min. The absorbance ratio of 700 nm/530 nm was determined as a function of time to monitor the assembly progression. TEM images were also obtained from parallel samples.

Temperature-controlled sequential assembly of DNA-AuNPs was achieved by incubating the reaction mixture first at 61 °C for 60 min, then at 55 °C for 60 min, and finally at 45 °C for another 60 min. At 61 °C, 50 nm AuNPs functionalized with complementary 15 n.t. sequences were assembled, and the assembly was complete after 60 min. Reducing the incubation temperature to 55 °C resulted in the assembly of 20 nm AuNPs functionalized with the 15 n.t. DNA sequences that contained a single base mismatch. After 60 min at 55 °C, further decrease of the incubation temperature to 45 °C gave rise to the assembly of 10 nm AuNPs functionalized with the DNA sequences that contained two base mismatches.

5.2.6 Transmission Electron Microscopy (TEM) experiments

Transmission electron microscopy (TEM) experiments were carried out with a 200 kV JEOL 2100 TEM. To monitor AuNP-DNA assembly, nanoparticle solution was dropped onto Carbon Type-B, 400 mesh copper grids (Ted Pella) at

different time points throughout the designed temperature programs. Excess solution was removed by absorbent paper and air-dried prior to imaging.

Sequential assembly of 50 nm and 20 nm gold nanoparticles

In a single tube, a reaction mixture contained 75 nM of Linker DNA in 300 mM NaCl and 10 mM Tris-HCl pH 7.4, 0.75 nM 20 nm AuNP-DNA1, 0.05 nM 50 nm AuNP-DNA2M, and 0.37 nM 20 nm AuNP-DNA1M. This mixture was aliquoted in 200 μ L PCR tubes and incubated at 40 °C for 60 min, followed by 49 °C for another 60 min. The absorbance ratio of 700 nm/530 nm was determined as a function of time to monitor the assembly progression. Parallel samples were also prepared for analysis by TEM.

Temperature-controlled sequential assembly of DNA-AuNPs was achieved by incubating the reaction mixture first at 40 °C for 60 min and then at 49 °C for 60 min. Two AuNP-DNA probes (50 nm and 20 nm) probes representing a single mismatch, and two mismatches were included. At 40 °C, 50 nm AuNPs functionalized with sequences containing two base mismatches (DNA2M) assembled. Increasing the incubation temperature to 49 °C resulted in the assembly of 20 nm AuNPs functionalized with the 15 n.t. DNA sequences that contained a single base mismatch.

5.3 Results and discussion

As discussed throughout this thesis, DNA-assembled AuNPs show a very interesting temperature-dependent assembly kinetic phenomenon. As the assembly temperature increases, there is an increase in the assembly rate that is observed up to a critical temperature (T_{crit}). At temperatures higher than T_{crit} , the assembly kinetics are drastically reduced. By plotting the assembly rate as a function of temperature, temperature-dependent assembly kinetics (TDAK) profiles can be observed. Parameters that impact the TDAK profile was discussed in Chapter 3 and the application of TDAK profiles to devise a method to detect SNPs was discussed in Chapter 4. Here, we develop a strategy to sequentially control the assembly of different DNA-AuNPs in a single solution. We first study the temperature-dependent assembly kinetics for DNA-AuNPs that differ by single base mismatches. We then identify temperatures where assembly occurs for one DNA-AuNP system, but not for others. This enables us to devise a temperature program that can selectively assembly different DNA-AuNPs in solution.

5.3.1 Temperature-dependent assembly kinetics of DNA-AuNPs with base mismatches

The unique TDAK profiles could be used to design precise control and selective assembly of different DNA-AuNPs. To test this hypothesis, we examined the temperature-dependent assembly rates using three AuNPs functionalized with DNA sequences containing no mismatch (completely complementary) (DNA0M),

one base mismatch (DNA1M), and two base mismatches (DNA2M) with respect to the Linker DNA (Figure 5-2).

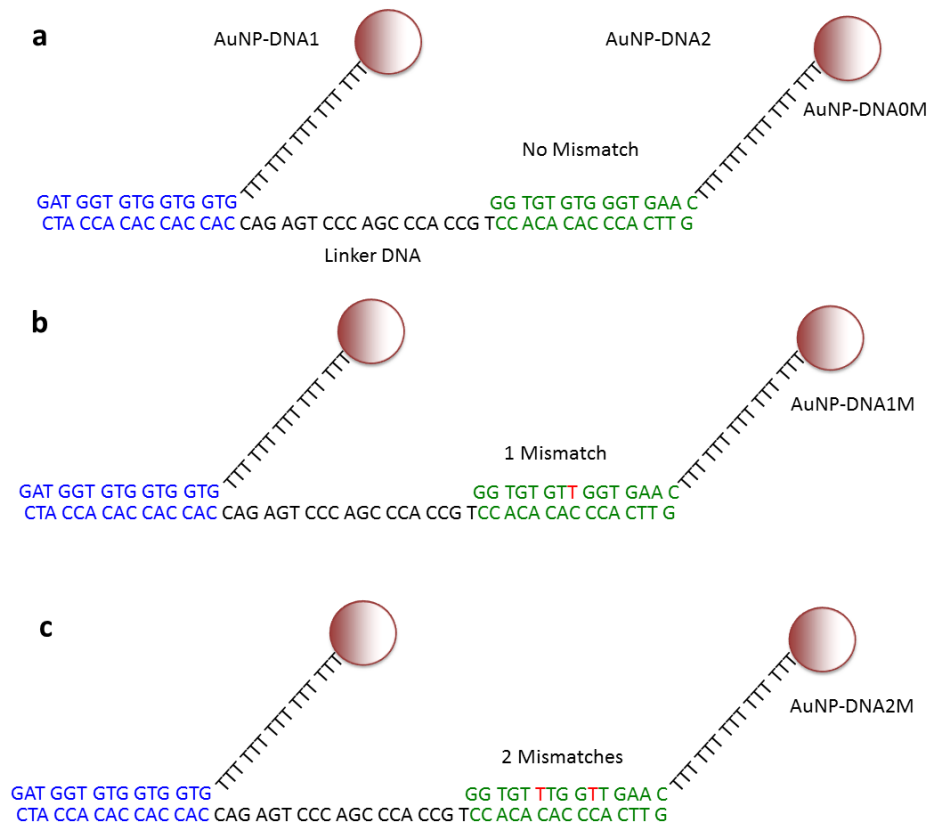


Figure 5-2. Schematic showing assembly of AuNPs using DNA sequences containing no mismatch (a), a single-base mismatch (b) or two-base mismatches (c). DNA1 on the first AuNP hybridizes to one end of the Linker DNA, and DNA2 on the second AuNP hybridizes to the other end of the Linker DNA. Three sequences of AuNP-DNA2 represent no mismatch (DNA0M), one base mismatch (DNA1M), and two base mismatches (DNA2M) in the 15 n.t. hybridizing region.

Figures 5-3, 5-4 and 5.5 show the progression of AuNP assembly over a period of 60 minutes at various temperatures. These represent three sequences of DNA that have no mismatch (Figure 5-3), one base mismatch (Figure 5-4), and two base mismatches (Figure 5-5) with respect to the linker DNA. From these measurements, we have obtained TDAK profiles for each of the three DNA-AuNP systems (Figure 5-6). In all three cases, there is a sharp transition for the assembly rate from maximum at T_{crit} to minimum at a temperature higher than T_{crit} . The T_{crit} values for the sequences containing zero, one and two base mismatches are 64 °C, 60 °C, and 49 °C, respectively.

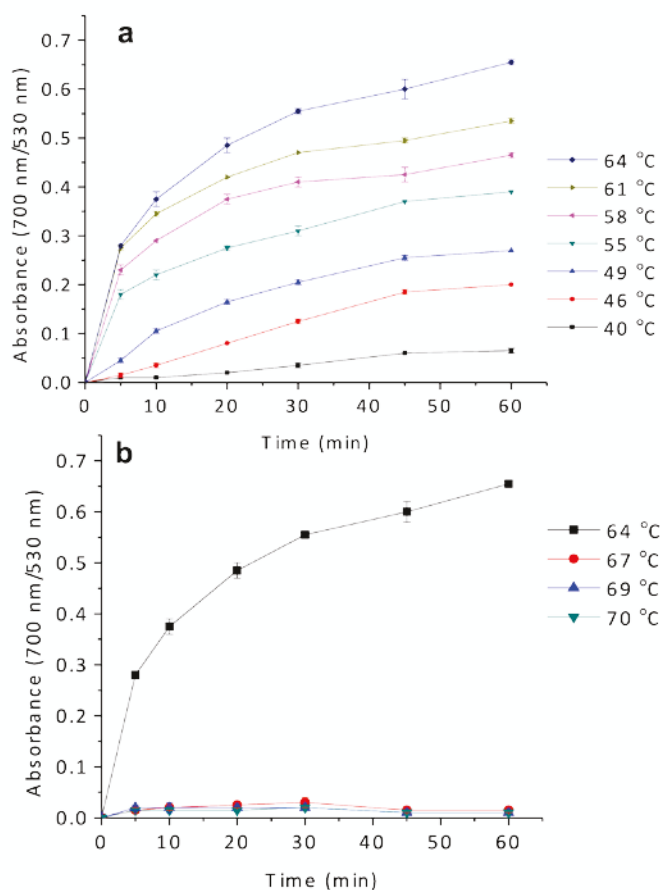


Figure 5-3 Effect of temperature on the assembly of AuNP-DNA1 (20 nm) and AuNP-DNA0M (20 nm) using a Linker DNA. Assembly was monitored over time by measuring the absorbance ratio of 700 nm/530 nm. The system is schematically represented in Figure 5-2(a). Note that the 15 n.t. of DNA1 are complementary to one end of the Linker DNA and that DNA0M contains no base mismatch in the 15 n.t. hybridizing region. The concentrations of the three DNA probes were 0.75 nM AuNP-DNA1, 0.75 nM AuNP-DNA1M, and 75 nM Linker DNA. (a) The assembly rate increases with the increase of temperature from 40 °C to 64 °C. (b) The assembly rate decreases drastically with further increases of temperature higher than 64 °C.

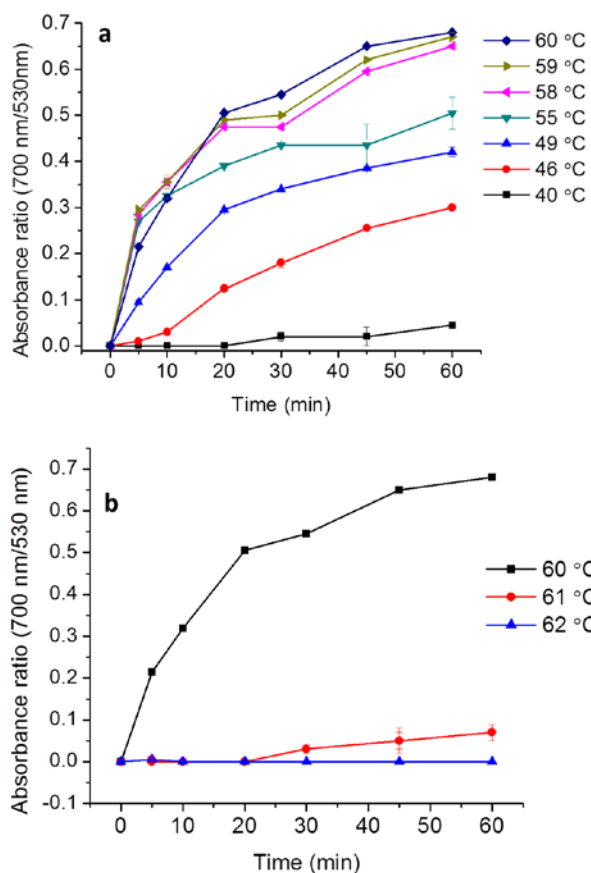


Figure 5-4. Effect of temperature on the assembly of AuNP-DNA1 (20 nm) and AuNP-DNA1M (20 nm) using a Linker DNA. Assembly was monitored over time by measuring the absorbance ratio of 700 nm/530 nm. The system is schematically represented in Figure 5-2(b). Note that the 15 n.t. of DNA1 are complementary to one end of the Linker DNA and that DNA1M contains a single base mismatch in the 15 n.t. hybridizing region. The concentrations of the three DNA probes were 0.75 nM AuNP-DNA1, 0.75 nM AuNP-DNA1M, and 75 nM Linker DNA. (a) The assembly rate increases with the increase of temperature from 40 °C to 60 °C. (b) The assembly rate decreases drastically with further increases of temperature higher than 60 °C.

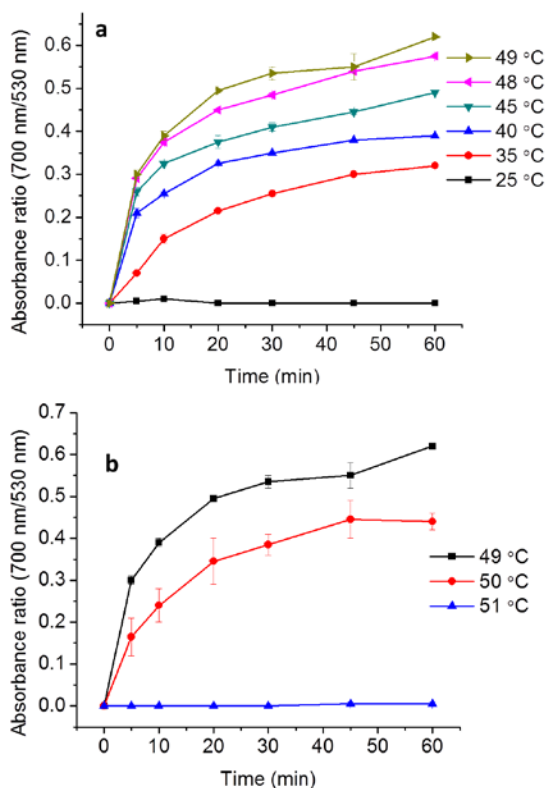


Figure 5-5. Effect of temperature on the assembly of AuNP-DNA1 (20 nm) and AuNP-DNA2M (20 nm) using a Linker DNA. Assembly was monitored over time by measuring the absorbance ratio of 700 nm/530 nm. The system is schematically represented in Figure 5-2(c). Note that the 15 n.t. of DNA1 are complementary to one end of the Linker DNA and that DNA2M contains two base mismatches in the 15 n.t. hybridizing region. The concentrations of the three DNA probes were 0.75 nM AuNP-DNA1, 0.75 nM AuNP-DNA2M, and 75 nM Linker DNA. (a) The assembly rate increases with the increase of temperature from 25 °C to 49 °C. (b) The assembly rate decreases drastically with further increases of temperature higher than 49 °C.

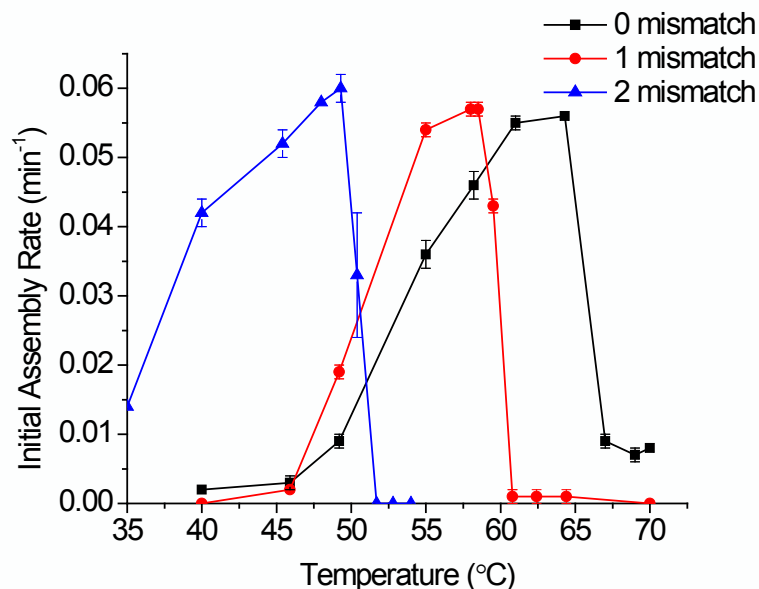


Figure 5-6. The TDAK profiles showing assembly rates as a function of temperature for assembling AuNPs functionalized with DNA that contains zero (black), one (red), or two (blue) base mismatches with respect to the linker DNA, as illustrated in Figure 5-2.

To confirm that assembly was occurring at T_{crit} values, but not at higher temperatures as predicted by the TDAK profiles, we used TEM to characterize the assemblies at different temperatures after one hour of incubation (Figure 5-7). The TEM images show that the assemblies are formed at T_{crit} (Figure 5-7 (a), (b) and (c)). No assembly at temperatures 2-3 °C higher than T_{crit} (Figure 5-7(d), (e) and (f)). In the absence of linker DNA, there is no assembly formation under any of the temperature conditions (Figure 5-7 (g), (h), and (i)). Therefore, the results

from both the absorbance ratio measurements (Figures 5-3, 5-4, and 5-5) and the TEM images (Figure 5-7) consistently show the importance of critical temperatures (T_{crit}) for the rapid assembly of AuNPs modified with desired DNA sequences.

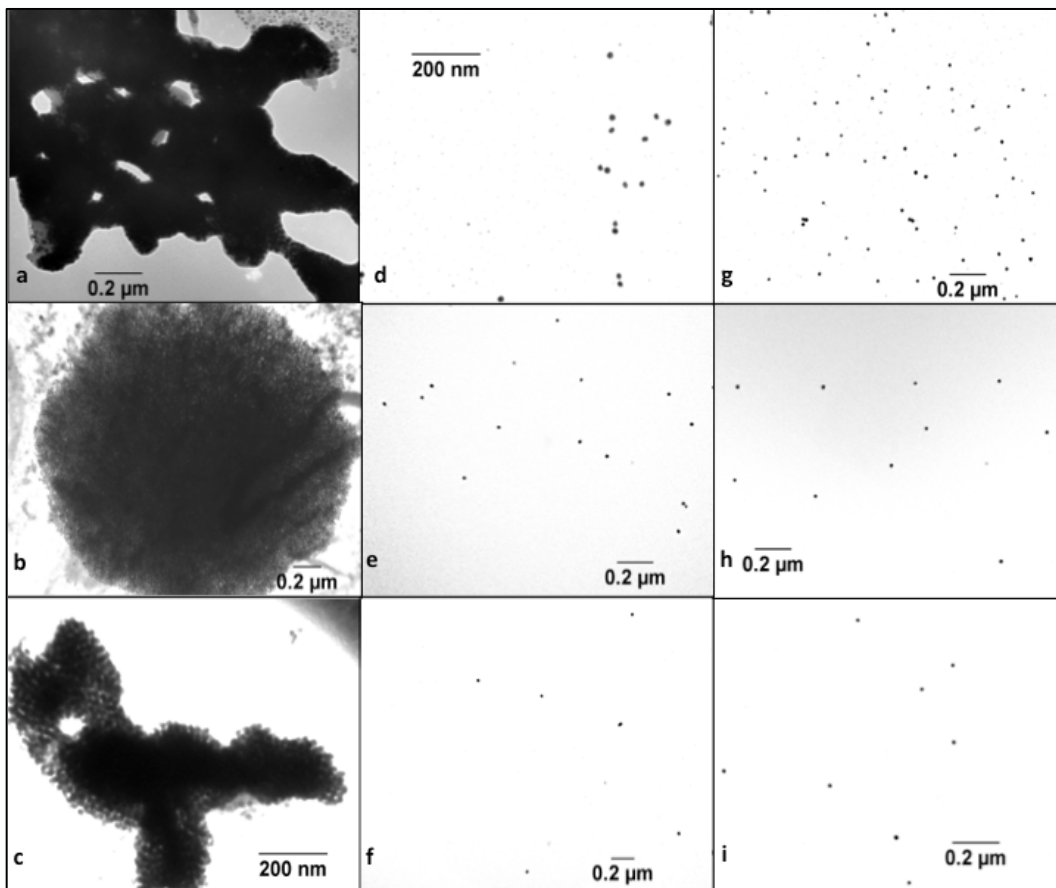


Figure 5-7. Transmission electron microscope images showing DNA-assembled AuNPs at the T_{crit} (a, b, and c) and the absence of assembly at temperatures slightly higher than T_{crit} (d, e, and f). (a) Assembly of AuNP-DNA1 and AuNP-DNA0M (no mismatch) using Linker DNA, as illustrated in Figure 5-2(a), at an incubation temperature of $T_{\text{crit}} = 64\text{ }^{\circ}\text{C}$ for 60 minutes. (b) Assembly of AuNP-DNA1 and AuNP-DNA1M (containing one mismatch) using Linker DNA as illustrated in Figure 5-2(b), at the critical temperature

(T_{crit}) of 60 °C for 60 minutes. (c) Assembly of AuNP-DNA1 and AuNP-DNA2M (containing two base mismatches) using Linker DNA, as illustrated in Figure 5-2(c), at the T_{crit} of 49 °C for 60 minutes. (d) Same as (a) except that the incubation temperature was 67 °C. No assembly was observed at this temperature 3 °C higher than T_{crit} . (e) Same as (b) except that the incubation temperature was 62 °C. No assembly was observed at this temperature 3 °C higher than T_{crit} . (f) Same as (c) except that the incubation temperature was 51 °C. No assembly was observed at this temperature 2 °C higher than T_{crit} . (g) Same as (b) except there was no Linker DNA. No assembly was observed. (h) Same as (c) except there was no Linker DNA. No assembly was observed. (i) Same as (c) except there was no Linker DNA. No assembly was observed

5.3.2 Temperature controlled assembly of 20 nm AuNPs differing by base mismatches

The unique T_{crit} values and TDAK profiles for the different DNA sequences suggest a possibility of strategically controlling the assembly of DNA-functionalized nanoparticles. This ability would be particularly useful if the assembly of different DNA-nanomaterials was required in a particular order. We achieved this by taking advantage of the maximal assembly occurring at T_{crit} and the negligible assembly at temperatures slightly higher than T_{crit} . This is distinguished from temperature-programmed assembly of DNA-AuNPs that is based on the different melting temperatures of DNA sequences.¹⁹⁶

To demonstrate the feasibility of sequential assembly of different DNA-AuNPs in the same solution, we used three DNA-AuNPs that were functionalized with DNA containing no mismatch (DNA0M), a single mismatch (DNA1M), and two

mismatches (DNA2M) with respect to the Linker DNA. Although all three DNA-AuNPs were present in the same tube, only AuNP-DNA0M assembled during the first 30 minutes of incubation at 61 °C. Subsequent assembly of AuNP-DNA1M occurred at 55 °C. Finally, AuNP-DNA2M (containing two base mismatches) assembled at 45 °C. This temperature-controlled sequential assembly (Figure 5-8a) is consistent with the T_{crit} for the three systems (Figure 5-6). To further confirm the controlled assembly of the three DNA-AuNP systems at the respective T_{crit} conditions, we repeated the assembly experiments of the three systems in three separate tubes. The results (Figure 5-8b) support the sequential assembly approach (Figure 5-8a) and agree with the T_{crit} (Figure 5-6).

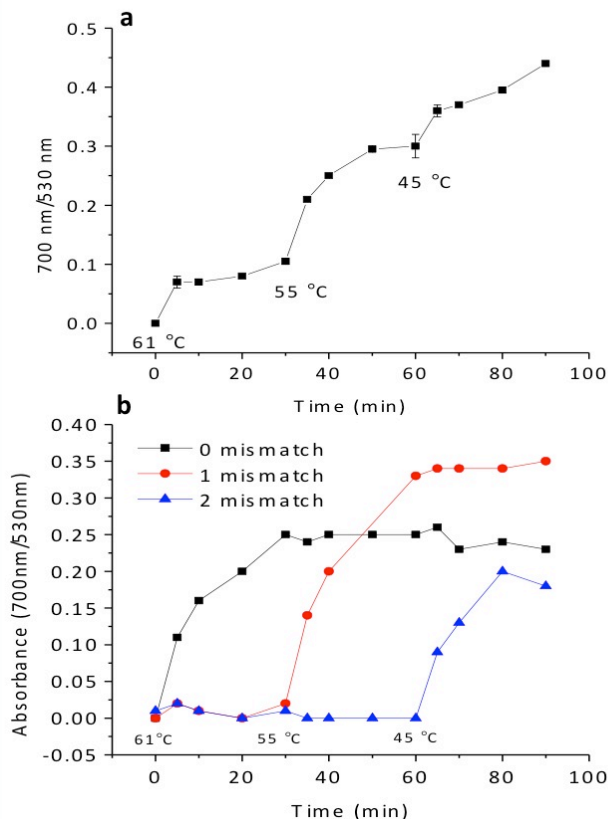


Figure 5-8. a) Temperature-controlled sequential assembly of AuNPs functionalized with DNA containing no mismatch (DNA0M) one-base mismatch (DNA1M), and two-base mismatches (DNA2M). AuNP-DNA0M and AuNP-DNA1 assembled with the Linker DNA during the initial 30 minutes at 61 °C. AuNP-DNA1M and AuNP-DNA1 assembled with Linker DNA during the second 30 minutes at 55 °C. AuNP-DNA2M and AuNP-DNA1 assembled with the Linker DNA during the final 30 minutes at 45 °C. (b) Three separate tubes each contained solutions representing one of the scenarios shown in Figure 5-2. The first tube contained AuNP-DNA0M (no mismatch), AuNP-DNA1, and DNA Linker. The second tube contained AuNP-DNA1M (one mismatch), AuNP-DNA1, and DNA Linker. The third tube contained AuNP-DNA2M (two mismatches), AuNP-DNA1. All three tubes were incubated at 61 °C for 30 minutes, only assembly in the first tubes was observed for AuNPs functionalized with DNA sequences complementary to the Linker DNA. No assembly was observed from the other two tubes

containing AuNPs functionalized with DNA of single or two mismatches. Assembly of DNA-AuNPs occurred at 55 °C in the second tube that contained AuNPs functionalized with DNA of a single mismatch. AuNPs functionalized with DNA sequences containing two base mismatches did not assemble until the temperature was reduced to 45 °C. Controlling the assembly of DNA-AuNPs by increasing the temperature with time.

5.3.3 Temperature-controlled assembly of differently sized DNA-AuNPs

We further verified the T_{crit} -controlled sequential assembly by visualizing the assembly with TEM. To help analyze the assembly process, we conjugated the three different DNA sequences (containing 0, 1, or 2 mismatches) with three different sizes of AuNPs (50 nm, 20 nm and 10 nm) (Figure 5-9).

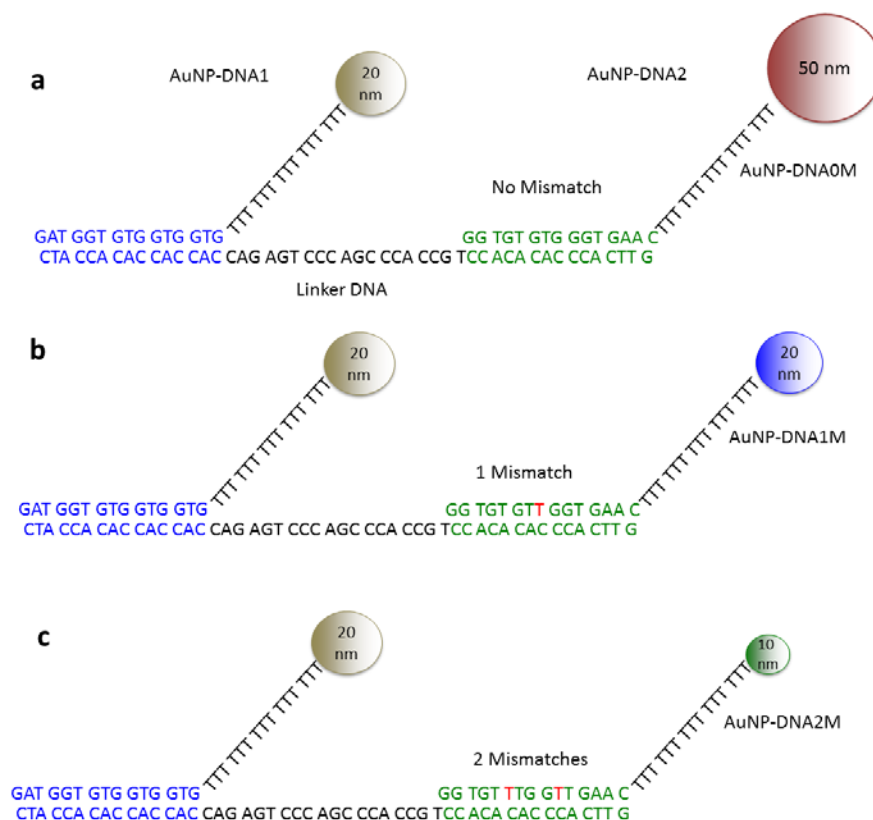


Figure 5-9. Schematic showing assembly of AuNPs using DNA sequences containing no mismatch (a), a single-base mismatch (b), or two-base mismatches (c). DNA1 on the first AuNP hybridizes to one end of the DNA Linker, and DNA2 on the second AuNP hybridizes to the other end of the DNA Linker. Three sequences of AuNP-DNA2 represent no mismatch (DNA0M), one base mismatch (DNA1M), and two base mismatches (DNA2M) in the 15 n.t. hybridizing region. DNA0M (containing no mismatches) was conjugated to 50 nm AuNPs. DNA1M (containing one mismatch) was conjugated to 20 nm AuNPs. DNA2M (containing two mismatches) was conjugated to 10 nm AuNPs.

The different sizes of the DNA-functionalized AuNPs allow TEM to differentiate the sequential assemblies. To further verify that temperatures selected from TDAK profiles could be used to control the assembly, we monitored the assembly kinetics using 50 nm, 20 nm and 10 nm AuNPs functionalized with DNA0M (Figure 5-10), DNA1M (Figure 5-4) and DNA2M (Figure 5-11), respectively. These different sized AuNPs functionalized with sequences that differ by base mismatches were expected to assemble at different times throughout the temperature program to 20 nm AuNPs functionalized with DNA1.

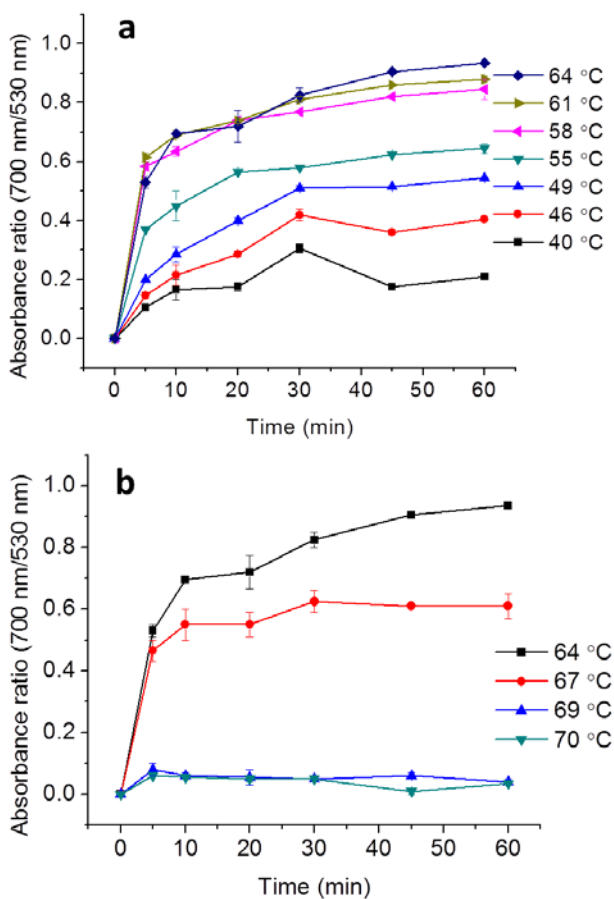


Figure 5-10. Effect of temperature on the assembly of AuNP-DNA0M (50 nm) and AuNP-DNA1 (20 nm) with a Linker DNA. Assembly was monitored over time by measuring the absorbance ratio of 700 nm/530 nm. The system is schematically represented in Figure 5-9(a). Note that the 15 n.t. of DNA1 are complementary to one end of the Linker DNA and that the 15 n.t. of DNA0M are complementary to the other end of the Linker DNA. The concentrations of the three DNA probes were 0.75 nM AuNP-DNA1, 0.1 nM AuNP-DNA0M and 75 nM Linker DNA. (a) The assembly rate increases with the increase of temperature from 40 °C to 64 °C. (b) The assembly rate decreases drastically with further increases of temperature higher than 64 °C.

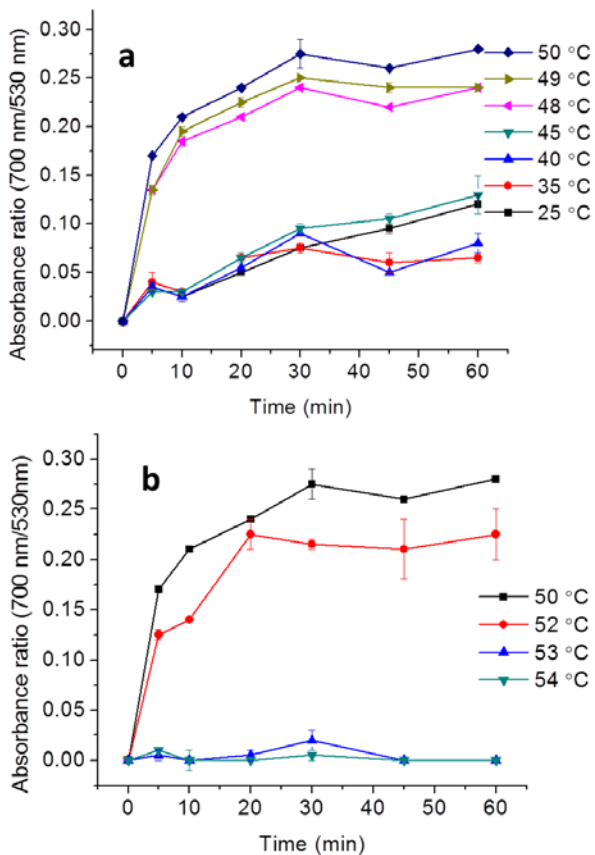


Figure 5-11. Effect of temperature on the assembly of AuNP-DNA2M (10 nm) and AuNP-DNA1 (20 nm) with a Linker DNA. Assembly was monitored over time by measuring the absorbance ratio of 700 nm/530 nm. The system is schematically represented in Figure 5-9(c). Note that the 15 n.t. of DNA1 are complementary to one end of the Linker DNA and that DNA2M contains two base mismatches in the 15 n.t. hybridizing region. The concentrations of the three DNA probes were 0.75 nM AuNP-DNA1, 7 nM AuNP-DNA2M, and 75 nM Linker DNA. (a) The assembly rate increases with the increase of temperature from 25 °C to 50 °C. (b) The assembly rate decreases drastically with further increases of temperature higher than 50 °C.

The AuNPs were mixed with the Linker DNA and incubated first at 61 °C for 60 minutes, then at 55 °C for 60 minutes and finally at 45 °C for 60 minutes. The assembly was monitored with both absorbance (Figure 5-12b) and TEM (Figure 5-13). At time 0, no assembly was observable (Figure 5-13a). After 60 minutes of incubation at 61 °C, the 50 nm AuNP-DNA0M and the 20 nm AuNP-DNA1 assembled (Figure 5-13b). The 20 nm AuNP-DNA1M and 10 nm AuNP-DNA2M remain dispersed (Figure 5-13c). The temperature was then decreased to 55 °C and the solution was incubated at this temperature for another 60 minutes. Both the 50 nm AuNP-DNA0M and the 20 nm AuNP-DNA1M are assembled to the 20 nm AuNP-DNA1 (Figure 5-13d). The 10 nm AuNP-DNA2M remain not assembled (Figure 5-13e). After 120 minutes, the temperature was reduced to 45 °C to allow the 10 nm AuNP-DNA2M to assemble to the 20 nm AuNP-DNA1, thus all three sizes of AuNPs are assembled (Figure 5-13f). These results are exactly expected of these particles as they assemble sequentially in a single solution at different temperatures.

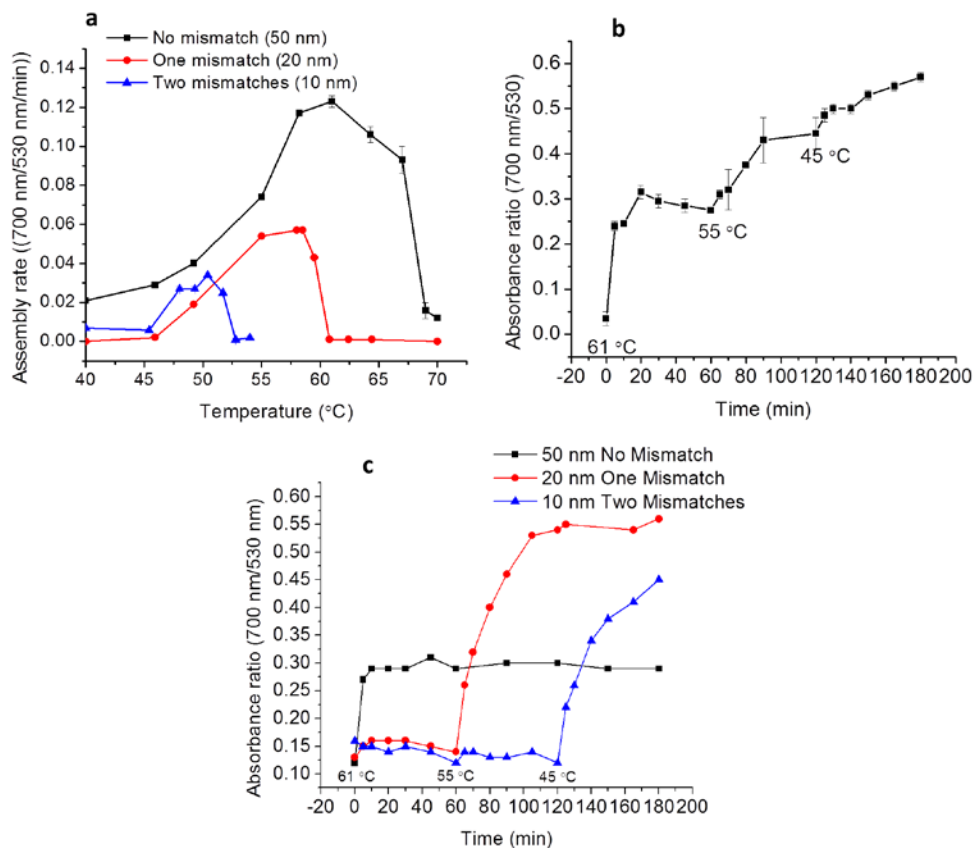


Figure 5-12. (a) The TDAK profiles showing assembly rates as a function of temperature for assembling different sized AuNPs functionalized with DNA that contains zero (black), one (red), or two (blue) base mismatches with respect to the linking DNA. (b) Temperature-controlled sequential assembly of DNA-AuNPs by incubating DNA probes first at 61 °C for 60 minutes, then at 55 °C for 60 minutes, and finally at 45 °C for another 60 minutes. In a single tube, the solution contained 20 nm AuNP-DNA1 and all three AuNP-DNA probes (50 nm, 20 nm and 10 nm) as shown in Figure 5-9, representing no mismatch, a single mismatch, and two mismatches, respectively. At 61 °C, AuNPs functionalized with complementary 15 n.t. sequences were assembled, and the assembly was complete after 60 minutes. Reducing the incubation

temperature to 55 °C resulted in the assembly of AuNPs functionalized with the 15 n.t. DNA sequences that contained a single base mismatch. After 60 minutes at 55 °C, further decrease of the incubation temperature to 45 °C gave rise to the assembly of AuNPs functionalized with the DNA sequences that contained two base mismatches. (c) Temperature-controlled assembly of DNA-AuNPs by incubating the DNA probes first at 61 °C for 60 minutes, then at 55 °C for 60 minutes, and finally at 45 °C for another 60 minutes. Different from that in (b), three separate tubes each contained solutions representing one of the scenarios shown in Figure 5-9. The first tube contained 20 nm AuNP-DNA1, Linker DNA, and 50 nm AuNP-DNA0M (no mismatch). The second tube contained 20 nm AuNP-DNA1, Linker DNA, and 20 nm AuNP-DNA1M (one base mismatch). The third tube contained 20 nm AuNP-DNA1, Linker DNA, and 10 nm AuNP-DNA2M (two mismatches). At 61 °C for 60 minutes, only assembly in the first tube was observed for AuNPs functionalized with DNA sequences complementary to the Linker DNA. No assembly was observed from the other two tubes containing AuNPs functionalized with DNA of single or two mismatches. Assembly of DNA-AuNPs occurred at 55 °C in the second tube that contained AuNPs functionalized with DNA of a single mismatch. AuNPs functionalized with DNA sequences containing two base mismatches did not assemble until the temperature was reduced to 45 °C. Concentrations of DNA probes used were 0.03 nM 50 nm AuNP-DNA0M, 0.25 nM 20 nm AuNP-DNA1M, 2.3 nM 10 nm AuNP-DNA2M, 0.75 nM 20 nm AuNP-DNA1 and 75 nM Linker DNA.

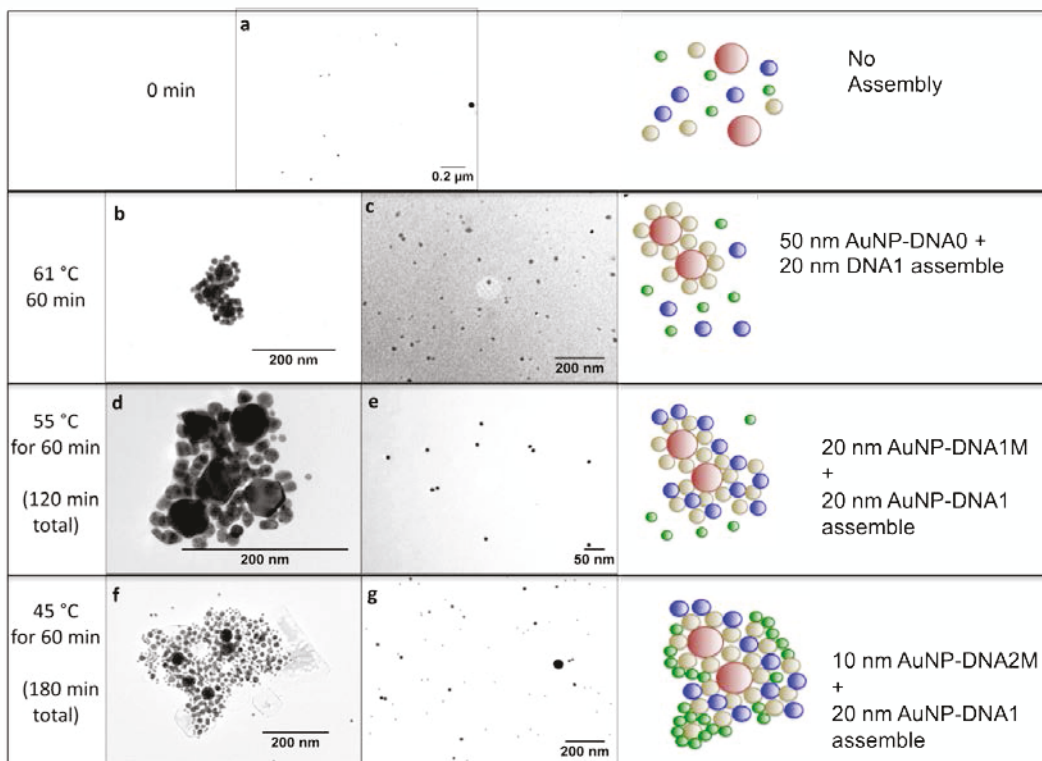


Figure 5-13. Transmission electron microscopy (TEM) images showing temperature-controlled sequential assembly of different sized AuNPs in a single solution. (a) 0 minutes; (b) and (c) at 61 °C for 60 minutes; (d) and (e) at 55 °C for another 60 minutes; (f) and (g) at 45 °C for another 60 minutes; (g) Control solution with no Linker DNA. Temperature-controlled sequential assembly of DNA-AuNPs by incubating DNA probes first at 61 °C for 60 minutes, then at 55 °C for 60 minutes, and finally at 45 °C for another 60 minutes. In a single tube the solution contained 20 nm AuNP-DNA1, 50 nm AuNP-DNA0M, 20 nm AuNP-DNA1M, and 10 nm AuNP-DNA0M as shown in Figure 5-9, representing no mismatch, a single mismatch, and two mismatches. At 61 °C, AuNPs functionalized with complementary 15 n.t. sequences were assembled (20 nm AuNP-DNA1 and 50 nm AuNP-DNA0M) (b), while 20 nm AuNP-DNA1M and 10 nm AuNP-DNA2M remain not assembled (c). Reducing the incubation temperature to 55 °C resulted in the assembly of AuNPs functionalized with the 15 n.t. DNA sequences that

contained a single base mismatch (20 nm AuNP-DNA1M) (d), while DNA sequences with two base mismatches remained not assembled (10 nm AuNP-DNA2M) (e). After 60 minutes at 55 °C, further decrease of the incubation temperature to 45 °C gave rise to the assembly of AuNPs functionalized with the DNA sequences that contained two base mismatches (f). No assembly was observed in the absence of the Linker DNA (g). Cartoon representations of the predicted DNA-AuNP assembly at each time point are placed next to the corresponding TEM images.

5.3.4 Controlling the assembly of different DNA-AuNPs by increasing the temperature

Another very interesting phenomenon observed in the TDAK profiles for DNA-assembled AuNPs is that at lower temperatures, sequences with more base mismatches have higher assembly kinetics. For example, at 40 °C DNA2M-AuNP has faster assembly kinetics compared to DNA1M-AuNP and DNA0M-AuNP and at 55 °C DNA1M-AuNP has faster assembly kinetics compared to DNA0M-AuNP (Figure 5-6). This is very surprising, as one would expect more stable DNA to have faster assembly kinetics, as complementary DNA is more thermodynamically stable. The nature of this phenomenon is still not clear and will be subject to future studies. There have been a few reports of mismatched DNA equilibrating faster than perfectly matched DNA on a surface and this effect could contribute to the faster assembly kinetics at lower temperatures for sequences with a higher degree of mismatch.¹⁹⁸⁻²⁰⁰

Based on this observation, another way to control the assembly of different DNA-AuNPs in solution is to make use of the faster assembly kinetics for two base

mismatch probes at lower temperatures compared to that of one or no base mismatch probes. For example, while the assembly of AuNPs with a single base mismatch (DNA1M) was minimal at 40 °C, assembly for AuNPs with two base mismatches (DNA2M) occurred at 40 °C (Figure 5-14). We therefore predicted that in a single solution, AuNPs with two base mismatches would assemble at a lower temperature (40 °C), and only after increasing the temperature, would the assembly of AuNPs with a single base mismatch occur. To test our hypothesis, we combined the 20 nm AuNP-DNA1, the 20 nm AuNP-DNA1M and the 50 nm AuNP-DNA2M with the Linker DNA in a single solution. We then incubated the mixture at 40 °C for one hour to facilitate the assembly of AuNP-DNA2M with AuNP-DNA1. We then increased the assembly temperature to 49 °C for one hour to facilitate the assembly of AuNP-DNA1M with AuNP-DNA1. Throughout this process, assembly was monitored with both absorbance (Figure 5-15a) and TEM (Figure 5-16). At 40 °C, AuNP-DNA1 and AuNP-DNA2M assembled whereas AuNP-DNA1M did not (Figure 5-15b). When the temperature was increased to 49 °C after one hour, both the AuNP-DNA2M and AuNP-DNA1M assemble to AuNP-DNA1 (Figure 5-15b). TEM images from the AuNPs of the different sizes are consistent with the expected sequential assembly of the AuNPs (Figure 5-16). This strategy is very distinct, and has not been reported before.

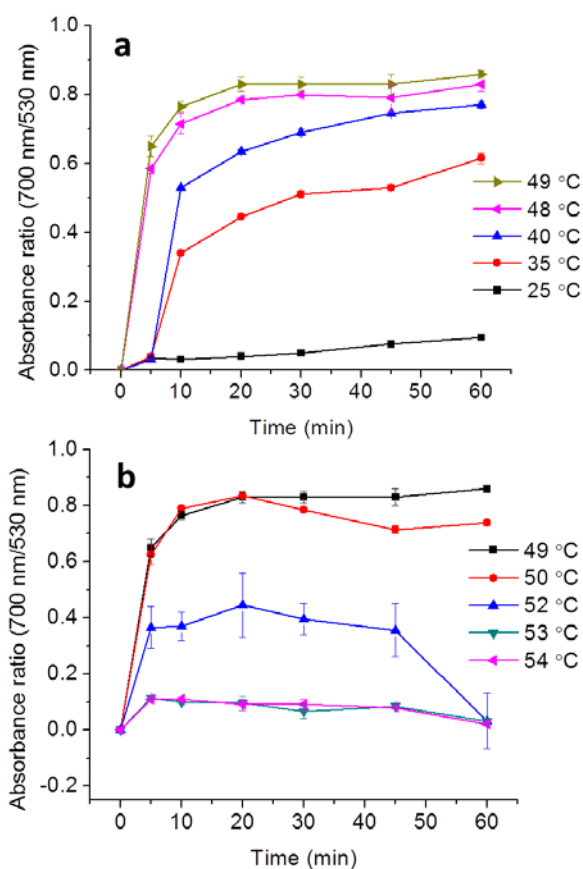


Figure 5-14. Effect of temperature on the assembly of AuNP-DNA2M (50 nm) and AuNP-DNA1 (20 nm) and Linker DNA. Assembly was monitored over time by measuring the absorbance ratio of 700 nm/530 nm. The concentrations of the three DNA probes were 0.75 nM AuNP-DNA1 (20 nM), 0.1 nM AuNP-DNA2M (50 nm), and 75 nM Linker DNA. (a) The assembly rate increases with the increase of temperature from 25 °C to 49 °C. (b) The assembly rate decreases drastically with further increases of temperature higher than 49 °C.

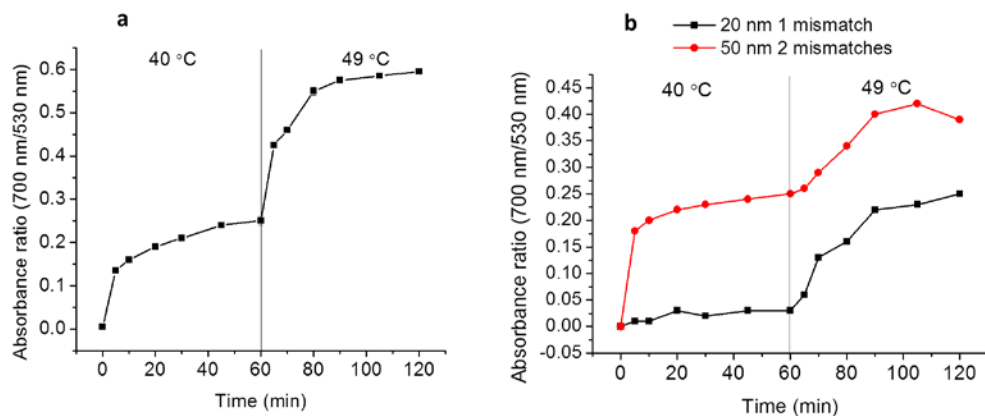


Figure 5-15. Controlling the assembly of DNA-AuNPs by increasing the temperature with time. (a) Assembly of DNA-AuNPs in a single solution containing 20 nm AuNP-DNA1, 20 nm AuNP-DNA1M, and 50 nm AuNP-DNA2M. (b) Assembly of 20 nm AuNP-DNA1 and 20 nm AuNP-DNA1M (black); and assembly of 20 nm AuNP-DNA1 and 50 nm AuNP-DNA2M (red) in separate tubes.

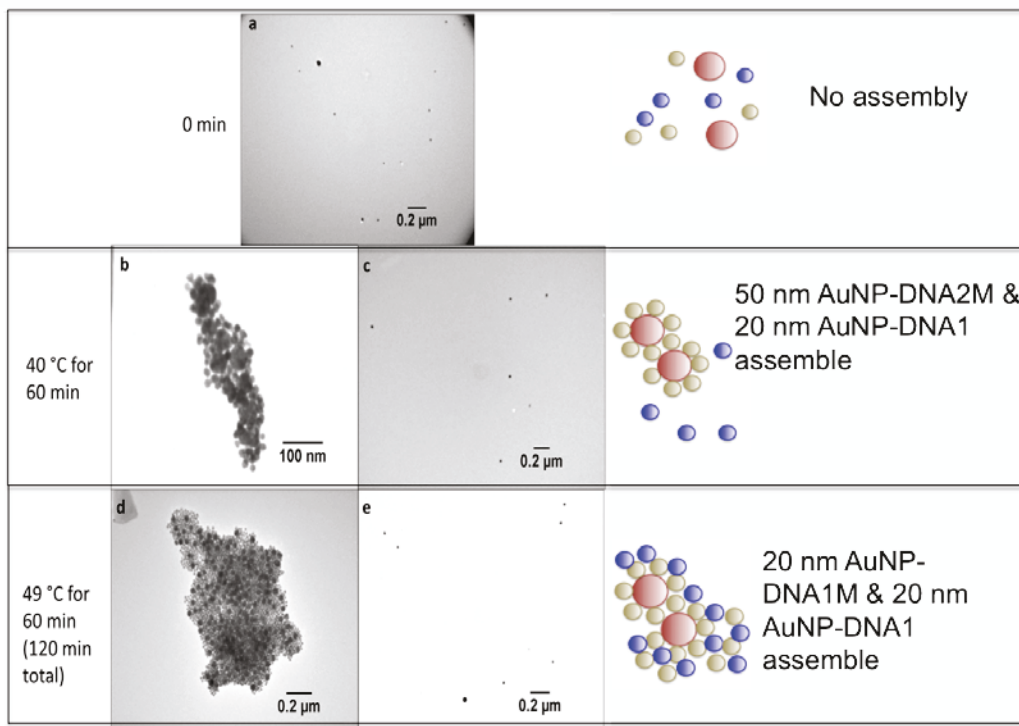


Figure 5-16. Transmission electron microscopy (TEM) images showing temperature-controlled sequential assembly of different-sized AuNPs in a single solution. This strategy is distinct because an increase in temperature is used to control the assembly versus a decrease in temperature. (a) 0 minutes; (b) and (c) after 60 minutes at 40 °C; (d) after 60 minutes at 40 °C followed by 60 minutes at 49 °C; (e) after 60 minutes at 40 °C followed by 60 minutes at 49 °C (same temperature program as in (d)) but with no Linker DNA. Temperature-controlled sequential assembly of DNA-AuNPs was achieved by incubating DNA probes first at 40 °C for 60 minutes, then at 49 °C for 60 minutes. In a single tube, the solution contained 20 nm AuNP-DNA1, 20 nm AuNP-DNA1M, and 50 nm AuNP-DNA2M, representing a single mismatch, and two mismatches. At 40 °C, AuNPs functionalized with sequences containing two base mismatches were assembled (20 nm AuNP-DNA1 and 50 nm AuNP-DNA2M) (b), while 20 nm AuNP-DNA1M remained not assembled (c). Increasing the incubation temperature to 49 °C resulted in the assembly of AuNPs functionalized with the 15 n.t. DNA sequences that contained a single base mismatch (20 nm AuNP-DNA1M) (d), No assembly

was observed when there was no Linker DNA (e). Concentrations of DNA probes used were 0.05 nM 50 nm AuNP-DNA2M, 0.37 nM 20 nm AuNP-DNA1M, 0.75 nM 20 nm AuNP-DNA1 and 75 nm Linker DNA. Cartoon representations of the predicted DNA-AuNP assembly at each time point are placed next to the corresponding TEM images.

5.4 Conclusions

In summary, a strong relationship was observed between the temperature and assembly rates of DNA-AuNPs. After a critical temperature, further increase in assembly temperature results in drastically reduced assembly rates. By understanding assembly that occurs at different temperatures, we can strategically control the sequence of assembly of DNA-AuNPs that differ by single base mismatches. The objective of controlled sequential assembly can be achieved by either decreasing assembly temperature, or by increasing assembly temperature as a function of time. Tools for controlling the assembly of nanoparticles is important for advancement for nanotechnology-based applications. The precise selective nature of the control achieved using this strategy provides a new tool for rationally assembling nanoparticle building blocks into more complex structures.

Chapter 6 – Conclusions and Future work

I have explored how temperature impacts the assembly kinetics of DNA-functionalized AuNPs and discovered a novel trend. The drastic decrease in assembly kinetics with further increase in temperature past a critical temperature is unique to DNA-AuNPs and could be harnessed for important applications, such as diagnostic development and designing strategies to control the assembly of DNA-AuNPs in solution. Specifically, Chapter 2 and 3 introduce the temperature-dependent assembly kinetic phenomenon and explores how various experimental parameters impact the profile. Chapters 4 and 5 focus mainly on applying the temperature-dependent assembly kinetic profile for the development of a colorimetric assay to detect single nucleotide polymorphisms, and designing a strategy to sequentially to control the assembly of different DNA-AuNPs in a single solution. In the following paragraphs, I will summarize the conclusions from each research chapter in detail.

In Chapter 2, I studied the influence of temperature on the assembly kinetics of DNA-AuNPs and discovered that there is a sharp transition from maximum to minimum assembly kinetics, as temperature is increased past a critical temperature. I compared this temperature-dependent assembly profile to the melting profile for the same DNA-AuNP system. The melting transition occurs at a higher temperature than the temperature-dependent assembly kinetic transition. The sharp transition in the temperature-dependent assembly kinetic transition is a novel discovery. With the many important applications of DNA-AuNPs, this

finding can provide a simple way to manipulate the assembly of DNA-functionalized nanomaterials. Specifically, this discovery can be used to develop novel diagnostics and strategies to assemble complex nanostructures.

In Chapter 3, I focused on studying how various parameters impact the temperature-dependent assembly kinetic profile. Because Chapter 2 was the first reporting of this phenomenon, it is important to determine how different parameters can influence not only the critical temperature, but also the temperature range where maximal to minimal assembly kinetics are observed. For example, in designing assay applications, it is important to determine how different concentrations of sodium chloride and DNA linker impact the profile, as these parameters may fluctuate between samples. Briefly, as sodium chloride concentration increases and DNA coverage on the AuNP surface increases, the critical temperature increases as well. The knowledge gained in this research improves the understanding of which parameters and to what extent they influence the temperature-dependent assembly kinetics of DNA-AuNPs

In Chapter 4, I applied the temperature-dependent assembly kinetic phenomenon to develop a colorimetric assay to detect single nucleotide polymorphisms (SNPs). When a single base mismatch is induced into the linker DNA with respect to the probe DNA on the AuNP surface, a shift in the temperature-dependent assembly profile can be observed. To enhance the selectivity of this assay, various experimental parameters were optimized including sodium chloride concentration and interparticle distance. I then applied this strategy to detect a clinically relevant SNP that confers drug resistance in *Mycobacterium tuberculosis*.

In Chapter 5, I applied the temperature-dependent assembly kinetic phenomenon to design strategies to sequentially control the assembly of different DNA-AuNPs in a single solution. By inducing base mismatches (0, 1, or 2) into the DNA on the AuNP surface, the temperature-dependent assembly kinetic profiles were shifted to lower temperatures, accordingly. After determining these profiles, temperatures can be selected where there is fast assembly kinetics for one system, but not for others. Based on identifying these temperatures, a temperature program can be designed to sequentially assemble different DNA-nanoparticles in a single solution. This was confirmed using UV/Vis absorption spectroscopy and transmission electron microscopy. This research demonstrates the potential of temperature-dependent assembly kinetics of DNA-AuNPs for the control over the assembly of different nanomaterials. This could be applied to develop novel nanostructures and metamaterials that could display unique properties.

The strategies and principles described in this thesis begin to explore how temperature-dependent assembly kinetics can be used to develop bioassays and ways to manipulate the assembly of AuNPs in solution. To broaden the potential of this concept, more research can be conducted. In this thesis the temperature-dependent assembly kinetics was studied only using DNA-AuNPs. To make use of the full potential of this phenomenon for the construction on novel materials, it would be valuable to study how temperature impacts the assembly kinetics of other DNA-functionalized nanomaterials, such as silver nanoparticles,²⁹ magnetic nanoparticles,³⁰ and quantum dots.³¹ This knowledge could be used to develop

more sensitive analytical techniques (i.e. the use of quantum dots for enhanced detection) or to develop materials with interesting new properties.

It would be valuable to extend temperature-dependent assembly kinetics to control the assembly of other nanostructures, such as 3D crystal structures. In the work presented in this thesis, the 3D structures generated were unstructured. Recent work in this field has shown that the 3D crystallization of polyvalent DNA-AuNPs is achievable and that different lattice structures can be predicted based on the linker DNA chosen.^{126,127,201} Our work has the potential to advance this research area, as it would enable controlled assembly of different lattice structures in solution, which could be very important implications in materials development.

The bottom up assembly of nanoparticle superlattices to generate plasmonic materials is desirable because materials can be developed with properties that do not exist in nature. For example, the formation of these materials can provide a means to manipulate electromagnetic fields on the nanoscale, which has important applications in fiber optics. With theoretical simulations, it is possible to predict the plasmonic properties that nanoparticle assemblies can afford. However, it is challenging to achieve these structures from a bottom up assembly approach. DNA has demonstrated to be a powerful tool in assembling nanoparticles to form metamaterials with unique properties.¹³⁶ Temperature-dependent assembly kinetics of nanomaterials could be useful in achieving more complex nanoparticle assemblies that display novel properties to advance material science.

References

1. Michalet, X. *et al.* Quantum dots for live cells, in vivo imaging, and diagnostics. *Science (80)*. **307**, 538 (2005).
2. Smith, A. M. & Nie, S. Semiconductor nanocrystals: structure, properties, and band gap engineering. *Acc. Chem. Res.* **42**, 190 (2010).
3. Smith, A. M., Duan, H., Mohs, A. M. & Nie, S. Bioconjugated quantum dots for in vivo molecular and cellular imaging. *Adv. Drug. Deliv. Rev.* **60**, 1226 (2008).
4. Daniel, M. C. & Astruc, D. Gold Nanoparticles: Assembly, Supramolecular Chemistry, Quantum-Size-Related Properties, and Applications Toward Biology, Catalysis, and Nanotechnology. *Chem. Rev.* **104**, 293 (2004).
5. Jun, Y.-W., Seo, J.-W. & Cheon, J. Nanoscaling laws of magnetic nanoparticles and their applicabilities in biomedical sciences. *Acc. Chem. Res.* **41**, 179 (2008).
6. Xia, Y., Xiong, Y., Lim, B. & Skrabalak, S. E. Shape-controlled synthesis of metal nanocrystals: Simple chemistry meets complex physics? *Angew. Chem. Int. Ed.* **48**, 60 (2009).

7. Kim, J., Piao, Y. & Hyeon, T. Multifunctional nanostructured materials for multimodal imaging, and simultaneous imaging and therapy. *Chem. Soc. Rev.* **38**, 372 (2009).
8. Yavuz, M. S. *et al.* Gold nanocages covered by smart polymers for controlled release with near-infrared light. *Nat. Mater.* **8**, 935 (2009).
9. Lal, S., Clare, S. E. & Halas, N. J. Nanoshell-enabled photothermal cancer therapy: Impending clinical impact. *Acc. Chem. Res.* **41**, 1842 (2008).
10. Rosi, N. L. & Mirkin, C. A. Nanostructures in biodiagnostics. *Chem. Rev.* **105**, 1547 (2005).
11. Anker, J. N. *et al.* Biosensing with plasmonic nanosensors. *Nat. Mater.* **7**, 442 (2008).
12. Shipway, A. N., Katz, E. & Willner, I. Nanoparticle arrays on surfaces for electronic, optical, and sensor applications. *ChemPhysChem* **1**, 18 (2000).
13. Ozbay, E. Plasmonics: merging photonics and electronics at nanoscale dimensions. *Science* **311**, 189 (2006).
14. Schuller, J. A. *et al.* Plasmonics for extreme light concentration and manipulation. *Nat. Mater.* **9**, 193 (2010).

15. Maier, S. A. *et al.* Local detection of electromagnetic energy transport below the diffraction limit in metal nanoparticle plasmon waveguides. *Nat. Mater.* **2**, 229 (2003).
16. Badia, A. *et al.* Self-Assembled Monolayers on Gold Nanoparticles. *Chem. Eur. J.* **2**, 359 (1996).
17. Min, Y., Akbulut, M., Kristiansen, K., Golan, Y. & Israelachvili, J. The role of interparticle and external forces in nanoparticle assembly. *Nat. Mater.* **7**, 527 (2008).
18. Cutler, J. I. *et al.* Polyvalent nucleic acid nanostructures. *J. Am. Chem. Soc.* **133**, 9254 (2011).
19. Rosi, N. L. *et al.* Oligonucleotide-modified gold nanoparticles for intracellular gene regulation. *Science (80)*. **312**, 1027 (2006).
20. Elghanian, R., Storhoff, J. J., Mucic, R. C., Letsinger, R. L. & Mirkin, C. A. Selective colorimetric detection of polynucleotides based on the distance-dependent optical properties of GNPs. *Science (80)*. **277**, 1078 (1997).
21. Taton, T. A. Scanometric DNA array detection with nanoparticle probes. *Science (80)*. **289**, 1757 (2000).
22. Alivisatos, A. P. *et al.* Organization of “nanocrystal molecules” using DNA. *Nature* **382**, 609 (1996).

23. Lim, D.-K., Jeon, K.-S., Kim, H. M., Nam, J.-M. & Suh, Y. D. Nanogap-engineerable Raman-active nanodumbbells for single-molecule detection. *Nat. Mater.* **9**, 60 (2010).
24. Seeman, N. C. DNA in a material world. *Nature* **421**, 427 (2003).
25. Rothmund, P. W. K. Folding DNA to create nanoscale shapes and patterns. *Nature* **440**, 297 (2006).
26. Stulz, E. DNA architectonics: towards the next generation of bio-inspired materials. *Chem. Eur. J.* **18**, 4456 (2012).
27. Mirkin, C. A., Letsinger, R. L., Mucic, R. C. & Storhoff, J. J. A DNA-based method for rationally assembling nanoparticles into macroscopic material. *Nature* **382**, 607 (1996).
28. Storhoff, J. J. & Mirkin, C. A. Programmed materials synthesis with DNA. *Chem. Rev.* **99**, 1849 (1999).
29. Lee, J.-S., Lytton-Jean, A. K. R., Hurst, S. J. & Mirkin, C. A. Silver nanoparticle-oligonucleotide conjugates based on DNA with triple cyclic disulfide moieties. *Nano Lett.* **7**, 2112 (2007).
30. Cutler, J. I., Zheng, D., Xu, X., Giljohann, D. A. & Mirkin, C. A. Polyvalent oligonucleotide iron oxide nanoparticle “click” conjugates. *Nano Lett.* **10**, 1477 (2010).

31. Mitchell, G. P., Mirkin, C. A. & Letsinger, R. L. Programmed assembly of DNA functionalized quantum dots. *J. Am. Chem. Soc.* **121**, 8122 (1999).
32. Sun, Y. & Xia, Y. Shape-controlled synthesis of gold and silver nanoparticles. *Science* **298**, 2176 (2002).
33. Eustis, S. & El-Sayed, M. A. Why gold nanoparticles are more precious than pretty gold: noble metal surface plasmon resonance and its enhancement of the radiative and nonradiative properties of nanocrystals of different shapes. *Chem. Soc. Rev.* **35**, 209 (2006).
34. Stratakis, M. & Garcia, H. Catalysis by supported gold nanoparticles: beyond aerobic oxidative processes. *Chem. Rev.* **112**, 4469 (2012).
35. Sperling, R. A., Gil, P. R., Zhang, F., Zamella, M. & Parak, W. J. Biological applications of gold nanoparticles. *Chem. Soc. Rev.* **37**, 1896 (2008).
36. Hill, H. D., Millstone, J. E., Banholzer, M. J. & Mirkin, C. A. The role radius of curvature plays in thiolated oligonucleotide loading on gold nanoparticles. *ACS Nano* **3**, 418 (2009).
37. Hurst, S. J., Lytton-Jean, A. K. R. & Mirkin, C. A. Maximizing DNA loading on a range of gold nanoparticle sizes. *Anal. Chem.* **78**, 8313 (2006).
38. Giljohann, D. A. *et al.* Gold nanoparticles for biology and medicine. *Angew. Chem. Int. Ed.* **49**, 3280 (2010).

39. Saha, K., Agasti, S. S., Kim, C., Li, X. & Rotello, V. M. Gold nanoparticles in chemical and biological sensing. *Chem. Rev.* **112**, 2739 (2012).
40. Ghosh, S. K. & Pal, T. Interparticle coupling effect on the surface plasmon resonance of gold nanoparticles: From theory to applications. *Chem. Rev.* **107**, 4797 (2007).
41. Boisselier, E. & Astruc, D. Gold nanoparticles in nanomedicine: preparations, imaging, diagnostics, therapies and toxicity. *Chem. Soc. Rev.* **38**, 1759 (2009).
42. Wilson, R. The use of gold nanoparticles in diagnostics and detection. *Chem. Soc. Rev.* **37**, 2028 (2008).
43. Liu, J., Cao, Z. & Lu, Y. Functional nucleic acid sensors. *Chem. Rev.* **109**, 1948 (2009).
44. Tuerk, C. & Gold, L. Systematic evolution of ligands by exponential enrichment: RNA ligands to bacteriophage T4 DNA polymerase. *Science (80)*. **249**, 505 (1990).
45. Hamula, C., Guthrie, J., Zhang, H., Li, X. C. & Le, X.-F. Selection and analytical applications of aptamers. *Trends Anal. Chem.* **25**, 681 (2006).
46. Jhaveri, S. D. *et al.* Designed signaling aptamers that transduce molecular recognition to changes in fluorescence intensity. *J. Am. Chem. Soc.* **122**, 2469 (2000).

47. Ellington, A. D. & Szostak, J. W. In vitro selection of RNA molecules that bind specific ligands. *Nature* **345**, 818 (1990).
48. Mendonsa, S. D. & Bowser, M. T. In vitro evolution of functional DNA using capillary electrophoresis. *J. Am. Chem. Soc.* **126**, 20 (2004).
49. Berezovski, M. *et al.* Nonequilibrium capillary electrophoresis of equilibrium mixtures: a universal tool for development of aptamers. *J. Am. Chem. Soc.* **127**, 3165 (2005).
50. Lou, X. *et al.* Micromagnetic selection of aptamers in microfluidic channels. *Proc. Natl. Acad. Sci. U.S.A.* **106**, 2989 (2009).
51. Shangguan, D. *et al.* Aptamers evolved from live cells as effective molecular probes for cancer study. *Proc. Natl. Acad. Sci. U.S.A.* **103**, 11838 (2006).
52. Hamula, C. *et al.* Selection and analytical applications of aptamers binding microbial pathogens. *Trends Anal. Chem.* **30**, 1587 (2011).
53. Gold, L., Polisky, B., Uhlenbeck, O. & Yarus, M. Diversity of oligonucleotide functions. *Annu. Rev. Biochem.* **64**, 763 (1995).
54. Prodan, E., Radloff, C., Halas, N. J. & Nordlander, P. A hybridization model for the plasmon response of complex nanostructures. *Science* **302**, 419 (2003).

55. Jin, R., Wu, G., Li, Z., Mirkin, C. A. & Schatz, G. C. What Controls the Melting Properties of DNA-Linked Gold Nanoparticle Assemblies. *J. Am. Chem. Soc.* **125**, 1643 (2003).
56. Storhoff, J. J., Elghanian, R., Mucic, R. C., Mirkin, C. A. & Letsinger, R. L. One-pot colorimetric differentiation of polynucleotides with single base imperfections using gold nanoparticle probes. *J. Am. Chem. Soc.* **120**, 1959 (1998).
57. Huang, C.-C., Huang, Y.-F., Cao, Z., Tan, W. & Chang, H.-T. Aptamer-modified gold nanoparticles for colorimetric determination of platelet-derived growth factors and their receptors. *Anal. Chem.* **77**, 5735 (2005).
58. Liu, J. & Lu, Y. A colorimetric lead biosensor using DNAzyme-directed assembly of gold nanoparticles. *J. Am. Chem. Soc.* **125**, 6642 (2003).
59. Liu, J. & Lu, Y. Fast colorimetric sensing of adenosine and cocaine based on a general sensor design involving aptamers and nanoparticles. *Angew. Chem. Int. Ed.* **45**, 90 (2006).
60. Liu, J. & Lu, Y. Accelerated color change of gold nanoparticles assembled by DNAzymes for simple and fast colorimetric Pb²⁺ detection. *J. Am. Chem. Soc.* **126**, 12298 (2004).
61. Sato, K. Rapid aggregation of gold nanoparticles induced by non-cross-linking DNA hybridization. *J. Am. Chem. Soc.* **125**, 8102 (2003).

62. Li, H. & Rothberg, L. Colorimetric detection of DNA sequences based on electrostatic interactions with unmodified gold nanoparticles. *Proc. Natl. Acad. Sci. U.S.A* **101**, 14036 (2004).
63. Doria, G. F., Franco, D. R. & Baptista, P. Nanodiagnostics: fast colorimetric method for single nucleotide polymorphism/mutation detection. *IET Nanobiotechnol.* **1**, 53 (2007).
64. Wei, H., Li, B., Li, J., Wang, E. & Dong, S. Simple and sensitive aptamer-based colorimetric sensing of protein using unmodified gold nanoparticle probes. *Chem. Commun.* **36**, 3735 (2007).
65. Wang, L., Liu, X., Hu, X., Song, S. & Fan, C. Unmodified gold nanoparticles as a colorimetric probe for potassium DNA aptamers. *Chem. Commun.* 3780 (2006).
66. Chen, S. J. Colorimetric determination of urinary adenosine using aptamer-modified gold nanoparticles. *Biosens. Bioelectron.* **23**, 1749 (2008).
67. Bunz, U. H. & Rotello, V. M. Gold nanoparticle-fluorophore complexes: sensitive and discerning “noses” for biosystems sensing. *Angew. Chem. Int. Ed.* **49**, 3268 (2010).

68. Dulkeith, E. *et al.* Fluorescence quenching of dye molecules near gold nanoparticles: radiative and nonradiative effects. *Phys. Rev. Lett.* **89**, 203002 (2002).
69. Dulkeith, E. *et al.* Gold nanoparticles quench fluorescence by phase induced radiative rate suppression. *Nano Lett.* **5**, 585 (2005).
70. Dubertret, B., Calame, M. & Libchaber, A. J. Single-mismatch detection using gold-quenched fluorescent oligonucleotides. *Nat. Biotechnol.* **19**, 680 (2001).
71. Song, S. *et al.* Gold-nanoparticle-based multicolor nanobeacons for sequence-specific DNA analysis. *Angew. Chem. Int. Ed.* **48**, 8670 (2009).
72. Zhang, J. *et al.* Apatamer-based multiicolor fluorescent gold nanoprobe for multiplex detection in homogenous solution. *Small* **6**, 201 (2010).
73. Maxwell, D. J., Taylor, J. R. & Nie, S. Self-assembled nanoparticle probes for recognition and detection of biomolecules. *J. Am. Chem. Soc.* **124**, 9606 (2002).
74. Liu, J., Lee, J. H. & Lu, Y. Quantum dot encoding of aptamer-linked nanostructures for one-pot simultaneous detection of multiple analytes. *Anal. Chem.* **79**, 4120–4125 (2007).
75. Prigodich, A. E. *et al.* Multiplexed nanoflares: mRNA detection in live cells. *Anal. Chem.* **84**, 2062 (2012).

76. Zheng, D., Seferos, D. S., Giljohann, D. A., Patel, P. C. & Mirkin, C. A. Aptamer nano-flares for molecular detection in living cells. *Nano Lett.* **9**, 3258–61 (2009).
77. Prigodich, A. E. *et al.* Nano-flares for mRNA regulation and detection. *ACS Nano* **3**, 2147 (2009).
78. Seferos, D. S., Prigodich, A. E., Giljohann, D. A., Patel, P. C. & Mirkin, C. A. Polyvalent DNA Nanoparticle Conjugates Stabilize Nucleic Acids 2009. *Nano Lett.* **9**, 308 (2009).
79. Seferos, D. S., Giljohann, D. A., Hill, H. D., Prigodich, A. E. & Mirkin, C. A. Nano-flares: probes for transfection and mRNA detection in living cells. *J. Am. Chem. Soc.* **129**, 15477 (2007).
80. Taton, T. A., Mirkin, C. A. & Letsinger, R. L. Scanometric DNA Array Detection with Nanoparticle Probes. *Science (80)*. **289**, 1757 (2000).
81. Wang, Y. *et al.* Ultrasensitive colorimetric detection of protein by aptamer-Au nanoparticles conjugates based on a dot-blot assay. *Chem Commun.* 2520 (2008).
82. Liu, J., Mazumdar, D. & Lu, Y. A simple and sensitive “dipstick” test in serum based on lateral flow separation of aptamer-linked nanostructures. *Angew. Chem. Int. Ed.* **45**, 7955 (2006).

83. Moskovits, M. & Uersi, U. Surface-enhanced spectroscopy. *Rev. Mod. Phys.* **57**, 783 (1985).
84. Banholzer, M. J., Millstone, J. E., Qin, L. & Mirkin, C. A. Rationally designed nanostructures for surface-enhanced Raman spectroscopy. *Chem. Soc. Rev.* **37**, 885 (2008).
85. Porter, M. D., Lipert, R. J., Siperko, L. M., Wang, G. & Narayanan, R. SERS as a bioassay platform: fundamentals, design, and applications. *Chem. Soc. Rev.* **37**, 1001 (2008).
86. Graham, D. The next generation of advanced spectroscopy: surface enhanced Raman scattering from metal nanoparticles. *Angew. Chem. Int. Ed.* **49**, 9325 (2010).
87. Kendall, C., Hutchings, J., Barr, H., Shepard, N. & Stone, N. Exploiting the diagnostic potential of biomolecular fingerprinting with vibrational spectroscopy. *Faraday Discuss* **149**, 256 (2011).
88. Xu, H., Bjerneld, E., Käll, M. & Börjesson, L. Spectroscopy of Single Hemoglobin Molecules by Surface Enhanced Raman Scattering. *Phys. Rev. Lett.* **83**, 4357 (1999).
89. Hao, E. & Schatz, G. C. Electromagnetic fields around silver nanoparticles and dimers. *J. Chem. Phys.* **120**, 357 (2004).

90. Camden, J. P., Dieringer, J. A., Zhao, J. & Van Duyne, R. P. Controlled plasmonic nanostructures for surface-enhanced spectroscopy and sensing. *Acc. Chem. Res.* **41**, 1653 (2008).
91. Graham, D. *et al.* Functionalized nanoparticles for bioanalysis by SERRS. *Biochem. Soc. Trans.* **37**, 697 (2009).
92. Faulds, K., Barbagallo, R. P., Keer, J. T., Smith, W. E. & Graham, D. SERS as a more sensitive technique for the detection of labelled oligonucleotides compared to fluorescence. *Analyst* **129**, 567 (2004).
93. Stokes, R. J. *et al.* Quantitative enhanced Raman scattering of labeled DNA from gold and silver nanoparticles. *Small* **3**, 1593 (2007).
94. Faulds, K., McKenzie, F. & Smith W. E. Graham, D. Quantitative simultaneous multianalyte detection of DNA by dual-wavelength surface-enhanced Raman scattering. *Angew. Chem. Int. Ed.* **46**, 1829 (2007).
95. Lim, D.-K. *et al.* Highly uniform and reproducible surface-enhanced Raman scattering from DNA-tailorable nanoparticles with 1-nm interior gap. *Nat. Nanotechnol.* **6**, 452 (2011).
96. Chou, L. Y. T., Zagorovsky, K. & Chan, W. C. W. DNA assembly of nanoparticle superstructures for controlled biological delivery and elimination. *Nat. Nanotechnol.* **9**, 148 (2014).

97. Stebe, K. J., Lewandowski, E. & Ghosh, M. Oriented assembly of metamaterials. *Science* **325**, 159 (2009).
98. Cao, A., Lu, R. & Veser, G. Stabilizing metal nanoparticles for heterogeneous catalysis. *Phys. Chem. Chem. Phys.* **12**, 13499 (2010).
99. Tan, S. J., Campolongo, M. J., Luo, D. & Cheng, W. Building plasmonic nanostructures with DNA. *Nat. Nanotechnol.* **6**, 268 (2011).
100. Sun, Y. *et al.* Metallic nanostructures assembled by DNA and related applications in surface-enhancement Raman scattering (SERS) detection. *J. Mater. Chem.* **21**, 16675 (2011).
101. Guerrini, L., McKenzie, F., Wark, A. W., Faulds, K. & Graham, D. Tuning the interparticle distance in nanoparticle assemblies in suspension via DNA-triplex formation: correlation between plasmonic and surface-enhanced Raman scattering responses. *Chem. Sci.* **3**, 2262 (2012).
102. Tan, S. J., Campolongo, M. J., Luo, D. & Cheng, W. Building plasmonic nanostructures with DNA. *Nat. Nanotechnol.* **6**, 268 (2011).
103. Choi, C. L. & Alivisatos, A. P. From artificial atoms to nanocrystal molecules: preparation and properties of more complex nanostructures. *Annu. Rev. Phys. Chem.* **61**, 369 (2010).
104. Wilner, O. I. & Willner, I. Functionalized DNA nanostructures. *Chem. Rev.* **112**, 2528 (2012).

105. Murphy, C. J., Gole, A. M., Hunyadi, S. E. & Orendorff, C. J. One-Dimensional Colloidal Gold and Silver Nanostructures. *Inorg. Chem.* **45**, 7544 (2006).
106. Kumar, A., Hwang, J.-H., Kumar, S. & Nam, J. Tuning and assembling metal nanostructures with DNA. *Chem. Commun.* **49**, 2597 (2013).
107. Zanchet, D., Micheel, C. M., Parak, W. J., Gerion, D. & Alivisatos, a. P. Electrophoretic Isolation of Discrete Au Nanocrystal/DNA Conjugates. *Nano Lett.* **1**, 32 (2001).
108. Claridge, S. A., Liang, H. W., Basu, S. R., Fréchet, J. M. J. & Alivisatos, A. P. Isolation of Discrete Nanoparticle - DNA Conjugates for Plasmonic Applications. *Nano Lett.* **8**, 1202 (2008).
109. Mastroianni, A. J., Claridge, S. A. & Alivisatos, A. P. Pyramidal and chiral groupings of gold nanocrystals assembled using DNA scaffolds. *J. Am. Chem. Soc.* **131**, 8455 (2009).
110. Yan, W. *et al.* Self-assembly of chiral nanoparticle pyramids with strong R/S optical activity. *J. Am. Chem. Soc.* **134**, 15114 (2012).
111. Xu, X., Rosi, N. L., Wang, Y., Huo, F. & Mirkin, C. A. Asymmetric functionalization of gold nanoparticles with oligonucleotides. *J. Am. Chem. Soc.* **128**, 9286 (2006).

112. Maye, M. M., Nykypanchuk, D., Cuisinier, M., Lelie, D. Van Der & Gang, O. Stepwise surface encoding for high-throughput assembly of nanoclusters. *Nat. Mater.* **8**, 398 (2009).
113. Deng, Z., Tian, Y., Lee, S.-H., Ribbe, A. E. & Mao, C. DNA-encoded self-assembly of gold nanoparticles into one-dimensional arrays. *Angew. Chem. Int. Ed.* **44**, 3582 (2005).
114. Beyer, S., Nickels, P. & Simmel, F. C. Periodic DNA nanotemplates synthesized by rolling circle amplification. *Nano Lett.* **5**, 719 (2005).
115. Ding, B. *et al.* Gold nanoparticle self-similar chain structure organized by DNA origami. *J. Am. Chem. Soc.* **132**, 3248 (2010).
116. Kuzyk, A. *et al.* DNA-based self-assembly of chiral plasmonic nanostructures with tailored optical response. *Nature* **483**, 311 (2012).
117. Le, J. D. *et al.* DNA-Templated Self-Assembly of Metallic Nanocomponent Arrays on a Surface. *Nano Lett.* **4**, 2342 (2004).
118. Sharma, J., Chhabra, R., Liu, Y., Ke, Y. & Yan, H. DNA-templated self-assembly of two-dimensional and periodical gold nanoparticle arrays. *Angew. Chem. Int. Ed.* **45**, 730 (2006).
119. Zheng, J. *et al.* Two-dimensional nanoparticle arrays show the organizational power of robust DNA motifs. *Nano Lett.* **6**, 1502 (2006).

120. Sharma, J. *et al.* Control of Self-Assembly of DNA Tubules Through Integration of Gold Nanoparticles. *Science (80)*. **323**, 112 (2009).
121. Reynolds, R. A., Mirkin, C. A. & Letsinger, R. L. Homogeneous, Nanoparticle-Based Quantitative Colorimetric Detection of Oligonucleotides. *J. Am. Chem. Soc.* **122**, 3795 (2000).
122. Storhoff, J. J. *et al.* What Controls the Optical Properties of DNA-Linked Gold Nanoparticle Assemblies? *J. Am. Chem. Soc.* **122**, 4640 (2000).
123. Macfarlane, R. J. *et al.* Assembly and organization processes in DNA-directed colloidal crystallization. *Proc. Natl. Acad. Sci. U.S.A.* **106**, 10493 (2009).
124. Hurst, S. J., Hill, H. D. & Mirkin, C. A. “Three-dimensional hybridization” with polyvalent DNA-gold nanoparticle conjugates. *J. Am. Chem. Soc.* **130**, 12192 (2008).
125. Li, Z. & Mirkin, C. A. G-quartet-induced nanoparticle assembly. *J. Am. Chem. Soc.* **127**, 11568 (2005).
126. Park, S. Y. *et al.* DNA-programmable nanoparticle crystallization. *Nature* **451**, 553 (2008).
127. Nykypanchuk, D., Maye, M. M., van der Lelie, D. & Gang, O. DNA-guided crystallization of colloidal nanoparticles. *Nature* **451**, 549 (2008).

128. Hill, H. D. *et al.* Controlling the Lattice Parameters of Gold Nanoparticle FCC Crystals with Duplex DNA Linkers. *Nano Lett.* **58**, 2341 (2008).
129. Macfarlane, R. J. *et al.* Nanoparticle superlattice engineering with DNA. *Science (80)*. **334**, 204 (2011).
130. Auyeung, E. *et al.* Synthetically programmable nanoparticle superlattices using a hollow three-dimensional spacer approach. *Nat. Nanotechnol.* **7**, 24 (2012).
131. Li, T. I. N. G., Sknepnek, R. & Olvera de la Cruz, M. Thermally active hybridization drives the crystallization of DNA-functionalized nanoparticles. *J. Am. Chem. Soc.* **135**, 8535 (2013).
132. Macfarlane, R. J. *et al.* Establishing the design rules for DNA-mediated programmable colloidal crystallization. *Angew. Chem. Int. Ed.* **49**, 4589 (2010).
133. Li, T. I. N. G., Sknepnek, R., Macfarlane, R. J., Mirkin, C. A. & de la Cruz, M. O. Modeling the crystallization of spherical nucleic acid nanoparticle conjugates with molecular dynamics simulations. *Nano Lett.* **12**, 2509 (2012).
134. Smith, D. R., Pendry, J. B. & Wiltshire, M. C. K. Metamaterials and negative refractive index. *Science* **305**, 788 (2004).

135. Solomon, M. J. Directions for targeted self-assembly of anisotropic colloids from statistical thermodynamics. *Curr. Opin. Colloid Interface Sci.* **16**, 158 (2011).
136. Young, K. L. *et al.* Using DNA to design plasmonic metamaterials with tunable optical properties. *Adv. Mater.* **26**, 653 (2014).
137. Dreyfus, R. *et al.* Simple Quantitative Model for the Reversible Association of DNA Coated Colloids. *Phys. Rev. Lett.* **102**, 048301 (2009).
138. Lee, O.-S., Prytkova, T. R. & Schatz, G. C. Using DNA to Link Gold Nanoparticles, Polymers and Molecules: a Theoretical Perspective. *J. Phys. Chem. Lett.* **1**, 1781 (2010).
139. Gibbs-Davis, J. M., Schatz, G. C. & Nguyen, S. T. Sharp melting transitions in DNA hybrids without aggregate dissolution: proof of neighboring-duplex cooperativity. *J. Am. Chem. Soc.* **129**, 15535 (2007).
140. Long, H., Kudlay, A. & Schatz, G. C. Molecular dynamics studies of ion distributions for DNA duplexes and DNA clusters: salt effects and connection to DNA melting. *J. Phys. Chem. B* **110**, 2918 (2006).
141. Akamatsu, K. *et al.* A DNA duplex with extremely enhanced thermal stability based on controlled immobilization on gold nanoparticles. *Nano Lett.* **6**, 491 (2006).

142. Chen, C., Wang, W., Ge, J. & Zhao, X. S. Kinetics and thermodynamics of DNA hybridization on gold nanoparticles. *Nucleic Acids Res.* **37**, 3756 (2009).
143. Maye, M. M., Nykypanchuk, D., van der Lelie, D. & Gang, O. A simple method for kinetic control of DNA-induced nanoparticle assembly. *J. Am. Chem. Soc.* **128**, 14020 (2006).
144. Prigodich, A. E. *et al.* Tailoring DNA structure to increase target hybridization kinetics on surfaces. *J. Am. Chem. Soc.* **132**, 10638 (2010).
145. Nykypanchuk, D., Maye, M. M., van der Lelie, D. & Gang, O. DNA-based approach for interparticle interaction control. *Langmuir* **23**, 6305 (2007).
146. Maye, M. M., Nykypanchuk, D., van der Lelie, D. & Gang, O. DNA-regulated micro- and nanoparticle assembly. *Small* **3**, 1678 (2007).
147. Tan, Y. N., Lee, K. H. & Su, X. A study of DNA design dependency of segmented DNA-induced gold nanoparticle aggregation towards versatile bioassay development. *RSC Adv.* **3**, 21604 (2013).
148. Oh, J.-H. & Lee, J.-S. Designed hybridization properties of DNA-GNP conjugates for ultrasensitive detection of single base mutation in breast cancer gene BRCA1. *Anal. Chem.* **83**, 7364 (2011).
149. Liu, J. & Lu, Y. Non-Base Pairing DNA Provides a New Dimension for Controlling Aptamer-Linked Nanoparticles and Sensors Adenosine-

- Responsive Aptamer-Linked AuNP Disassem-. *J. Am. Chem. Soc.* **129**, 8634 (2007).
150. Sikder, M. D. H. & Gibbs-Davis, J. M. The Influence of Gap Length on Cooperativity and Rate of Association in DNA-Modified Gold Nanoparticle Aggregates. *J. Phys. Chem. C* **116**, 11694 (2012).
151. Smith, B. D., Dave, N., Huang, P. J. & Liu, J. Assembly of DNA-Functionalized Gold Nanoparticles with Gaps and Overhangs in Linker DNA. *J. Phys. Chem. C* **115**, 7851 (2011).
152. Nam, J. M., Park, S. J. & Mirkin, C. A. Bio-barcodes based on oligonucleotide-modified nanoparticles. *J. Am. Chem. Soc.* **124**, 3820 (2002).
153. Jones, M. R. *et al.* DNA-nanoparticle superlattices formed from anisotropic building blocks. *Nat. Mater.* **9**, 913 (2010).
154. Macfarlane, R. J. *et al.* Assembly and organization processes in DNA-directed colloidal crystallization. *Proc. Natl. Acad. Sci. U.S.A* **106**, 10493 (2009).
155. Pinto, Y. Y. *et al.* Sequence-encoded self-assembly of multiple-nanocomponent arrays by 2D DNA scaffolding. *Nano Lett.* **5**, 2399 (2005).
156. Le, J. D. *et al.* DNA-Templated Self-Assembly of Metallic Nanocomponent Arrays on a Surface. *Nano Lett.* **4**, 2343 (2004).

157. Zhang, J., Liu, Y., Ke, Y. & Yan, H. Periodic square-like gold nanoparticle arrays templated by self-assembled 2D DNA Nanogrids on a surface. *Nano Lett.* **6**, 248 (2006).
158. Song, T. & Liang, H. Synchronized assembly of gold nanoparticles driven by a dynamic DNA-fueled molecular machine. *J. Am. Chem. Soc.* **134**, 10803 (2012).
159. Liu, J. Adsorption of DNA onto gold nanoparticles and graphene oxide: surface science and applications. *Phys. Chem. Chem. Phys.* **14**, 10485 (2012).
160. Leunissen, M. E., Dreyfus, R., Sha, R., Seeman, N. C. & Chaikin, P. M. Quantitative study of the association thermodynamics and kinetics of DNA-coated particles for different functionalization schemes.pdf. *J. Am. Chem. Soc.* **132**, 1903 (2010).
161. Witten, K. G., Bretschneider, J. C., Eckert, T., Richtering, W. & Simon, U. Assembly of DNA-functionalized gold nanoparticles studied by UV/Vis-spectroscopy and dynamic light scattering. *Phys. Chem. Chem. Phys.* **10**, 1870 (2008).
162. Osinkina, L. *et al.* Tuning DNA binding kinetics in an optical trap by plasmonic nanoparticle heating. *Nano Lett.* **13**, 3140 (2013).

163. Buchkremer, A. *et al.* Stepwise thermal and photothermal dissociation of a hierarchical superaggregate of DNA-functionalized gold nanoparticles. *Small* **7**, 1397 (2011).
164. Lee, O.-S. & Schatz, G. C. Molecular Dynamics Simulation of DNA-Functionalized Gold Nanoparticles. *J. Phys. Chem. C* **113**, 2316 (2009).
165. Katz, E. & Willner, I. Integrated nanoparticle-biomolecule hybrid systems: synthesis, properties, and applications. *Angew. Chem. Int. Ed.* **43**, 6042 (2004).
166. Feldkamp, U. & Niemeyer, C. M. Rational design of DNA nanoarchitectures. *Angew. Chem. Int. Ed.* **45**, 1856 (2006).
167. Lu, Y. & Liu, J. Smart nanomaterials inspired by biology: dynamic assembly of error-free nanomaterials in response to multiple chemical and biological stimuli. *Acc. Chem. Res.* **40**, 315 (2007).
168. Zhao, W., Brook, M. A. & Li, Y. Design of gold nanoparticle-based colorimetric biosensing assays. *ChemBiochem* **9**, 2363 (2008).
169. Geerts, N. & Eiser, E. DNA-functionalized colloids: Physical properties and applications. *Soft Matter* **6**, 4647 (2010).
170. Lin, C., Liu, Y. & Yan, H. Designer DNA Nanoarchitectures. *Biochemistry* **48**, 1663 (2009).

171. Xue, X., Wang, F. & Liu, X. One-step, room temperature, colorimetric detection of Mercury (Hg^{2+}) using DNA/nanoparticle conjugates. *J. Am. Chem. Soc.* **130**, (2008).
172. Lee, J.-S., Han, M. S. & Mirkin, C. A. Colorimetric detection of mercuric ion (Hg^{2+}) in aqueous media using DNA-functionalized gold nanoparticles. *Angew. Chem. Int. Ed.* **46**, 4093 (2007).
173. Zhao, W., Lam, J. C., Chiuman, W., Brook, M. A. & Li, Y. Enzymatic cleavage of nucleic acids on gold nanoparticles: A generic platform for facile colorimetric biosensors. *Small* **4**, 810 (2008).
174. Demers, L. M. *et al.* A fluorescence-based method for determining the surface coverage and hybridization efficiency of thiol-capped oligonucleotides bound to gold thin films and nanoparticles. *Anal. Chem.* **72**, 5535 (2000).
175. Zu, Y., Ting, A. L., Yi, G. & Gao, Z. Sequence-selective recognition of nucleic acids under extremely low salt conditions using nanoparticle probes. *Anal. Chem.* **83**, 4090 (2011).
176. Oh, J. & Lee, J.-S. Salt concentration-induced dehybridisation of DNA-gold nanoparticle conjugate assemblies for diagnostic applications. *Chem. Commun.* **46**, 6382 (2010).

177. Maye, M. M., Kumara, M. T., Nykypanchuk, D., Sherman, W. B. & Gang, O. Switching binary states of nanoparticle superlattices and dimer clusters by DNA strands. *Nat. Nanotechnol.* **5**, 116 (2010).
178. Protozanova, E., Yakovchuk, P. & Frank-Kamenetskii, M. D. Stacked-unstacked equilibrium at the nick site of DNA. *J. Mol. Biol.* **342**, 775 (2004).
179. Yakovchuk, P., Protozanova, E. & Frank-Kamenetskii, M. D. Base-stacking and base-pairing contributions into thermal stability of the DNA double helix. *Nucleic Acids Res.* **34**, 564 (2006).
180. Peterson, A. W., Heaton, R. J. & Georgiadis, R. M. The effect of surface probe density on DNA hybridization. *Nucleic Acids Res.* **29**, 5163 (2001).
181. Wong, I. Y. & Melosh, N. A. An electrostatic model for DNA surface hybridization. *Biophys. J.* **98**, 2954 (2010).
182. Irving, D., Gong, P. & Levicky, R. DNA surface hybridization: comparison of theory and experiment. *J. Phys. Chem. B* **114**, 7631 (2010).
183. Kirk, B. W., Feinsod, M., Favis, R., Kliman, R. M. & Barany, F. Single nucleotide polymorphism seeking long term association with complex disease. *Nucleic Acids Res.* **30**, 3295 (2002).

184. Cao, Y. C., Jin, R. & Mirkin, C. A. Nanoparticles with Raman spectroscopic fingerprints for DNA and RNA detection. *Science (80)*. **297**, 1536 (2002).
185. Nickerson, D. A. *et al.* Automated DNA diagnostics using an ELISA-based oligonucleotide ligation assay. *Proc. Natl. Acad. Sci. U. S. A.* **87**, 8923 (1990).
186. Chen, X., Livak, K. J. & Kwok, P. A Homogeneous, Ligase-Mediated DNA Diagnostic Test. *Genome Res.* **8**, 549 (1998).
187. Ross, P., Hall, L., Smirnov, I. & Haff, L. High level multiplex genotyping by MALDI-TOF mass spectrometry. *Nat. Biotechnol.* **16**, 1347 (1998).
188. Schouten, J. P. *et al.* Relative quantification of 40 nucleic acid sequences by multiplex ligation-dependent probe amplification. *Nucleic Acids Res.* **30**, e57 (2002).
189. Livak, K. J. Allelic discrimination using fluorogenic probes and the 5' nuclease assay. *Genet. Anal.* **14**, 143 (1999).
190. Xu, X., Han, M. S. & Mirkin, C. A. A gold-nanoparticle-based real-time colorimetric screening method for endonuclease activity and inhibition. *Angew. Chem. Int. Ed.* **46**, 3468 (2007).
191. Lee, J. H., Wang, Z., Liu, J. & Lu, Y. Highly sensitive and selective colorimetric sensors for uranyl (UO_2^{2+}): development and comparison of

- labeled and label-free DNAzyme-gold nanoparticle systems. *J. Am. Chem. Soc.* **130**, 14217 (2008).
192. Liu, J. & Lu, Y. Stimuli-responsive disassembly of nanoparticle aggregates for light-up colorimetric sensing. *J. Am. Chem. Soc.* **127**, 12677–12683 (2005).
193. Han, M. S., Lytton-Jean, A. K. R., Oh, B.-K. K., Heo, J. & Mirkin, C. A. Colorimetric screening of DNA-binding molecules with gold nanoparticle probes. *Angew. Chem. Int. Ed.* **45**, 1807 (2006).
194. Wu, Z. *et al.* Inhibitory Effect of Target Binding on Hairpin Nanoparticle Assembly for Light-up Colorimetric Protein Assay. *Anal. Chem.* **82**, 3890 (2010).
195. Williams, D. L. *et al.* Contribution of rpoB Mutations to Development of Rifamycin Cross-Resistance in Mycobacterium tuberculosis Contribution of rpoB Mutations to Development of Rifamycin Cross-Resistance in Mycobacterium tuberculosis. *Antimicrob. Agents. Chemother.* **42**, 1853 (1998).
196. Dillenback, L. M., Goodrich, G. P. & Keating, C. D. Temperature-programmed assembly of DNA: Au nanoparticle bioconjugates. *Nano Lett.* **6**, 16 (2006).

197. Sobczak, J.-P. J., Martin, T. G., Gerling, T. & Dietz, H. Rapid folding of DNA into nanoscale shapes at constant temperature. *Science (80)*. **338**, 1458 (2012).
198. Naef, F., Lim, D., Patil, N. & Magnasco, M. DNA hybridization to mismatched templates: A chip study. *Phys. Rev. E* **65**, 040902 (2002).
199. Sorokin, N. V *et al.* Discrimination between perfect and mismatched duplexes with oligonucleotide gel microchips: role of thermodynamic and kinetic effects during hybridization. *J. Biomol. Struct. Dyn.* **22**, 725 (2005).
200. Dai, H., Meyer, M., Stepaniants, S., Ziman, M. & Stoughton, R. Use of hybridization kinetics for differentiating specific from non-specific binding to oligonucleotide microarrays. *Nucleic Acids Res.* **30**, e86 (2002).
201. Macfarlane, R. J. *et al.* Nanoparticle superlattice engineering with DNA. *Science (80)*. **334**, 204 (2011).